Wideband MEMS energy harvesters utilizing nonlinear springs

Son Duy Nguyen

Department of Informatics
Faculty of Mathematics and Natural Sciences
University of Oslo

Thesis submitted for the degree
of Philosophiae Doctor

November 2012

Series of dissertations submitted to the
Faculty of Mathematics and Natural Sciences, University of Oslo
No. 1306

ISSN 1501-7710

Cover: Inger Sandved Anfinsen.
Printed in Norway: AIT Oslo AS.

Produced in co-operation with Akademika publishing.
The thesis is produced by Akademika publishing merely in connection with the thesis defence. Kindly direct all inquiries regarding the thesis to the copyright holder or the unit which grants the doctorate.

Abstract

Micro-scale energy harvesting from motion has received increasing research interest. The energy harvesters can be used as replacements for batteries in low-power wireless electronic devices. Conventional vibration energy harvesters are designed as linear resonance structures. These have a very narrow bandwidth and operate efficiently only when the excitation frequency is very close to the resonant frequency of the harvester. The narrow bandwidth limits their applications in real-world environments that have a wide spectrum of frequencies or varying vibration spectra.

This thesis investigates a method to extend the bandwidth of the energy harvesters. We exploit nonlinearities of suspensions, in particular *softening and bistable characteristics*, to widen the harvesting bandwidth. The nonlinear-spring characteristics are obtained purely through *their geometrical design* without relying on extra features such as permanent magnets that can interfere with the surroundings.

Two electrostatic energy harvesters are designed, fabricated and characterized based on microelectromechanical systems (MEMS). The first harvester with *a quad-angled spring*, which displays *a softening characteristic*, is made by through-wafer-thickness deep-reactive ion etching onto a silicon wafer. The experimental results show that a 13-fold increase in the bandwidth of the harvester with the angled springs and an average output power increase of 68% compared with that of linear-vibrating energy harvesters at a broadband random vibration of $7\times10^{-4}\ g^2/Hz$.

We also find that the harvester is tolerant to variations both in the center frequency and bandwidth of vibration, and can perform close to its theoretical maximum with wideband vibrations.

The second MEMS electrostatic energy harvester with *curved springs* is fabricated on a silicon-on-insulator wafer using bulk micro-fabrication technology. The curved springs display *an asymmetrical bistable behavior* obtained purely through geometrical design. The experimental results with a white noise vibration at $4{\times}10^{-3}\ g^2/Hz$ show that the harvester bandwidth reaches 715 Hz, representing the largest bandwidth reported in the literature so far.

Such wideband harvesters are well-suited to extract power from a wide spectrum of vibrations or from sources with a wide range of variability in the spectrum.

Preface

This thesis is submitted in partial fulfillment of the requirements for the degree of *Philosophiae Doctor (Ph.D)* at the Department of Informatics, Faculty of Mathematics and Natural Sciences, University of Oslo. The thesis consists of a set of eight papers, including five journal articles and three conference papers, and an extensive Introduction.

The work in this thesis was carried out at the Department of Micro and Nano Systems Technology (IMST), Vestfold University College (HiVe) from August 2008 to November 2012 under the supervision of *Professor Einar Halvorsen*. Twenty-five percent of that time was allocated to duty work at HiVe and three months, July 2010-October 2010, was allocated for a cooperative research project between HiVe and U.C. Berkeley. The period for the PhD study is therefore equivalent to three years. I spent the entire period of my PhD studies at HiVe, except for a four-month period, April 2011-August 2011, when I was at U.C. Berkeley as a visiting researcher fabricating the last prototype.

Work for the thesis was part funded by The Research Council of Norway under the project "*Device concepts for micro energy harvesting*", No. 191282.

Son Duy Nguyen.

November 2012.

Acknowledgements

First and foremost, I am deeply grateful to my supervisor, Professor Einar Halvorsen for the advice, guidance, support and patience both in technical and non-technical matters. I have learned many, many things that I will carry with me for the rest of my life.

My gratitude then goes to Dean Duy-Tho Do and Associate Professor Nhon Van Vo for their efforts to give me and other Vietnamese students the chance to study at Vestfold Univerity College (HiVe), Norway.

Next, I would like to thank Dean Duy-Tho Do, the representative of the Faculty of Technology and Maritime Sciences, Associate Professor Nils Høivik and Tone Gran, the representative of the Department of Micro and Nano Systems Technology (IMST) for providing with financial means and laboratory facilities. I am thankful also to the people working in the clean-room laboratories for their help and kindness. I especially want to mention Engineer Zekija Ramic and Chief Engineering Ragnar Dahl Johansen at the IMST clean room, HiVe, Process Engineering Manager Sia Parsa at the Marvell Nano Lab, University of California (U.C.), Berkeley, Chief Scientist Geir Uri Jensen and Research Scientist Andreas Volg at SINTEF ICT.

I would like to thank Professor Yngvar Berg and the Department of Informatics, Oslo University for giving me the opportunity to carry out my PhD studies.

My gratitude goes to The Norwegian Centre for International Cooperation in Higher Education (SIU) and Dr. Igor Paprotny, Professor Richard White, and Professor Paul Wright at U.C. Berkeley for providing me the chance to research at their facilities.

I would like to thank all the members in the Energy Harvesting Group for their useful presentations and discussions, Associate Professor Svein Husa, Research Scientist Lars-Cyril Blystad at SINTEF ICT (former member), Research Fellow Sukhdeep Kaur (Binny), Research Fellow Cuong Phu Le, and Research Fellow Zhaochu Zang.

Thanks to Mrs. Van and all Vietnamese students in HiVe. Without you, the winter in Norway would be colder.

to my family

my parents, my wife Uyen+, my niece Boi Ngoc, my sister Sophia,
and my brother Hoang.

Contents

CONTENTS

List of Figures

Acronyms

AC	Alternating Current
AlN	Aluminium Nitride
DC	Direct Current
DRIE	Deep Reactive Ion Etching
FEM	Finite Element Method
LPVCP	Low Pressure Vapor Chemical Deposition
MEMS	Microelectromechanical Systems
RFID	Radio Frequency Identification
PCB	Printed Circuit Board
PSD	Power Spectral Density
PZT	Lead Zirconate Titanate
SEM	Scanning Electron Microscope
SOI	Silicon-On-Insulator
TPMS	Tire Pressure Monitoring System
WiseMAC	Wireless Sensor Medium Access Control
WSN	Wireless Sensors Node

Manuscript and published papers enclosed as annexes to the thesis

Journal articles

[1] S. D. Nguyen, E. Halvorsen and I. Paprotny, "Bistable springs for wideband MEMS energy harvesters," vol. **102**, no. 02, *Applied Physics Letters*, p. 023904, Jan 2013.

[2] S. D. Nguyen, E. Halvorsen and G. U. Jensen, "Wideband MEMS energy harvester driven by colored noise," **submitted to** *IEEE/ASME Journal of Microelectromechanical Systems*, Nov 2012.

[3] S. D. Nguyen and E. Halvorsen, "Nonlinear springs for bandwidth-tolerant vibration energy harvesting," *IEEE/ASME Journal of Microelectromechanical Systems*, vol. **20**, no. 6, pp.1225-1227, Dec 2011.

[4] S. D. Nguyen, E. Halvorsen, G. U. Jensen and A. Vogl, "Fabrication and characterization of a wideband MEMS energy harvester utilizing nonlinear springs," *Journal of Micromechanics and Microengineering*, vol. **20**, no. 12, p. 125009 (11p), Dec 2010.

[5] L. G. W. Tvedt, S. D. Nguyen, and E. Halvorsen, "Nonlinear behavior of an electrostatic energy harvester under wide- and narrowband excitation," *IEEE/ASME Journal of Microelectromechanical Systems*, vol. **19**, no. 2, pp. 305-316, Apr 2010.

Conference proceedings

[6] S. D. Nguyen, N. H. T. Tran, E. Halvorsen and I. Paprotny, "Design and fabrication of MEMS electrostatic energy harvester with nonlinear springs and vertical sidewall electrets," *Proceedings of PowerMEMS 2011* (Seoul, Korea, Nov 15-18 2011), pp.126-129, 2011.

[7] S. D. Nguyen and E. Halvorsen, "Analysis of vibration energy harvesters utilizing a variety of nonlinear springs, " *Proceedings of PowerMEMS 2010* (Leuven, Belgium, Nov 30 Dec 3), pp.331-334, 2010.

[8] S. D. Nguyen and E. Halvorsen, "Wideband energy harvester utilizing nonlinear springs," *Proceedings PowerMEMS 2009* (Washington D.C., USA, Dec 1-4, 2009) pp.411-414, 2009.

List of other publications not enclosed in the thesis

Book chapter

[9] E Halvorsen and S. D. Nguyen, "MEMS electrostatic energy harvester with nonlinear springs," a book chapter of *Advance in Energy Harvesting Methods*, *Springer*, Editors: Niell Elvin and Alper Erturk, to be published.

Conference papers

[10] S. D. Nguyen, I. Paprotny, E. Halvorsen and R. M. White, "Fabrication of Nonlinear Wideband MEMS Energy Harvester with Vertical Sidewall Electrets," *BSAC IAB meeting* (California, USA, Sep 2011), BPN639, 2011.

[11] N.H.T. Tran , S. D. Nguyen and E. Halvorsen, "Design of nonlinear springs for MEMS vibration energy harvesting applications," *Micromechanics and Micro systems Europe Workshop* (Tonsberg, Norway, Jun 19-22, 2011), 2011.

[12] E. Halvorsen and S. D. Nguyen, "Numerical simulation of MEMS energy harvesters driven by band-limited random noise, " *Solid State System Symposium* (HCM city, Vietnam, Jun 16-18, 2010), 2010.

Chapter 1

Introduction

1.1 Vibration energy harvesters

1.1.1 Motivations

Wireless sensor networks are part of the new and high technology of spatially distributed autonomous sensors developed to monitor physical or environmental conditions. Currently, wireless sensor nodes (WSNs) are powered by batteries. However, batteries have limited lifetimes and must be regularly replaced or recharged. Some WSNs are not easily accessible such as embedded sensors, automotive tire pressure monitoring systems, and health monitoring sensors of bridge structures, machines, and underground power cable. The replacement or recharging is therefore costly. Application environments also can sometimes be too harsh to use batteries. Li-ion batteries cannot withstand temperatures higher than 60^0C [16].

Furthermore, the battery is usually the largest and most expensive component of the WSNs. Miniaturization without reducing their lifetimes is an obstacle as battery capacity is a function of battery size [17].

The power consumption of recent low-rate and short-range wireless communication technologies such as those using the sub-GHz Industrial, Scientific and Medical (ISM) radio frequency bands, IEEE 802.15.4 ZigBee protocol, and Bluetooth low-energy, continues to decrease. Bluetooth low energy devices consume a low power of 147 μW at the bit rate of 960 bits/second [18]. Radio frequency identification (RFID) using the ISM band is one of the wireless application with low-power consumption. Ricci et al. [19] presented an ultra-low power baseband processor for RFID systems. The baseband processor dissipates only 440-nW average power when operating at 800 kHz and 0.6 V.

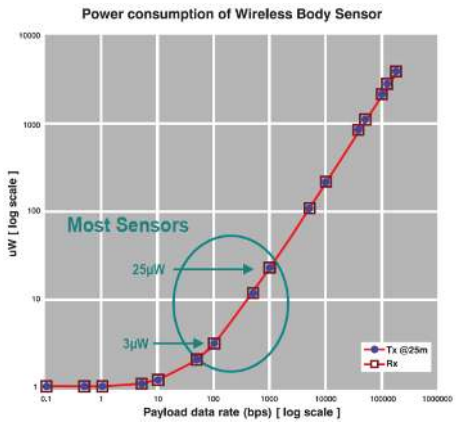

Figure 1.1: Average power versus payload data rate of a wireless sensor using the ZL70250 Transceiver from Microsemi [1]

Some other passive RFID tags consume ultra-low power of only 1 μW [20], 2 μW [21] and 16.7 μW [22].

Reghu Rajan, Microsemi CMPG company, presented a fully integrated ultra-low power sub-GHz ISM band transceiver, ZL70250 [1]. As indicated in Fig. 1.1, a wireless sensor using the ZL70250 transceiver consumes an average power of less than 25 μW for a data rate of lower than 1000 bps.

Besides the well-known standard IEEE 802.15.4 ZigBee protocol for low-rate, low-power, low-cost wireless networking, other protocols have been developed with the view to reduce power consumption of WSNs. El-Hoiydi and Decotignie [23] presented a sensor node that consumes 7 μW using a wireless sensor medium access control (WiseMAC) protocol with the WSNs transceiver compared with 13 μW when using the IEEE 802.15.4 ZigBee standard. Enz et al. [24] presented a relay sensor node consuming about 25 μW when forwarding 56-byte packets every 100 seconds using WiseMAC protocol, which is about 100 times less power than comparable solutions available at that time.

Because of the limitations of batteries, along with the reduction of power consumption and size of the WSNs, micro-scale energy harvesting from ambient sources is continually attracting interest from both the academic community and the industry. In low-power sensing applications with long life-time requirements, energy harvesters can be used to replace or recharge batteries.

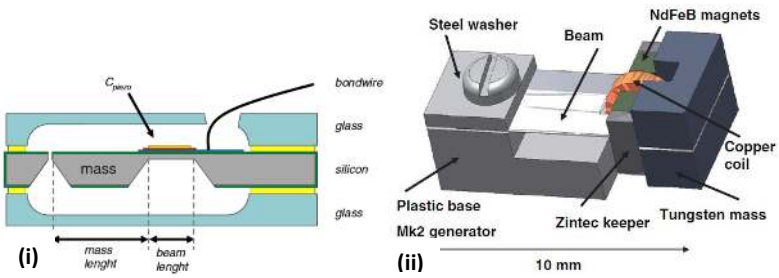

Figure 1.2: (i) Piezoelectric energy harvester (from Elfrink et al. [2]). (ii) Electromagnetic energy harvester (from Torah et al. [3]).

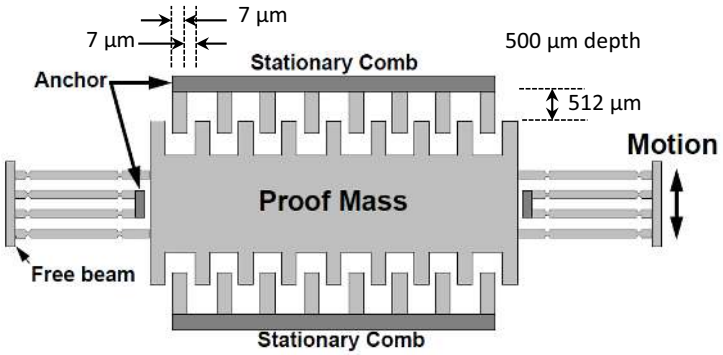

Figure 1.3: Electrostatic energy harvester (from Meninger et al. [4]). The bias means are not shown here.

Among the many forms of energy sources available for harvesting including chemicals, light, radio-frequency electromagnetic radiation, thermal gradients, and motion, the last of these is the most attractive because of its versatile and ubiquitous characteristics. Ambient motion from human body, structures, machinery, vehicles, or air/water flows form the main sources of energy for vibration energy harvesters. Research activity have demonstrated that vibration energy harvesters have a great potential in applications that need just a few microwatts [25; 26]. Energy harvesting is seen a major contributor to the future success of WSNs [27].

1.1.2 Principle of vibration energy harvesters

Present working solutions for vibration-to-electricity conversion are mainly based on three technologies: electromagnetic, piezoelectric, and electrostatic (or capacitive).

Electromagnetic energy harvesters are based on the relative movement of a permanent magnet and a coil as in conventional generators (Fig. 1.2-ii). The electromagnetic harvester for powering wristwatches such as the Seiko Kinetic watch, was invented by Hayakawa of Seiko Epson Corporation [28], and is one of the earliest commercial energy harvester products. However, electromagnetic harvesters are only suitable at macro scales, and scale poorly to MEMS size. Fabricating a macro-scale coil is an obstacle.

Piezoelectric devices are composed of piezoelectric material and electrodes on a supporting beam(s) or membrane and extract electrical energy from deformation of the piezoelectric material (Fig. 1.2-i). A piezoelectric energy harvester was first described in 1969 in a patent awarded to Ko [29]. The device converts body motion into electrical energy to power implants or pacemakers. Similarly, Schroeppel [30] presented a piezoelectric device that converts heart contractions for continuous electrical power generation. Later, piezoelectric harvesters were introduced for widespread applications in low-power wireless devices. Glynne-Jones et al. [31] and White et al. [32] presented the first vibration energy harvester based on thick film piezoelectric technology.

The advantage of piezoelectric harvesters is that there is no need of a bias to operate. Because of this convenience, piezoelectric harvesters have received much research focus in both the academic community [33; 34; 35; 36; 37; 38] and industry [39; 40]. However, piezoelectric harvesters are more complex to integrate; the piezoelectric material must be configured into micro-systems as the material needs to be poled in a strong electric field and at an elevated temperature [33].

Electrostatic harvesters with an appropriate bias use the displacement of the proof mass to vary capacitor(s) to generate the electrical energy (Fig. 1.3). MEMS-based electrostatic harvesters were firstly reported by Chandrakasan group at MIT [4; 41] and further developed by Roundy [42]. The major drawback of electrostatic harvesters is the requirement of a bias for its operation. The bias can be provided by electrets [43; 44; 45; 46; 47; 48], power management circuitry [4; 49], by recharged floating electrodes [50] or by large re-charged capacitor [51; 52].

Compared with electromagnetic or piezoelectric harvesters, electrostatic ones have the advantages:

- The capacitor configuration is easily integrated into micro-systems using standard MEMS manufacturing.
- The electromechanical coupling can be increased by increasing the bias. Electrets, the most common method for biasing them, have undergone rapid development in recent years. Potentials can reach -900 V on the horizontal surface of electrets [47] and about 100 V on the vertical surface of electrets [45]. Besides the traditional corona discharge [53; 54], many novel methods have been developed such as vacuum UV irradiation [47], and soft X-ray [48] or ion charging with ionic hair-dryers [44; 55].
- Because transducers, i.e. variable capacitors, and suspensions of electrostatic device are designed separately, there is greater freedom in designing the shape of the suspensions. Almost any shape that can be drawn while respecting the minimum critical dimensions of the process at hand is feasible.
- The tensile strength of silicon, the typical material for suspensions of electrostatic harvesters, is much higher than that of piezoelectric material such as Aluminium nitride (AlN). The failure stress of a silicon die with less than 300-μm thickness can vary from 500 - 1000 MPa [56] whereas the tensile strength of 0.94 μm thin film AlN is about 300 MPa [57]. By using parylene for suspensions of electrostatic harvesters [58], the tensile strength can be upwards of 4 GPa.

.

1.1.3 Potential applications

There are many potential applications of MEMS vibration energy harvesters to power low-power WSNs as indicated in Fig. 1.4. Energy harvesting from car-tire vibrations to power tire pressure monitoring systems (TPMSs) is one of the most promissing applications. As of September 2007, all cars sold in the United States must be equipped with a TPMS [15]. In the Eurozone, from November 1^{st} 2012 all cars must be installed with TPMS as well as all vehicles manufactured after November 1^{st} 2014 [59]. This mandatory regulation has led to a dramatic increasing in TPMS use that is seen as a very large market opportunity. Like many WSNs, TPMS modules are powered by batteries, which constitute one of the largest components in the module. MEMS energy harvesters are viewed as being the possible power solution for TPMSs in the future and thus have been received a lot of attention both academically [6; 7; 15; 60; 61; 62; 63] and from industry [64; 65; 66].

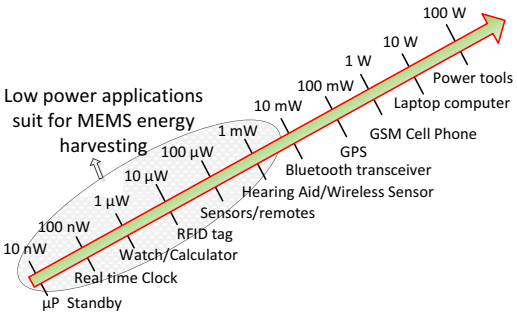

Figure 1.4: Power consumption of wireless sensor nodes (adapted from [5].)

Bridge stress monitoring [67], bridge health monitoring [68] or structural health monitoring [69] are other potential applications. Energy harvesters can be embedded into bridge or structural constructions to power these wireless monitoring sensors. Moreover, wearable sensors, and implantable sensors are other targets of MEMS vibration energy harvesters for applications [29; 30; 70; 71].

1.1.4 Fundamental limitations of vibration energy harvesters

Conventional vibration energy harvesters are usually designed as linear resonance structures [25; 72]. Resonance devices generate maximum power when the resonant frequency of the harvester matches the frequency of ambient vibrations. When a mismatch between excitation frequency and resonant frequency occurs, the output power of the harvester falls significantly. Resonance harvesters are therefore suited only for fixed narrow-band excitations. A frequency of 60 Hz for the magnetic force from the AC electric power field in the United States is an example of a fixed narrow-band excitation for energy harvesters [73; 74; 75].

However, most ambient vibrations such as car-tire vibrations [6], car vibrations [76], compressor base vibrations [37], railway vibrations [8] (Fig. 1.6) have wide frequency spectra or the main frequency peak can vary over time. Therefore, energy harvesters with fixed resonant frequency perform at very low efficiency under ambient vibrations.

An example of the spectrum (log-linear scale) of the tangential vibration of a car tire is shown in Fig. 1.5. The power spectrum density (PSD) of a typical resonance energy harvester with a bandwidth of 2.7 Hz (corresponding to the harvester giving the highest

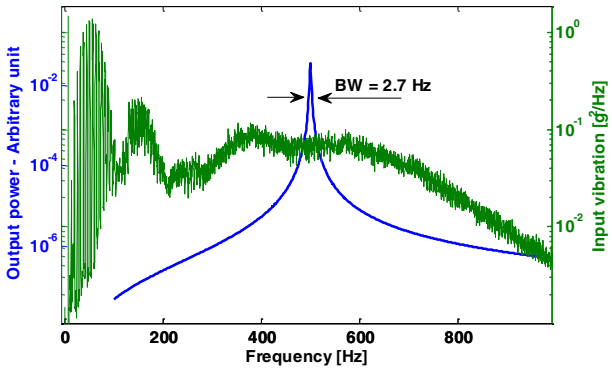

Figure 1.5: Power spectral density (PSD) of car-tire vibrations, measured on the E18 Highway, Norway, at a car speed of 50 km/h [6; 7]. An example of an output PSD of a resonance energy harvester with a bandwidth of 2.7 Hz, a quality factor of 185 and a resonant frequency of 500 Hz.

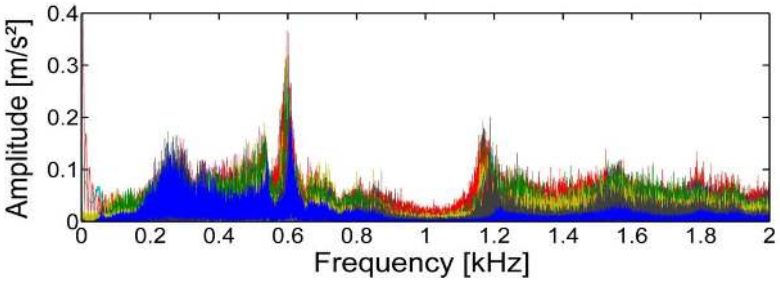

Figure 1.6: Superimposed frequency spectrum of 67 trains in the Arlberg-Tunnel, Germany from Wischke et al. [8]

output power reported in literature so far [63]) and 500-Hz resonant frequency, falling within the signal bandwidth, is also illustrated. It is clear that the resonance harvester is not optimal for this instance. Only vibration frequencies around the harvester's resonance drive it whereas the other frequencies are suppressed. There is a very high spectral weight at about 6 Hz, dominated by the tire revolution at 50 km/h, and many high peaks of comparable magnitude up to 100 Hz. A design of a MEMS energy harvester to operate around one of these peaks is infeasible for two reasons. First, these depend on the speed of the car and therefore vary when the car speeds change. Second, a harvester design at the micro-scale with low resonant frequency, of a few dozen Hertz, is a challenge as it would require a very narrow spring width to customize a low spring stiffness.

The broadband spectral vibration of these environments suggests that:

- it is possible to harvest vibration energy over a wide range of the spectrum; for example, the car-tire vibration spectrum spreads from 300 Hz to 700 Hz whereas the railway vibration spectrum is distributed over from 200 Hz to 600 Hz and 1200 Hz to 2000 Hz.
- the vibration energy harvesters need to have the working frequency range increased to be able to apply these in real vibration environments.

1.2 State-of-the-art methods to improve the working frequency range

There are two possible solutions to increase the working frequency range of energy harvesters: tuning of the resonant frequency and widen the bandwidth [77]. Tuning methods tune the resonant frequency of the energy harvester so that it matches the variable frequency of ambient vibrations. Methods that widen bandwidth broaden the response of the energy harvester to adapt a wideband spectrum of ambient vibrations.

The methods of both kinds of systems can be categorized as either active or passive. Active systems need an external action to modify their operation in response to changing excitation frequency. Active systems can use an external force [78; 79; 80], stiffness modification [81; 82; 83], or mechanical pre-load [84; 85]. However, these methods do not tune the system automatically; some have a low tuning range, while others require extra systems or energy.

In contrast, passive systems do not require user intervention or external energy resources to operate. These are therefore interesting to investigate, in particular for increasing the working frequency range of energy harvesters. One solution for a passive system that works at different frequencies is to use multi-devices as proposed by Sari et al. [86], Shahruz [87], Liu et al [88] or the commercial device developed by MicroGen Systems, Inc. [89]. However, the method has quite a low volume efficiency as there is only one device working at any time for a single tone. Gu and Livermore [90] produced a passive self-tuning energy harvester by using centrifugal force. This method, although very interesting, is only applied for rotational motion.

The Duffing equation describing an oscillator with a cubic nonlinearity is used as an approximate model for numerous nonlinear systems such as mechanical, structural, civil, aeronautical, ocean, electrical, control systems [91; 92]. Duffing oscillator is widely studied in nonlinear dynamics. Nonlinear behavior, e.g. jumps, bifurcations, wider frequency responses for frequency down-sweeps of softening springs or frequency up-sweeps of hardening springs, is observed in the response of nonlinear oscillator systems with a Duffing spring (Fig. 1.7).

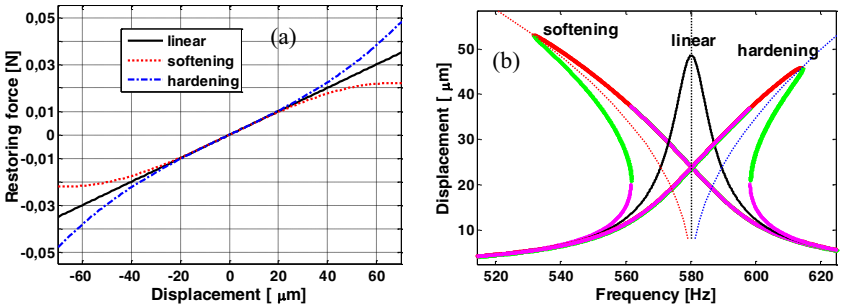

Figure 1.7: An example of nonlinear oscillator system with a Duffing spring. (a) Force-displacement curves for linear spring (zero cubic nonlinearity), softening spring (negative cubic nonlinearity) and hardening spring (positive cubic nonlinearity). (b) Frequency response curves of the displacement for linear, softening and hardening springs.

In the context of energy harvesting, non-linearities of suspensions have been proposed as a promising solution to enlarge the bandwidth. The nonlinear suspensions that have been considered can be classified into three types: hardening, softening and bistable suspensions.

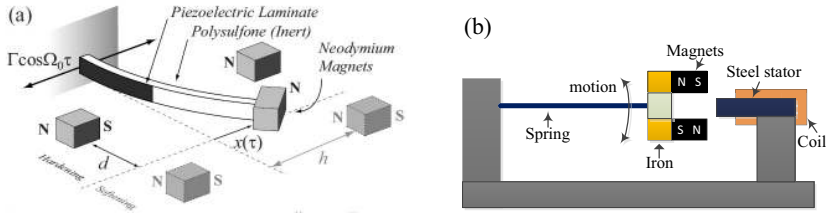

Figure 1.8: (a) Schematic of the proposed nonlinear piezoelectric energy harvester using permanent magnets from Stanton et al. [9]. (b) Nonlinear electromagnetic energy harvester using permanent magnets, adapted from Burrow et al. [10; 11].

Hardening systems were exploited early in the development of vibration mechanical systems by Kao et al. [93] or Soliman [94]. More recently, hardening suspensions are again being proposed for vibration harvesters to widen the bandwidth in many research works [9; 95; 96; 97; 98; 99; 100; 101; 102]. Mechanical end stops [103; 104; 105; 106; 107] give similar behavior as hardening springs.

Hardening suspensions as well as end-stops have the capability to increase harvesting bandwidth rather than power relative to that of tuned linear devices [108]. This is because the hardening suspensions restrict the displacement of the proof mass and therefore limit the output power. In this respect, softening suspensions are more promising because these give larger displacements and potentially higher output power than those with hardening suspensions.

The softening behavior was first introduced by Burrow et al. [10] and later by Stanton et al. [9] where permanent magnets were used (see Fig. 1.8). The Burrow prototype shows both softening and hardening behavior within the same structural system whereas the Stanton harvester shows softening or hardening responses depending on the position of stationary magnets. Not only is this technique shown to increase the bandwidth of the device but experimental results additionally verified the capability to outperform linear resonance harvesters [9].

In a similar approach to using magnets, many symmetric bistable energy harvesters were developed later by a number of other researchers [109; 110; 111; 112; 113; 114; 115; 116; 117]. The bistable harvesters show their performance can outperform the linear device covering a wide bandwidth.

Indeed, following Burrow's design, energy harvesters exhibiting softening, hardening, or bistable behavior can be produced by changing the distance between any number of movable and stationary magnet [116; 117]. However, the presence of the magnets

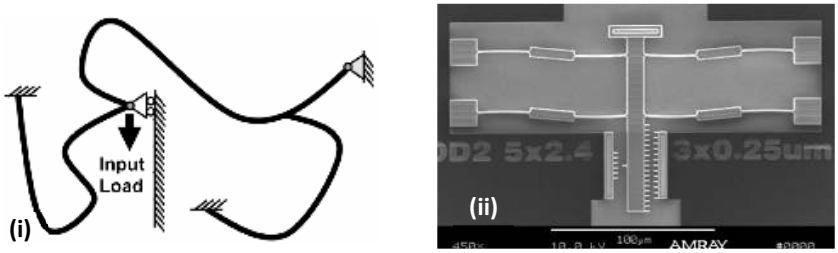

Figure 1.9: (i) A typical spring design generated from the design methodology used in the nonlinear spring synthesis developed by Jutte and Kota [12]. (ii) Asymmetric softening/bistable segmented-springs for actuator applications from Wittwer et al. [13].

can introduce an undesired force on the proof mass of the harvester when placed close to magnetic materials. Conversely, the field from the magnets could affect other nearby electronic devices or magnetic sensors. Moreover, by adding magnets, the fabrication process requires additional material and additional device volume to accommodate two separated magnets.

It would therefore be more interesting and significant to consider other methods to obtain softening or bistable characteristics in suspensions without using permanent magnets. Jutte and Kota [12] presented an approach to develop compliant elements of any prescribed nonlinear stiffness, e.g. asymmetrical softening. However, the spring shapes obtained are often not simple and requires large spaces (see Fig. 1.9-(i)). Segmented-springs have been used to create asymmetrical softening or bistable springs used in many MEMS applications such as switches, relays, shutters, and low-power sensing arrays [13; 118; 119; 120]. The segmented-springs have also been proposed by Ando et al. [121] for MEMS energy harvester to widen the bandwidth. However, an energy harvester with segmented-springs has not been experimentally verified so far.

Another nonlinear spring - a curved spring was proposed and verified by experiments for a long-travel MEMS electrostatic actuator [122; 123]. The curved spring was proposed for MEMS electrostatic energy harvester to widen bandwidth in another work [124] that is related to the work of this thesis.

Table 1.1 summarizes the various approaches in making nonlinear suspensions that have been presented in the literature so far.

Table 1.1: A list of reported methods to create nonlinearities in proof-mass suspensions. EM: Electromagnetic. PZ: Piezoelectric. ES: Electrostatic

Source	Approach	Nonlinearity	Device scale	Transducer
Soliman2008 [125]	End-stops (for beam)	Hardening	Mesoscale	EM
Spreemann2010 [98]	End-stops (for beam)	Hardening	Mesoscale	PZ
Blystad2011 [126]	End-stops (for proof mass)	Hardening	Mesoscale	PZ
Matsumoto2011 [127]	End-stops (for proof mass)	Hardening	MEMS	ES
Liu2011 [105]	End-stops (for proof mass)	Hardening	MEMS	PZ
Marinkovic2009 [128], Marzencki2009 [97], Hajati2011 [99], Marinkovic2012 [101] and Dai2012 [100]	Stretching at large deflections	Hardening	MEMS	PZ
Burrow2007/8 [10; 11]	Magnetic forces	Softening & hardening	Mesoscale	EM
Mann2009 [96]	Magnetic forces	Hardening	Mesoscale	EM
Stanton2009 [9]	Magnetic forces	Hardening	Mesoscale	PZ
Constantinou2012 [102]	Magnetic forces	Hardening	Mesoscale	EM
Gu2010 [90]	Centrifugal force	Hardening	Mesoscale	PZ
Cottone2009 [109]	Magnetic forces	Bi-stable	Mesoscale	PZ
Erturk2009 [129]	Magnetic forces	Bi-stable	Mesoscale	PZ
Ferrari2010 [111]	Magnetic forces	Bi-stable	Mesoscale	PZ
Barton2010 [110]	Magnetic forces	Bi-stable	Mesoscale	PZ
Stanton2009 [9]	Magnetic forces	Softening	Mesoscale	PZ
Ramlan2012 [116] and Tang2012 [117]	Magnetic forces	Softening, hardening & bi-stable	Mesoscale	PZ
Tran2011 [124]	Beam shape	Bistable	MEMS	ES
Ando2012 [121]	Beam shape	Bistable	MEMS	ES

1.3 Hypotheses and investigations of this study

The project aims to overcome the fundamental limitation of resonance vibration energy harvesters, namely, their narrow bandwidths. In real environment, a wide spectrum of vibrational frequencies or varying vibration spectra are commonly found. For better exploitation of broad spectrum vibrations, harvesters with broadband response need to be developed to take advance in potential applications. The underlying hypotheses of this work, its objectives, and definitive scope are given below.

Hypotheses:

We propose nonlinear suspensions, particularly springs with softening and bistable characteristics, to widen the bandwidth of vibration energy harvesters. Spring non-linearities can be obtained without the need to use permanent magnets, simply through geometrical design, a well-suited approach for micro-fabrication.

Nonlinear energy harvesters can have wider bandwidth than that of resonance harvesters without sacrificing harvested power. Especially, the average output power of the nonlinear harvester can be larger than that of a resonance harvester given the same linear stiffness under broadband white noise vibrations.

Moreover, nonlinear harvesters can be more tolerant to variations both in the center frequency and bandwidth of the vibration.

The project investigations

We investigate nonlinear springs with softening and bistable characteristics to widen the bandwidth of MEMS electrostatic energy harvesters. The project objectives include:

1. Characterization of a MEMS electrostatic energy harvester with clamped-guided springs (from a previous Master's thesis [130]) and lumped modeling in SPICE, a general-purpose circuit simulation tool, to understand the nonlinear harvester's response from its nonlinear springs.

2. Design of spring structures to obtain softening characteristic based on a purely geometrical design, lumped modeling of the complete electromechanical system in SPICE using a variety of excitation signals.

3. Design of a prototype of a MEMS electrostatic energy harvester using softening springs. Fabrication of the prototype using bulk micro-fabrication technology.

4. Characterization and analysis of the performance of the harvester prototype under various kinds of excitations, such as sinusoidal excitations, broad band white noise excitations, and colored noise excitations to evaluate the usefulness of the springs operating in the softening regime.

5. Design of a spring geometry to achieve bistable characteristics, modeling and design of a MEMS electrostatic energy harvester working in the bistable regime for possible further improvement of bandwidth and efficiency.

6. Fabrication of bistable-spring harvesters on silicon-on-insulator wafers using bulk micro-fabrication technology, considering also the possibility of embedded electrets.

7. Characterization of the MEMS harvester with bistable springs to verify further bandwidth improvement.

The following aspects fall outside the scope of the current project:

- A whole energy harvester based system including an energy harvester, a power conditioning circuitry, an energy storage device (super capacitors, re-charged batteries or Micro-Energy Cells [5]), and application sensors and wireless electronics. The power conditioning circuitry, the energy storage device, and application wireless electronics are not within the scope of this project.

- We study the MEMS electrostatic harvesters operating in continuous mode, not in switched mode [49]. The output port is connected to a load resistor.

- Electrostatic harvesters require a bias to work. We consider the bias outside scope of this project, and use external bias voltages as simulated electrets or external bias.

1.4 Outline of the thesis

This thesis is based on a collection of manuscript and published papers including five journal papers [131; 132; 133; 134; 135] and three conference papers [136; 137; 138]. Chapter 2 contains the highlights of the results presented in the manuscript and published papers. Chapter 3 includes conclusions and outlook. Perspectives for future work follow at the end of Chapter 3. The manuscript and published papers are attached in the final part of this thesis after the list of publications.

Chapter 2

Summary

This chapter will highlight the main results presented in five journal articles, referred as Paper 1 [131], Paper 4 [132], Paper 5 [133], Paper 6 [134] and Paper 8 [135] and three conference papers, referred as Paper 2 [137], Paper 3 [136] and Paper 7 [138]. The order of this chapter follows the order of the papers which presents the logical progression of the research works.

2.1 Nonlinear behaviors of MEMS electrostatic energy harvester with clamped-guided springs

The first harvester prototype was designed in a previous master project [130] and fabricated in multiproject wafer foundry (from Tronics Microsystems S.A.). Fabrication involved deep-reactive ion etching (DRIE) of a silicon-on-insulator (SOI) wafer with 60-μm-thick device layer. The proof mass is suspended by a quad straight-spring that makes each spring as a clamped-guided support. A schematic drawing of the device and a scanning electron microscope (SEM) image of the spring are shown in Fig. 2.1-i and -ii, respectively.

From frequency up- and down-sweeps, the measured output voltage from the harvesters (Fig. 2.2-i) displays both softening and hardening behaviors. The nonlinearities are also observed when the device is driven by white noise vibrations (Fig. 2.2-ii).

The SPICE simulations with nonlinear springs displaying both spring softening and hardening (Fig. 2.3-i) verify that the nonlinear behaviors are due to

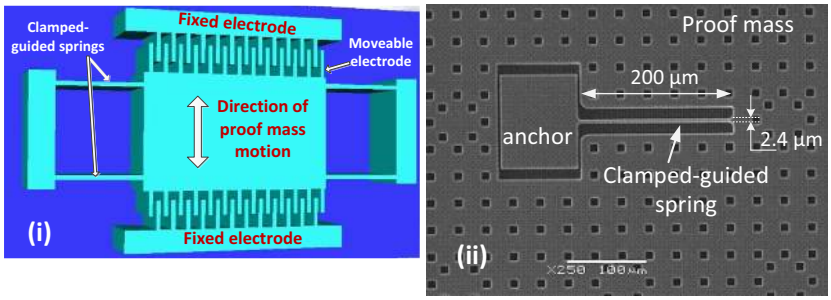

Figure 2.1: (i) Schematic drawing of the MEMS electrostatic energy harvester. (ii) SEM image of a straight spring (Photo: Tronics Microsystems S.A.).

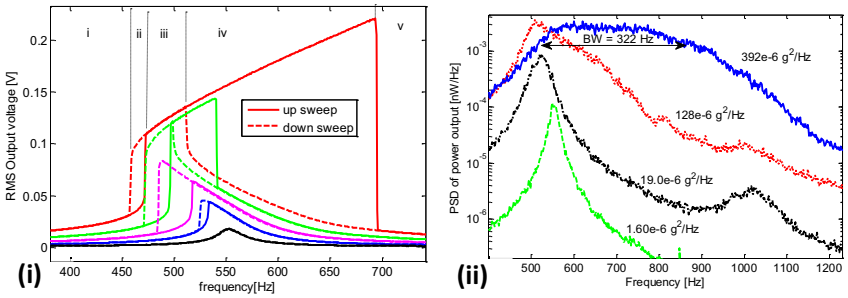

Figure 2.2: (i) Measured output voltage from frequency up- and down-sweeps with increasing RMS acceleration amplitudes, 0.010, 0.025, 0.055, 0.100, and 0.160 g (from lower to upper curve). (ii) Power spectral density (PSD) of output voltage under white noise vibrations.

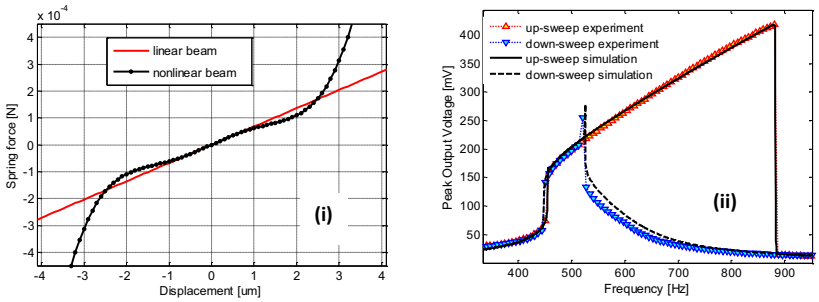

Figure 2.3: (i) Spring force-displacement curve is used in SPICE model for fitting the measured results. (ii) The fitting of SPICE simulations and experiments for frequency up- and down-sweeps at RMS acceleration amplitude of 0.21 g.

the springs (Fig. 2.3-ii). For clamped-guided springs, large displacements must produce tensile stresses in the springs and consequently the hardening behavior. The appearance of the softening behavior can be explained from the pre-stresses occurring in during fabrication. These pre-stresses could originate from packaging process and/or compressive residual stresses in the SOI wafers. Moreover, the device mounting onto PCB test boards and subsequent onto a shaker for testing can generate pre-stresses.

Spring softening enlarges the bandwidth of the energy harvester particularly in the lower frequency range whereas hardening widens the bandwidth at the higher frequencies. The experimental results suggest that bandwidths can be enhanced by both spring softening and hardening. Moreover, investigating the geometrical design of springs is another interesting way to obtain spring nonlinearities without relying on beam pre-stress.

These results are presented in the Paper 1.

2.2 Softening springs or hardening springs

While both spring softening and hardening characteristics augment bandwidth of energy harvesters, softening springs offer greater potential as these give larger displacements that hardening springs and hence potentially give higher output power, especially when the harvesters are driven by white noise vibrations. To

support this conclusion, we analyzed the three spring types: linear, softening, and hardening. Force-displacement curves are given in Fig. 2.4. The performance of the energy harvester suspended by each of these springs is calculated using the SPICE simulation tool.

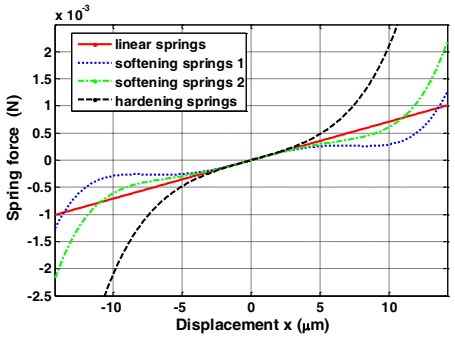

Figure 2.4: Force-displacement curves for linear, softening, and hardening springs. The softening springs 1 is more compliant than the softening springs 2.

Curves for the average output power vs. load resistance under white noise accelerations of $3.0\times\ 10^{-4}\ g^2/Hz$ for the different spring types are shown in Fig. 2.5-i. Similarly, the power spectral densities (PSDs) of output voltage at $2.8\times\ 10^{-4}\ g^2/Hz$ white noise acceleration are shown in Fig. 2.5-ii. We conclude that:

- Output power: greater output power yields are obtained from the harvesters with softening springs than those with linear springs and hardening springs.
- Bandwidth: both softening and hardening springs give larger bandwidth than linear springs but the most compliant springs, i.e. those corresponding to curve softening springs 1, give the largest bandwidth.

These numerical results suggest that softening springs are better disposed to provide enhancements to bandwidth of energy harvesters under white noise vibrations. Such harvesters not only extract energy over wider bandwidths but also yield higher output power than those with linear springs and hardening springs. For this reason, softening springs are of interest for further investigation.

These results are presented in the Paper 2.

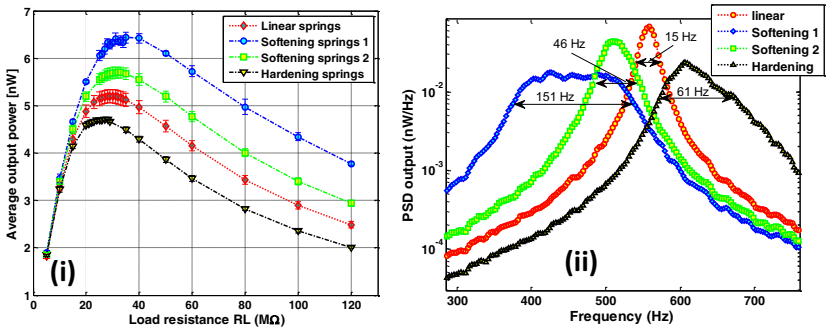

Figure 2.5: SPICE simulations. (i) Average output power vs. load resistance for the spring types under white noise excitation with a level of $3.0\times\ 10^{-4}\ g^2/Hz$. (ii) Power spectral density of the output voltage for the spring types from white noise with a level of $2.8\times10^{-4}\ g^2/Hz$.

2.3 Design of softening springs

Leland et al. [84] and Lesieutre et al. [139] introduced the ideal of using a compressive axial preload to reduce the stiffness of piezoelectric bimorph vibration energy harvester to tune the resonant frequency [84] or increasing the coupling coefficient [139]. Preloading is implemented by applying external forces to both two ends of the cantilever. However, the method does not automatically tune the resonance vibration of the cantilever and requires external action to adjust the preloading force.

As mentioned in the introduction, a spring with any prescribed asymmetric nonlinear load-displacement can be produced using the synthesis methodology devised by Jutte and Kota [12]. However, typical spring configurations that have been generated are usually complex and occupy large space.

Here, we will instead restrict our attention to simple, parametrized spaces of spring shapes to generate asymmetric spring softening. In particular, we design a spring configuration so that the axial compressive force automatically appears as the proof mass moves. The axial compressive force will make the springs become softer and therefore develop spring softening.

To obtain axial compressive force during displacement, the spring configuration is designed so that its length tends to shorten. The simplest design is to use

a straight spring but instead of having a horizontal layout as shown in Fig 2.6-i, the spring is inclined at an angle of α (Fig. 2.6-ii). The proof mass is usually suspended by a quad spring, so each spring has a clamped-guided support. The spring force-displacement curves of these springs, calculated by the finite element method (FEM), are shown in Fig. 2.6. The axial force of them is showed in Fig. 2.7.

The clamped-guided straight spring has a linear stiffness associated with the small axial force over displacements within about 1% of its length. With larger displacements, the axial force is always compressive (Fig. 2.7) and yields hardening. Hence, hardening springs are easily implemented.

From Fig. 2.6-ii, the inclined spring is linear for small displacements; for larger displacements in the positive direction, the spring exhibits hardening owing to the axial tensile force (Fig. 2.7). For large displacements in the negative direction, the spring ehxibits softening in the regime where the axial force is compressive. Therefore, asymmetric spring softening can be attained using inclined springs. Whereas the proof mass moves less in the hardening spring regime, in the softening regime it is much more. The mean position therefore corresponds to the softening spring regime and in consequence, the overall behavior is described as softening.

2.4 MEMS energy harvester with angled springs

Softening spring behavior can be obtained with inclined springs. As shown in Fig. 2.6-ii, the linear stiffness for small displacement of the inclined spring dramatically increases with increasing inclined angle α and therefore increasing resonant frequency of the harvester. To reduce variations in the linear stiffness when varying the inclined angle α, one more beam segment is added to the inclined spring; the spring is referred as an angled spring. A schematic drawing of the angled spring and its dimensions are shown in Fig. 2.8-i and the spring force-displacement curve calculated by FEM is shown in Fig. 2.8-ii. (*Paper 3*).

We developed a fabrication process specifically targeted toward prototyping MEMS energy harvester with the angled springs and high-aspect-ratio electrode gaps formed by full-wafer-thickness DRIE of a silicon wafer. Methods to protect the angled springs during fabrication using dummy protective structures and

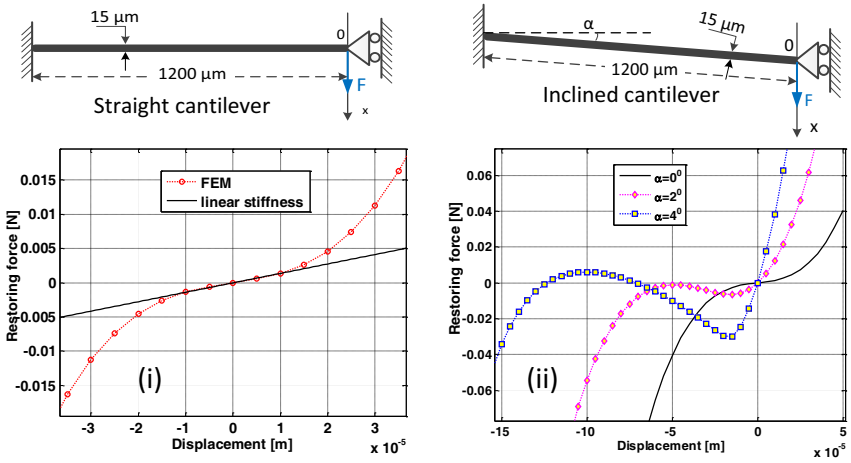

Figure 2.6: Force-displacement curves for (i) the straight cantilever and (ii) the inclined cantilever, calculated by the finite element method (FEM).

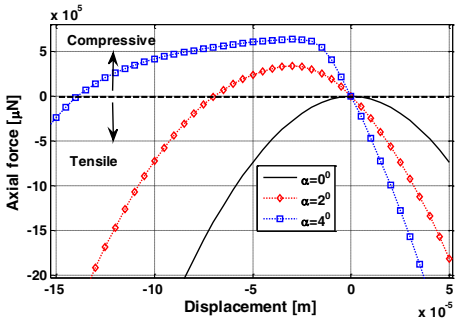

Figure 2.7: Axial force-displacement curves for various inclinations calculated by FEM. The positive values indicate axial compressive forces and the negative values indicate axial tensile forces.

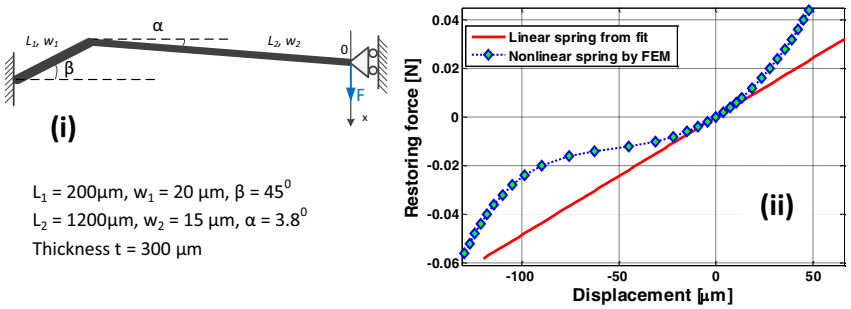

Figure 2.8: (i) Schematic drawing and dimensions of an angled spring. (ii) Spring force-displacement curve, calculated using FEM.

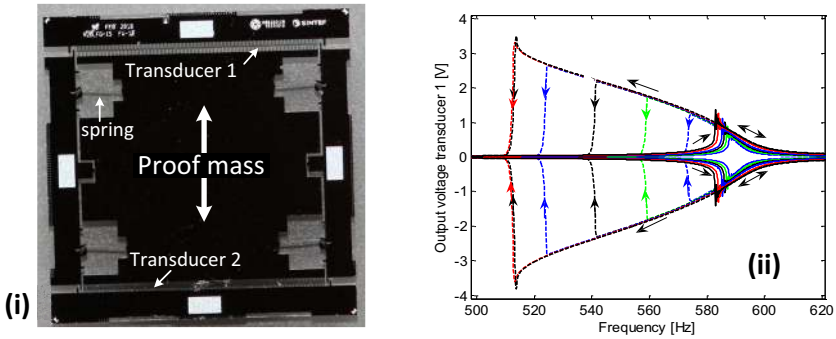

Figure 2.9: (i) MEMS electrostatic energy harvester with angled springs after fabrication. (ii) Measured frequency-response curves of the harvester under various frequency sweeps (directions are indicated by arrows). Peak acceleration amplitudes are 0.062, 0.088, 0.110, 0.135, 0.158 and 0.183 g (from lower to upper curve).

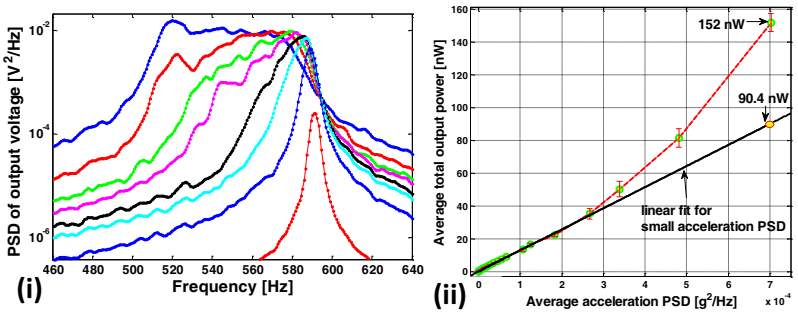

Figure 2.10: (i) Output spectrum of the harvester under white noise accelerations at various levels from 1.5×10^{-6} g^2/Hz to 7×10^{-4} g^2/Hz. (ii) Average output power vs. PSD of acceleration.

sacrificial structures are presented in *Paper 4* [132] and *Paper 6* [134]. The produced device is pictured in Fig. 2.9-i.

As seen in Fig. 2.9-ii, the harvester with angled springs displays softening spring effect including widened bandwidths for frequency down-sweeps.

The PSD of output voltage under white noise excitations is shown in Fig. 2.10-i. When vibrations increase, softening behavior, i.e. broadening of the bandwidth towards the lower frequency, can be observed to develop gradually. At vibration level of 7×10^{-4} g^2/Hz, the output spectrum is quite flat over a wide frequency range. This corresponds to a bandwidth of about 60.2 Hz, which is more than 13 times wider than the bandwidth at the lowest level. Hence, the nonlinear-spring design provides a wide bandwidth for sufficiently strong vibrations.

The average output power vs. acceleration PSD is shown in Fig. 2.10-ii. The energy harvester using angled springs is found to achieve 68% more power (151.9 nW and 90.4 nW) than a linear energy harvester for the broadband excitation of 7×10^{-4} g^2/Hz.

The experimental results verify that the harvester with softening springs not only widens bandwidth as would be expected, but also harvests more output power than a linear energy harvester for sufficiently strong broadband random vibrations. *The results are presented in Paper 4.*

Compare with a linear spring harvester, the angled-spring harvester also performs better under band-limited random vibrations over a range of vibration

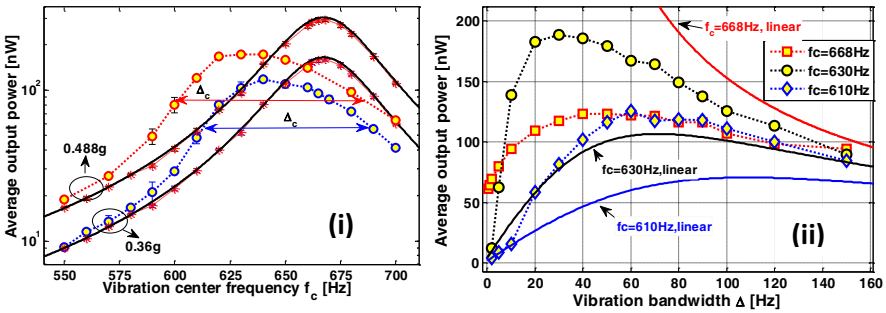

Figure 2.11: (i) Average output power vs. vibration center frequency, the vibration bandwidth of 50 Hz, the RMS acceleration amplitude of 0.360 g and 0.488 g. Dotted curves with circles : experiments. Dash-dot curves with asterisks: SPICE simulations. Solid curves: analytical calculation.(ii) Average output power vs. vibration bandwidth for different vibration center frequencies.

bandwidths and center frequencies. From Fig. 2.11-i, for random vibrations with a bandwidth of 50 Hz and varying center frequencies, the maximum output power of the nonlinear-spring harvester is seen to be 1.7 times lower than that of a linear-spring harvester but the 1-dB bandwidth is two times larger. For vibration center frequencies of 38 Hz and 58 Hz below the resonance frequency, the nonlinear-spring harvester always extracts more power than its linear-spring counterpart regardless of the vibration bandwidth (Fig. 2.11-ii). Therefore, the nonlinear spring design provides a device that also has considerably higher tolerance towards vibration bandwidth variations. *The results are presented in Papers 5 and 6.*

2.5 MEMS energy harvester with curved springs

The energy harvester with angled beams operates over a considerably wider bandwidth, i.e. 60 Hz around 550 Hz (see Fig. 2.10-i) representing relatively about 11% of the resonant frequency. With real-world vibration spectra in mind, for example the vibration from a car tire or train railway as shown in Figs. 1.6 and 1.5, it is interesting to see if this can be further improved.

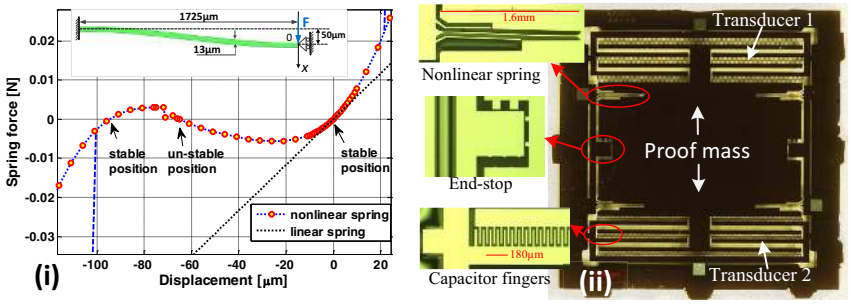

Figure 2.12: (i) Restoring force vs. displacement for the curved springs, calculated using FEM. (ii) MEMS electrostatic energy harvester with curved springs after fabrication.

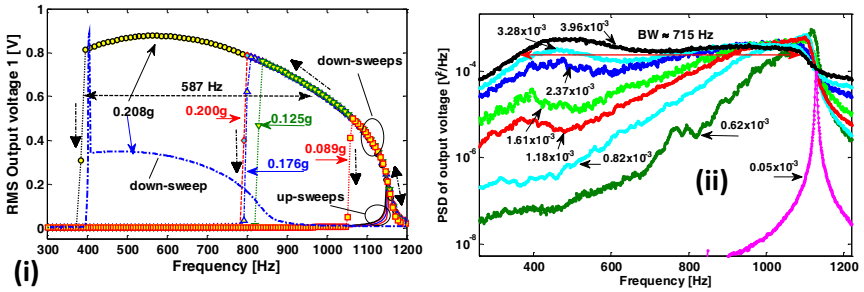

Figure 2.13: (i) Measured frequency-response curve under frequency up- and down-sweeps. (ii) Output power spectral density under white noise vibrations.

An curved spring was proposed and experimentally analyzed for use in a long-travel MEMS electrostatic actuator [122; 123]. We investigate a similar spring for use in a MEMS electrostatic energy harvester. Here, we designed the spring so that it has asymmetric bistable characteristic. The shape and dimensions of the curved spring are shown in the inset of Fig. 2.12-i.

A MEMS electrostatic energy harvester with curved springs (in Fig. 2.12-ii) was fabricated on an SOI wafer using bulk micro-fabrication technology. The side-walls of the capacitor fingers are oxidized to potentially allow for electret biasing. (*Paper 7*)

2. SUMMARY

The harvester's response under frequency sweeps at very small acceleration, where the proof mass moves in the linear spring regime, shows that the 3-dB bandwidth is about 2.8 Hz. For frequency down-sweep with larger acceleration (Fig. 2.13-i), the harvester 3-dB bandwidth of 578 Hz is achieved at a constant amplitude of 0.208 g.

For white noise excitation at a level of $4{\times}10^{-3}\ g^2/Hz$, the bandwidth reaches about 715 Hz, which is more than 250 times wider compared with that for the linear-spring regime.

Table 2.1 shows a comparison of the measured 3-dB bandwidths of some wideband energy harvesters presented in the literature against that obtained for the wideband device developed for this project.

The MEMS energy harvester with the curved springs attained the largest 3-dB bandwidth of 715 Hz, which is 10 times wider than the widest bandwidth reported so far, and the second largest normalized bandwidth of nearly 1. It is noted that the bandwidth in ref. [101], i.e. $BW = 70$ Hz and $NFB = 1.27$, were obtained from mechanical end-stops. The displacement as well as the output power are limited, almost flat at a small output power of 6 nW for a high sinusoidal amplitude with 3.2 g, to achieve a wideband response. (*The results are presented in Paper 8*)

Table 2.1: Comparison of the measured normalized bandwidth of some wideband energy harvesters (a: the rms acceleration, BW: 3-dB bandwidth, f_c: the central frequency of 3-dB bandwidth, NFB = BW/f_c: normalized frequency 3-dB bandwidth)

Ref.	Approach	Non-linearity	Device scale	a (g)	BW (Hz)	f_c (Hz)	NFB
Soliman08[125]	End-stops	Hardening	macro	0.1	5	96.5	0.05
Stanton09[9]	Magnetic forces (MF)	Softening	macro	0.3	3	12.1	0.25
Erturk09[129]	MF	Bistable	macro	0.35	1.5	7.25	0.21
Arrieta10[140]	MF	Bistable	macro	2	4.5	11.5	0.39
Ferrari10[111]	MF	Bistable	macro	0.3	7	14.5	0.48
Galchev11[141]	MF	–	macro	1	16	30	0.53
Matsumoto11[127]	End-stops	Hardening	MEMS	1.4	14	33	0.42
Marinkovic12[101]	End-stops	Hardening	MEMS	3.2	70	55	1.27
Liu11[105]	End-stops	Hardening	MEMS	1	17	36	0.47
Dai12[100]	Stretching	Hardening	MEMS	0.8	12	186	0.07
Wischke10[142]	MF & bias	Tuning frequency	macro	0.7	65	298	0.22
Ramlan12[116]	Magnetic forces (MF)	Bistable	macro	3	13	34.5	0.38
Angled springs	Beam shape	Softening	MEMS	$7e^{-4}$ g^2/Hz	60	543	0.11
Curved springs	Beam shape	Bistable	MEMS	$4e^{-3}$ g^2/Hz	**715**	730	0.98

Chapter 3

Conclusion and outlook

The project investigated on spring softening and bistable characteristics with the objective of widening the bandwidth of MEMS vibration energy harvesters. We successfully designed, modeled, and fabricated wideband MEMS electrostatic energy harvesters with softening springs and bistable springs. The nonlinear characteristics of the springs are obtained through geometrical design, a well-suited approach for micro-fabrication technology, without the need to use permanent magnets.

The experimental results for the harvester with angled springs operating in the softening regime showed that the bandwidth increases by more than 13-fold and the average output power increased by 68% compared with that of a resonance harvester with the same linear stiffness at a broadband random vibration of 7×10^{-4} g^2/Hz. Experiments with varying bandwidth and center frequency of vibration have shown that the softening-spring harvester gives an indication of the robustness towards variation in the vibration spectrum. The MEMS harvester of less than 1 cm^2 collected an average power of about 1 μW at 180 V, corresponding to an efficiency of 92% for a white noise excitation of 7.29×10^{-4} g^2/Hz. An output power of 7 μW was achieved for a similar device at 120-V bias and a frequency down-sweep at 0.36 g, corresponding to a power density of 536 μW/cm^3

Wideband MEMS electrostatic energy harvesters with bistable springs were fabricated on a silicon-on-insulator wafer using bulk micro-fabrication technology. The experimental results of this bistable-configured harvester showed the

bandwidth was much improved compared with that of the softening-configured harvester. Under white noise excitation at a level of 4×10^{-3} g^2/Hz, the harvester attained the largest bandwidth of 715 Hz compared with that of wideband harvesters reported in the literature so far.

Such wideband MEMS energy harvesters are well-suited to extract power from a wide spectrum of vibrations or from sources with a wide range of variability in the spectrum such as in car tires and railways.

Although the MEMS energy harvesters in both softening and bistable configuration demonstrate wide bandwidth responses, showing a dramatic enhancement in bandwidth compared with that of resonance harvesters, these still have their limitations.

The hysteresis in the frequency-sweeps response is the main difficultly. Harvesters with angled springs and curved springs display wideband response to only the frequency down-sweeps. For the up-sweeps, these display narrow bandwidths and respond with low-output power traces in the hysteresis regime. A proposal from Sebald et al. [143] to overcome this limitation is to use a fast burst perturbation to control the jump from the lower trace jump to the higher trace.

Another limitation of the nonlinear harvester is the requirement of sufficiently large white noise vibrations to provide a wideband response. The devices are unable to produce wide bandwidth response in low amplitude vibration environments. Thus these are more suited to strong ambient vibration conditions.

A fracture of the angled springs is a further limitation. These springs reach failure stresses before impacting their mechanical end tops. Many angled springs were broken during fabrication. The fabrication yield of bistable springs is much better. The fracture of the springs can be avoided by design or using high-yield-strain parylene for the springs, as suggested by Suzuki et al. [58].

There are some interesting ideas that can be further investigated to construct better bistable-configured energy harvesters.

The first idea involves charging the dielectric on the capacitor sidewall to make electrets that bias the device. Charging methods that can use include traditional Corona dis-charging, soft X-ray [45] or ionic charging with ionic hair-dryers [44].

A second idea to explore the use of power conditioning circuitry, storage device, application sensors and wireless electronics to build an entire vibration-based energy harvester. The ultra low-power ZL70250 Transceiver is a good candidate for wireless communication.

Wideband MEMS energy harvester for Tire Pressure Monitoring Systems (TPMS) applications is an interesting topic to investigate. As shown in Appendix B, the experimental results for the bistable-spring harvester subject to real car-tire vibrations show that the harvester is suitable because the harvester responds over a wide bandwidth for a wide spectrum of car-tire vibrations. However, the efficiency of the harvester needs to be improved because the resonance of the current design is outside the vibration spectra. Increasing the variable capacitance by designing longer traveling of the proof mass and/or the number capacitor fingers need also to be considered. Packaging the harvester die with embedded electrets remains a challenge and needs more study .

Chapter 4

List of publications enclosed in the thesis

[*Paper 1*] L. G. W. Tvedt, S. D. Nguyen, and E. Halvorsen, "Nonlinear behavior of an electrostatic energy harvester under wide- and narrowband excitation," *IEEE/ASME Journal of Microelectromechanical Systems*, vol. **19**, no. 2, pp. 305-316, Apr 2010.

[*Paper 2*] S. D. Nguyen and E. Halvorsen, "Analysis of vibration energy harvesters utilizing a variety of nonlinear springs, " *Proceedings of PowerMEMS 2010* (Leuven, Belgium, Nov 30 Dec 3), pp.331-334, 2010.

[*Paper 3*] S. D. Nguyen and E. Halvorsen, "Wideband energy harvester utilizing nonlinear springs," *Proceedings PowerMEMS 2009* (Washington D.C., USA, Dec 1-4, 2009) pp.411-414, 2009.

[*Paper 4*] S. D. Nguyen, E. Halvorsen, G. U. Jensen and A. Vogl, "Fabrication and characterization of a wideband MEMS energy harvester utilizing nonlinear springs," *Journal of Micromechanics and Microengineering*, vol. **20**, no. 12, p. 125009 (11p), Dec 2010.

[*Paper 5*] S. D. Nguyen and E. Halvorsen, "Nonlinear springs for bandwidth-tolerant vibration energy harvesting," *IEEE/ASME Journal of Microelectrome-*

chanical Systems, vol. **20**, no. 6, pp.1225-1227, Dec 2011.

[*Paper 6*] S. D. Nguyen, E. Halvorsen and G. U. Jensen, "Wideband MEMS energy harvester driven by colored noise," **submitted to** *IEEE/ASME Journal of Microelectromechanical Systems*, Nov 2012.

[*Paper 7*] S. D. Nguyen, N. H. T. Tran, E. Halvorsen and I. Paprotny, "Design and fabrication of MEMS electrostatic energy harvester with nonlinear springs and vertical sidewall electrets," *Proceedings of PowerMEMS 2011* (Seoul, Korea, Nov 15-18 2011), pp.126-129, 2011.

[*Paper 8*] S. D. Nguyen, E. Halvorsen and I. Paprotny, "Bistable springs for wideband MEMS energy harvesters," vol. **102**, no. 02, *Applied Physics Letters*, p. 023904, Jan 2013.

Paper No. 1

Tvedt2010 JMEMS, Journal Article

Title: “Nonlinear Behavior of an Electrostatic Energy Harvester Under Wide- and Narrowband Excitation”.

Authors: Lars Geir Whist Tvedt, Duy Son Nguyen, and Einar Halvorsen.

Journal: *EEE/ASME Journal of Microelectromechanical Systems.*

Volume: 19**, Issue:** 2**, page(s):** 305 – 316

Date of Publication: April 2010

Times Cited: 14 (from Web of Science, to Jan 2013)

Paper No. 2

Nguyen2010b PowerMEMS, Conference paper

Title: "Analysis of vibration energy harvesters utilizing a variety of nonlinear springs".

Authors: Son Duy Nguyen and Einar Halvorsen.

Proceedings of: *PowerMEMS 2010*

Page: 331 - 334

Date: Nov 30 – Dec 3

Place: Leuven, Belgium.

ANALYSIS OF VIBRATION ENERGY HARVESTERS UTILIZING A VARIETY OF NONLINEAR SPRINGS

Duy S. Nguyen* and Einar Halvorsen
Department of Micro and Nano Systems Technology, Vestfold University College, Norway
*Presenting Author: duy.s.nguyen@hive.no

Abstract: This paper reports a numerical investigation of the potential benefits of utilizing softening springs in comparison to linear springs and hardening springs for vibration energy harvesters. Our results show that the energy harvester using softening springs is better than the energy harvester using linear springs or hardening springs for broadband random vibrations. This is due to its potential to give both wider bandwidth and larger harvested power.

Keywords: MEMS, energy harvester, nonlinear systems, softening springs, hardening springs.

INTRODUCTION

Energy harvesting from motion is promising as means to power wireless sensor nodes in constructions, machinery and on the human body [1].

Most vibration-based energy harvesters are spring-mass-damper systems which generate maximum power when the resonant frequency of the device matches the frequency of the ambient vibration. As many environmental vibration spectra exhibit a range of frequencies [2], resonant vibration energy harvesters will have restricted applicability in these environments. Nonlinear stiffness has been exploited to increase the bandwidth of the energy harvesters to overcome this limitation [3]. Nonlinear stiffness could be a hardening spring [4] and/or a softening spring [5-6]. Nevertheless, comparisons of the potential benefits of using linear springs, softening springs and hardening springs for vibration energy harvesters have not yet been reported, in particular when the devices are driven by broadband random vibrations. In this paper, we report a numerical investigation of potential benefits of utilizing softening springs in comparison to linear springs and hardening springs for vibration energy harvesters.

MODELING ANALYSIS

The equations of motion for a resonant energy harvester with a linear electromechanical transducer can be written:

$$m\ddot{x} = -F_{sp}(x) - \alpha q - b\dot{x} + ma \qquad (1)$$

$$-R\dot{q} = V = \alpha x + \frac{1}{C}q \qquad (2)$$

where m is the proof mass, x its displacement, $F_{sp}(x)$ the spring force, q the charge, b the damping coefficient, a the negative of the package acceleration, R the load resistance, C the clamped capacitance and α coefficient determining the linear electromechanical coupling.

We consider a phenomenological spring force on the form:

$$F_{sp}(x) = k_1 x + k_3 x^3 + k_5 x^5 \qquad (3)$$

The term $k_1 x$ is the linear part of the force and the term $(k_3 x^3 + k_5 x^5)$ models the nonlinear part. The linear stiffness k_1 is kept constant. The positive constant k_5 represents nonlinear spring stiffness at large deflections. The k_3 is changed to have different nonlinear stiffness for intermediate deflections: hardening springs or softening springs as shown in Figure 1.

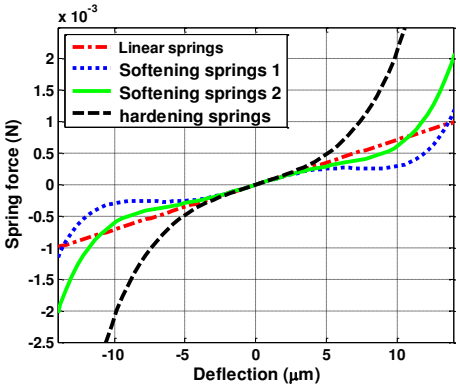

Figure 1: Spring force versus deflection for different springs: linear springs, softening springs 1, softening springs 2 (less soften than variety 1) and hardening springs.

Figure 2 shows the equivalent circuit for an energy harvester represented by the equations of motion (1) and (2). The selected parameters (table 1) are close to the dimension of the MEMS electrostatic energy harvester in [3].

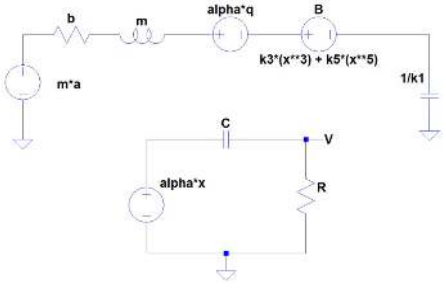

Figure 2: The equivalent circuit for the energy harvesters

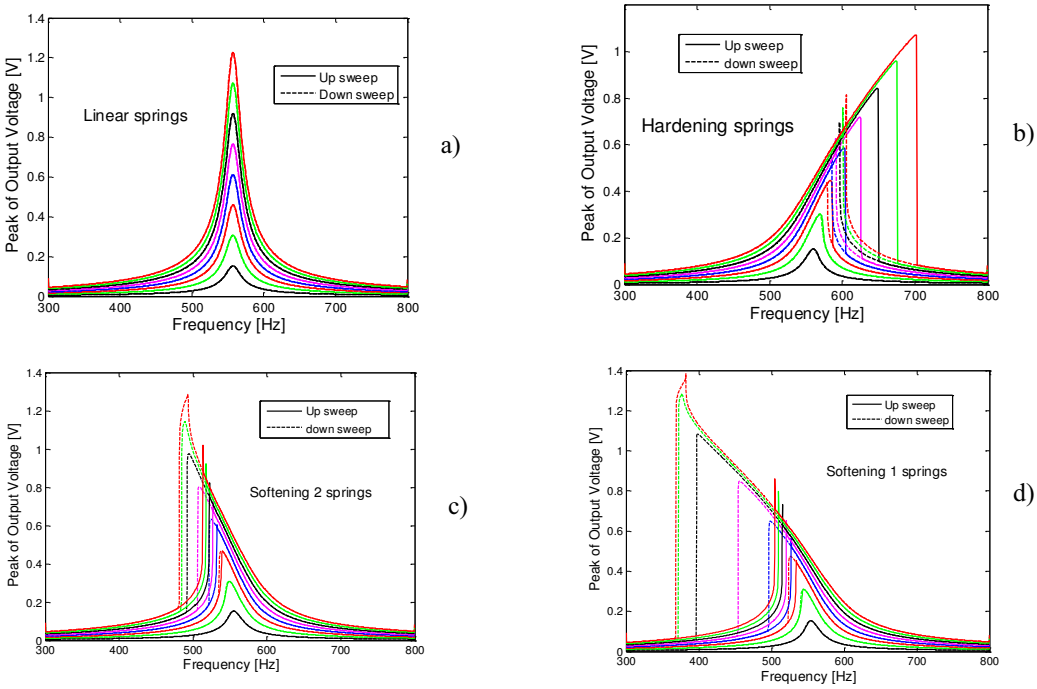

Figure 3: The frequency response for frequency sweeps at different peak excitation amplitudes of 0.05 g, 0.10 g, 0.15g, 0.20 g, 0.25 g, 0.30 g, 0.35 g and 0.40 g. a) linear springs b) hardening springs c) softening spring 2 d) softening springs 1

TABLE I. MODEL PARAMETERS

Symbol	Description	Value
m	Proof mass	5.76 mg
b	Mechanical damping	$7 \cdot 10^{-4}$ Ns/m
k_1	Linear stiffness	71 N/m
	Softening nonlinear stiffness 1	$-0.92 \cdot 10^{12}$ N/m^3
k_3	Softening nonlinear stiffness 2	$-0.6 \cdot 10^{12}$ N/m^3
	Hardening nonlinear stiffness	$0.9 \cdot 10^{12}$ N/m^3
k_5	Nonlinear stiffness	$5 \cdot 10^{21}$ N/m^5
C	Transducer capacitance	9.8 pF
α	A linear electromechanical coupling constant	$-1.84 \cdot 10^{5}$ V/m

RESULTS AND DISCUSION

Sinusoidal excitations

Figure 3 shows the output voltage of the energy harvester as a function of frequency for frequency up-sweeps and down-sweeps at different excitation amplitudes. For the linear springs, the resonance frequency does not change with increasing excitation amplitudes. Moreover, the output voltages of frequency up-sweeps and down-sweeps are identical (Fig. 3-a). For the nonlinear springs, the output voltage curves are the same as for the linear springs when the excitation amplitude is small, e.g. 0.05 g. When excitation amplitudes get larger so that the spring nonlinearity is pronounced, the resonant frequency is shifted toward higher frequency for hardening springs (Fig. 3-b) and to lower frequency for softening springs (Fig. 3-c, d). Consequently, the bandwidth of hardening springs is wider for frequency up-sweeps while the bandwidth of softening springs is wider for frequency down-sweeps. In addition, in comparing the two softening springs, the softening springs 1 obtain wider bandwidth than the softening springs 2 do.

White noise excitations

Figure 4 shows the average output power as a function of load resistance under broadband excitation at level of 3.0×10^{-4} g^2/Hz. When the load resistance is very small ($R \to 0$), the current i through it will be approximately the short circuit current, $i = \alpha C \dot{x}$, the system can be described by a nonlinear second order model whose reduced probability distribution of the velocity is independent of the mechanical nonlinearities and therefore gives the same output power for all types of springs [7]. The equations of motion (1) and (2) will then agree with [8] and it is understandable that no benefit of nonlinearities was found in that work. In our simulations, we see that the average output power is almost the same for different springs for small load resistances. When increasing the load resistance, the nonlinearity in the stiffness clearly affects the average

output power.

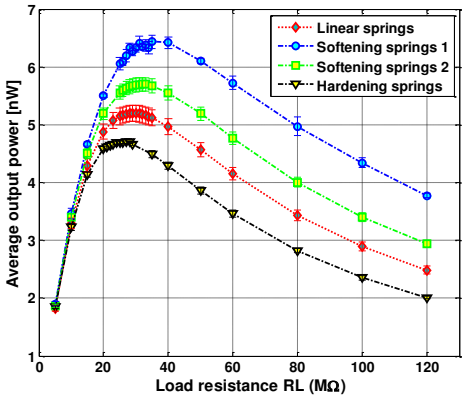

Figure 4: Average output power as a function of load resistance under broadband excitation at level of 3.0×10^{-4} g^2/Hz. The optimal loads are 25 MΩ, 29 MΩ, 32 MΩ and 35 MΩ for hardening springs, linear springs, softening springs 2 and softening springs 1, respectively.

Firstly, the optimal load resistance is slightly different for different springs. From [7], we know that the optimal load resistance for the linear spring harvester under the white noise excitation is given by ($R_{opt} = 1/\omega_0 C$) which is the same for all cases considered here. In Figure 4, we see that the most compliant springs, e.g. softening springs 1, have the largest optimal load resistance value (*35 MΩ*) while the hardening springs have the lowest optimal load resistance value (*25 MΩ*).

Secondly, the softening springs 1 obtain the highest average output power at the optimal load resistance while the hardening springs give the lowest average output power. That is still true if we compare the two cases for any choice of the same load resistance.

Figure 5 shows the output power spectral density (PSD) of different springs for various white noise excitation levels. When the white noise excitation level is small, e.g. 0.46×10^{-4} g^2/Hz, the output PSD is almost the same for different springs. Nevertheless, when excitations get larger, the nonlinearities in stiffness provide an enhanced bandwidth of the harvester. The hardening springs increase the bandwidth towards higher frequencies (Fig. 5-b) while the softening springs increase the bandwidth towards lower frequencies (Fig 5-c, d).

To compare the bandwidth for different springs, the output PSDs for different springs at the white noise excitation level of 2.8×10^{-4} g^2/Hz are shown together in Figure 6. At this excitation level, the 3-dB bandwidth of the softening springs 1 increase by about 2.5 and 10 times compared to the bandwidth of the hardening

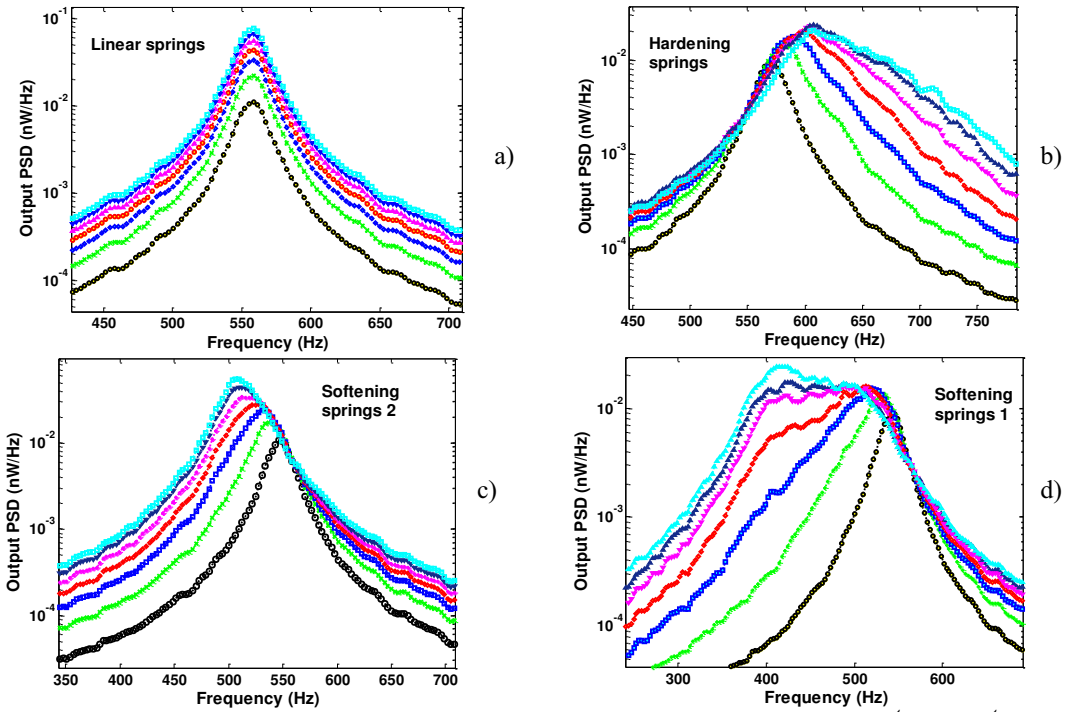

Figure 5: Output PSD as a function of frequency for many broadband excitation levels: 0.46×10^{-4}, 0.92×10^{-4}, 1.4×10^{-4}, 1.8×10^{-4}, 2.3×10^{-4}, 2.8×10^{-4}, 3.2×10^{-4} g^2/Hz. a) linear springs b) hardening springs c) softening spring 2 d) softening springs 1.

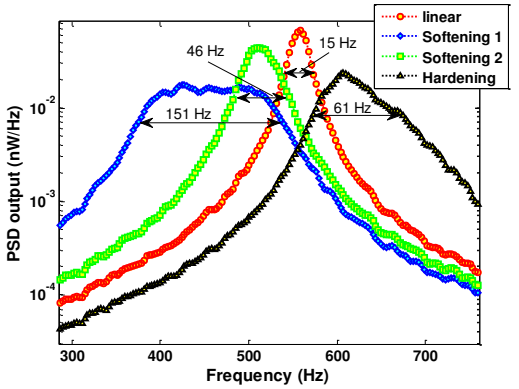

Figure 6: Output spectral density as a function of frequency under broadband excitation at level of 2.8×10^{-4} g^2/Hz. The bandwidth is calculated at 3-dB.

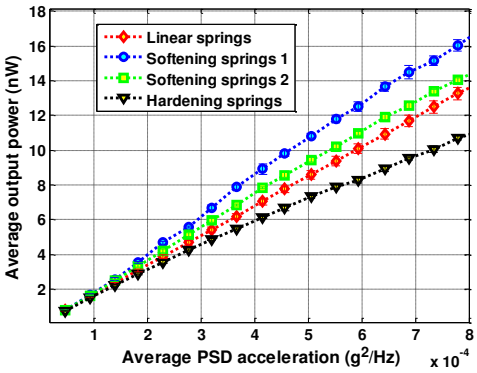

Figure 7: Average output power as a function of the average PSD of the excitation. The load resistance is the optimal load in Figure 4.

springs and linear springs respectively.

The most important criterion to evaluate the vibration energy harvester under white noise excitation must be the average harvested power. To compare the harvested power under white noise excitation for different springs, the average output power as a function of the average PSD of the excitation is depicted in Figure 7. For sufficiently intense white noise, the softening springs achieve higher average output power than the linear springs and the hardening springs do. Additionally, in Figure 7 we also observe that the softening springs 1 harvest more output power than the softening springs 2. So, both softening springs and hardening springs can enhance the bandwidth of the energy harvester, but softening springs have the advantage that they give more output power.

CONCLUSION

We have presented the potential benefit of using softening springs in comparison to linear springs and hardening springs for vibration energy harvesters. Through numerical calculations, we showed that the nonlinearities in the stiffness can provide an enhancement in the performance of the energy harvester.

For sinusoidal excitation, the hardening springs increase the bandwidth for frequency up-sweeps. In contrast, the softening springs increase the bandwidth for frequency down-sweeps.

For white noise excitation, we found that the nonlinearities in the stiffness can increase the bandwidth of the energy harvester. However, softening springs obtain more harvested power than either linear springs or hardening springs do. Furthermore, increased softening behavior in the stiffness will increase the bandwidth and the harvested power.

In conclusion, the softening springs are better than linear springs or hardening springs in designing energy harvester for random vibration environments. This is due to its potential to give both wider bandwidth and larger harvested power. Experimental results on a benefit of using softening springs for vibration energy harvester will be reported elsewhere [9].

ACKNOWLEDGEMENTS

This work was supported in part by The Research Council of Norway under grant no. 191282.

REFERENCES

[1] Mitcheson P D, Yeatman E M, Rao G K, Holmes A S and Green T C 2008 Energy Harvesting From Human and Machine Motion for Wireless Electronic Devices *Proceedings of the IEEE* **96** 1457--86

[2] Reilly E K, Miller L M, Fain R and Wright P 2009 A study of ambient vibrations for piezoelectric energy conversion *Technical Digest PowerMEMS 2009 (Wasington DC, USA, December 1-4, 2009)* 312-5

[3] Zhu D, Tudor M J and Beeby S P 2009 Strategies for increasing the operating frequency range of vibration energy harvesters: a review *Measurement Science and Technology* **21** 022001

[4] Marzencki M, Defosseux M and Basrour S 2009 MEMS Vibration Energy Harvesting Devices With Passive Resonance Frequency Adaptation Capability *Journal of Microelectromechanical Systems* **18** 1444-53

[5] Tvedt L G W, Nguyen D S and Halvorsen E 2010 Nonlinear Behavior of an Electrostatic Energy Harvester Under Wide- and Narrowband Excitation *Journal of Microelectromechanical Systems* **19** 305 -16

[6] Stanton S C, McGehee C C and Mann B P 2009 Reversible hysteresis for broadband magnetopiezoelastic energy harvesting *Applied Physics Letters* **95**

[7] Halvorsen E 2008 Energy Harvesters Driven by Broadband Random Vibrations *Journal of Microelectromechanical Systems* **17** 1061--71

[8] F.Daqaq M 2010 Response of uni-modal duffing-type harvesters to random forced excitations *Journal of Sound and Vibration* **329** 3621–31

[9] Nguyen D S, Halvosen E, Jensen G U and Vogl A 2010 Fabrication and characterization of a wideband MEMS energy harvester utilizing nonlinear springs *(unpublished)*

Paper No. 3

Nguyen2009 PowerMEMS, Conference paper

Title: "Wideband vibration energy harvesting utilizing nonlinear springs".

Authors: Son Duy Nguyen and Einar Halvorsen.

Proceedings of: *PowerMEMS 2009*

Page: 411 - 414

Date: Dec 1-4, 2009

Place: Washington DC, USA.

WIDEBAND VIBRATION ENERGY HARVESTING UTILIZING NONLINEAR SPRINGS

Duy Son Nguyen and Einar Halvorsen
Institute for Microsystem Technology, Vestfold University College, Norway

Abstract: Based on modeling and simulation, this paper investigates the use of nonlinear beams to extend the bandwidth of vibration energy harvesters. We have designed an electrostatic device with an asymmetric nonlinear suspension. A lumped model of the device, which we have implemented in a circuit simulator using parameters obtained from finite element analysis, is presented. We find that the harvester exhibits jumps during frequency and amplitude sweeps and broadening of the spectrum with increasing levels of broadband excitation. Our results show that considerable bandwidth enhancements can be achieved by utilizing nonlinear springs.

Keywords: energy harvester, nonlinear systems, electrostatic devices, vibrations.

INTRODUCTION

Designing energy harvesters to harvest energy from environmental motion with stochastic or varying vibration spectra has been a challenge. In our previous work [1], an in-plane overlap varying device with a nonlinear spring that displays both softening and stiffening behavior achieved a noticeable bandwidth enhancement without replying on impact of mechanical stoppers, resonance tuning or large electromechanical coupling. While impact on elastic stoppers [2] has much the same effect as stiffening springs, softening springs are different. In particular softening spring effects are interesting because they potentially allow larger displacements and suppress the dominance of mechanical over electrostatic forces.

Motivated by the experiments, this paper presents the use of nonlinear beams to extend the bandwidth of vibration energy harvesters. Fig. 1 shows the 3D geometry of the electrostatic energy harvester analyzed. It includes two fixed electrodes attached to the frame and two variable electrodes on the proof mass suspended by four nonlinear springs which are the key feature of our design. The beams have clamped support on the frame and the other ends are fixed on the proof mass. The geometry of the beams is similar to L-shaped beams, but with a joint angle of 131.2^0. The thickness of the beams or the whole device is 300 μm. The width and length of the first and second beam are 15 μm x 1200 μm and 25 μm x 200 μm, respectively, as shown in the right corner of Fig. 1. To obtain the softening regime, four beams are arranged asymmetrically as shown in the Fig. 1. As a result, the spring force versus the displacement of the proof mass was calculated by the finite element method (FEM) in Coventorware as shown in Fig. 2. A softening regime was achieved on one side from about 10 to 90 μm with a quite flat region (very small stiffness) from 30 μm to 90 μm. On the other side it is stiffening.

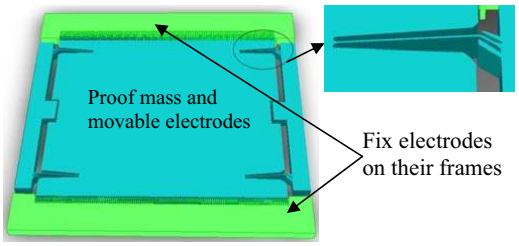

Fig. 1: The 3D layout of electrostatic energy harvester includes two fix electrodes and proof mass suspended by 4 nonlinear springs.

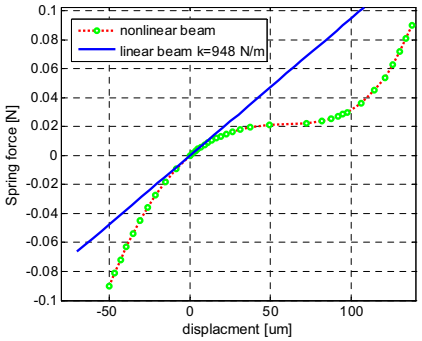

Fig. 2: The spring force vs. displacement of nonlinear springs, calculated by FEM in Coventorware.

ENERGY HARVESTER MODEL

Fig. 3 shows a schematic representation of the energy harvester which is a standard in-plane overlap varying device, except for the springs which are designed to achieve the nonlinear behavior. The model is a generalization of the model in [3]. The

mechanical part consists of the inertial mass m, mechanical damping b represented by a dashpot and the nonlinear beam suspensions. The electrical part consists of two out of phase variable capacitances C_1 and C_2, load resistors R_{L1} and R_{L2}, parasitic capacitances C_{p1} and C_{p2}, load capacitance C_L and an external bias V_e.

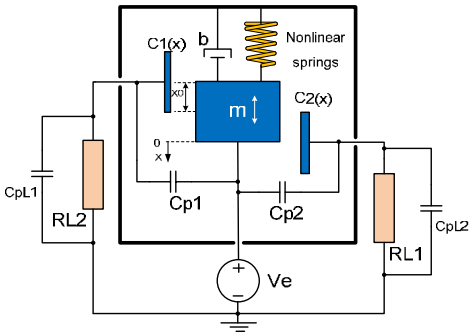

Fig. 3: Electrostatic energy harvester model including the mechanical and electrical part

In modeling of the variable capacitances, we use the parallel plate capacitor formula fit to FEM calculations. The inter-electrode capacitances C_1 and C_2 as functions of the displacement x of the proof mass are

$$C_1(x) = C_{p1} + C_{01}(1-\frac{x}{x_{01}}) \quad (1)$$

$$C_2(x) = C_{p2} + C_{02}(1-\frac{x}{x_{02}}) \quad (2)$$

where C_{01} and C_{02} are the initial capacitances. C_{p1} and C_{p2} represent parasitic capacitances.

The voltages V_{L1} and V_{L2} at the two ports are given by:

$$V_{L1/L2} = \frac{q_{1/2}}{C_{1/2}(x)} + V_e \quad (3)$$

where q_1 and q_2 are the charges on port 1 and port 2 respectively.

Newton's second law describing the motion of the damped mass-spring system is given by

$$m\ddot{x} + b\dot{x} + F_r + F_e = ma \quad (4)$$

Here, m is the mass and ma is the fictitious force. F_e is the electrical force, given by

$$F_e = \frac{1}{2}q_1^2\frac{d}{dx}(\frac{1}{C_1(x)}) + \frac{1}{2}q_2^2\frac{d}{dx}(\frac{1}{C_2(x)}) \quad (5)$$

and F_r is the spring force which is found from FEM and fitted to the polynomial form

$$F_r = \sum_{n=1}^{7} k_n x^n \quad (6)$$

Based on the above equations, the equivalent circuit for the nonlinear spring electrostatic energy harvester is shown in Fig. 4. In SPICE, each variable capacitor $C_{1/2}(x)$ is implemented as an arbitrary fixed capacitor connected in series with a behavioral voltage source [3]. The equivalent circuit includes two sub-circuits for the mechanical part and electrical part respectively. In the mechanical sub-circuit, we chose to split the spring force into the linear term implemented as a capacitor and the remaining nonlinear terms implemented as the behavioral source F_{rn}. We have also implemented a stopper force F_s which is not important at the acceleration levels considered here.

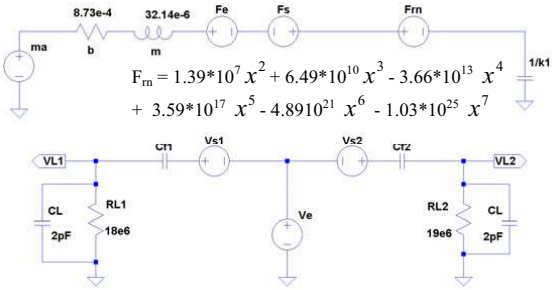

Fig. 4: The equivalent circuit for modeling electrostatic energy harvester.

Table 1: Parameters for nonlinear spring energy harvester.

Parameters	Symbol	Value
Spring constants	k_1	948 N/m
Transducer 1		
Initial finger overlap	x_{01}	110 μm
Initial capacitance	C_{01}	4.67 pF
Parasitic capacitance	C_{p1}	3.74 pF
Transducer 2		
Initial finger overlap	x_{02}	100 μm
Initial capacitance	C_{02}	4.25 pF
Parasitic capacitance	C_{p2}	3.71 pF

RESULTS AND DISCUSSION

In the following we consider a variety of vibration signals: frequency sweeps at fixed amplitude, amplitude sweeps at fixed frequency and broadband random noise with approximately flat power spectral density (PSD).

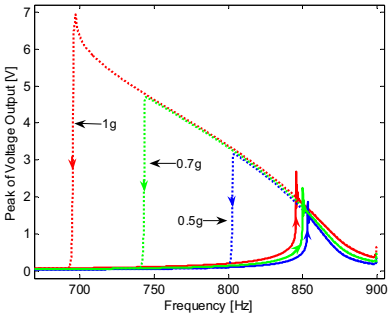

Fig. 5: Up and down frequency sweeps at 0.5g, 0.7g and 1g (peak) excitation with 30V bias. The direction of the arrows shows the direction of the frequency sweeps.

The frequency sweeps are from 600Hz to 900Hz (up-sweep) and from 900Hz down to 600Hz (down-sweep) in 40s. Fig. 5 shows the peak voltage across the first port as a function of frequency. During the forward sweep, the voltage output of the 0.5g (peak) excitation curve jumps up to a higher amplitude at frequency of about 853Hz and decreases with increasing frequency. When performing the frequency sweep downward, the voltage output increases incrementally as the excitation frequency decrease and jumps down to small amplitude value at the frequency of 800Hz, far away from the up-jump frequency, establishes a region of hysteresis or two-valued response. It is evident that two amplitude outputs coexist for any excitation frequency in the range from 800Hz to 853Hz. On increasing the amplitude, the two-valued response region considerably broadens from 743Hz to 850Hz for 0.7g (peak) and from 695Hz to 845Hz for 1g (peak) amplitude excitation. The jump phenomenon in frequency sweeps with the two-valued region appearing on the lower side of the response is a typical property of softening springs.

We also considered frequency sweeps at 0.8g (peak) amplitude excitation for three different bias voltages as shown in Fig. 6. At this level excitation, the voltage output is roughly proportional to the bias voltage away from the jumps. The up-jump frequencies are insensitive to the bias voltage while the down-jump frequencies are roughly insensitive.

Next we consider how the voltage output depends on the vibration amplitude while the driving frequency is kept constant. The driving frequency (840Hz) is selected in the multi-valued response region of the frequency sweeps in Fig 5. The sweeps of amplitude are either from a low to high value (up sweep) or from a high to low value (down sweep) for

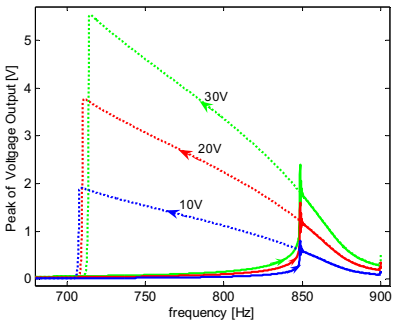

Fig. 6: Up and down frequency sweeps at 0.8g (peak) excitation for 10V, 20V and 30V bias.

three different bias voltages as shown in Fig. 7.

On the up sweep, the voltage output jumps up to the high amplitude value when the excitation reaches 1.4g (peak). After a short transient response, the voltage output continues to increase slowly. On the down sweep, the voltage output stays high beyond 1.4g (peak) where there is also a possible lower amplitude value and drops to small value at about 0.3g (peak). We also see that the jump frequencies are quite independent of the bias voltage. When the device is driven at 840Hz, a two-valued response exists between 0.3g and 1.4g (peak).

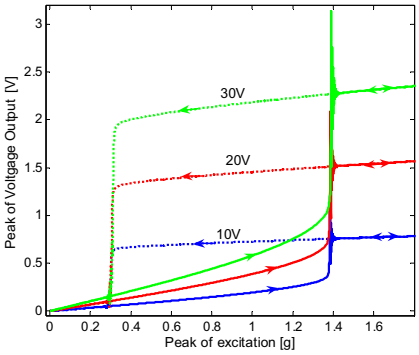

Fig. 7: Up and down amplitude sweeps at 840Hz vibration for 10V, 20V and 30V bias.

Now, we examine the output voltage when the device is driven by broadband random noise. The broadband excitations with a relatively flat PSD from 200Hz to 3000Hz were used. Fig. 8 shows the two-sided output PSD of the first port for many excitation levels from small to large average acceleration PSD values S_a. We notice that the bandwidth of the output considerably widens on increasing excitation (see table 2). Moreover, a shift to the left of the lower

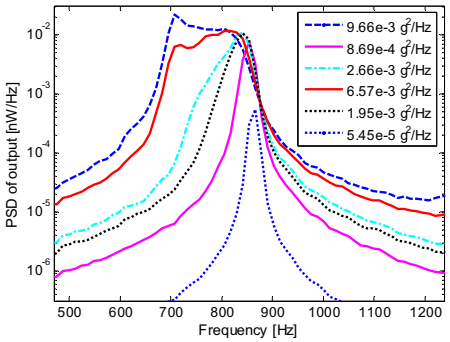

Fig. 8: Two side PSD of output at 30V bias with several levels of the average acceleration PSD

frequency at a half maximum power, f_1, demonstrates that the widening of bandwidth comes from the softening spring effect.

Table 2: The bandwidth of the output PSD for several levels of the acceleration PSD S_a

S_a (g^2/Hz)	Frequency at a half maximum power f_1 and f_2	Bandwidth $BW = f_2 - f_1$
5.45×10^{-5}	853Hz – 874Hz	21Hz
8.69×10^{-4}	842Hz – 865Hz	23Hz
1.95×10^{-3}	820Hz – 860Hz	40Hz
2.66×10^{-3}	814Hz – 857Hz	43Hz
6.57×10^{-3}	706Hz – 849Hz	143Hz
9.66×10^{-3}	695Hz – 820Hz	125Hz

These results show that the electrostatic energy harvesters utilizing nonlinear springs harvest energy in a much wider bandwidth than the similar energy harvester with linear springs, but it does not necessarily mean that nonlinear spring devices can harvest more (or less) power under wide band vibrations than the linear spring devices can. The average output power of the nonlinear spring harvester is compared with the average output power of a linear spring harvester, both having the same parameters except for the springs ($k_{linear} = k_1 = 948$ N/m, Fig. 2) as shown in Fig. 9. It can be seen that both harvest the same power for the same average acceleration PSD. We know from theory [4] that the effect of mechanical nonlinearities on output power depends on the load resistance. Experiments show that it may enhance performance for certain loads [5], though this is not the case here.

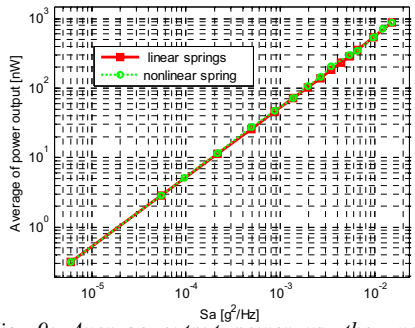

Fig. 9: Average output power vs. the average acceleration PSD for nonlinear and linear springs

CONCLUSION

We have modeled and simulated an energy harvester utilizing nonlinear springs to increase the device bandwidth. For narrowband excitations, we found jumps and multi-valued responses when sweeping either frequency or amplitude. The down sweep bandwidth is greatly enhanced. For broadband excitations, we found a significant bandwidth enhancement with increasing vibration strength while the average output power is the same as for the linear spring device. A prototype is being fabricated at the time of writing and its experimental characterization will be presented in future work.

ACKNOWLEDGEMENT

This work was supported in part by The Research Council of Norway under grant no. 191282.

REFERENCES

[1] Tvedt L G W, Nguyen D S and Halvorsen E 2009 Nonlinear Behavior of an Electrostatic Harvester Under Wide and Narrow Band Excitation (unpublished)

[2] Soliman M S M, Abdel-Rahman E M, El-Saadany E F and Mansour R R 2008 A wideband vibration-based energy harvester *J. Micromech. Microeng.* **18**

[3] Tvedt L G W, Blystad L-C J and Halvorsen E 2008 Simulation of an Electrostatic Energy Harvester at Large Amplitude Narrow and Wide Band Vibrations *Symposium on Design, Test, Integration and Packaging of MEMS/MOEMS - DTIP 2008*

[4] Halvorsen E 2008 Energy Harvesters Driven by Broadband Random Vibrations *J. Microelectromech. Syst.* **17** pp. 1061-1071

[5] Cottone F, Vocca H and Gammaitoni L 2009 Nonlinear Energy Harvesting *Phys. Rev. Lett.* **102** p. 080601

Paper No. 4

Journal of Micromechanics and Microengineering

Nguyen2010 JMM, Journal Article

Title: “Fabrication and characterization of a wideband MEMS energy harvester utilizing nonlinear springs”.

Authors: Son Duy Nguyen, Einar Halvorsen, Geir Uri Jensen and Andreas Vogl.

Journal: *Journal of Micromechanics and Microengineering*

Volume: 20**, Number:** 12**, page(s):** 125009 (11pp)

Date of Publication: Dec 2010

Times Cited: 14 (from Web of Science, to Jan 2013)

Paper No. 5

Nguyen2011 JMEMS, Journal Article

Title: "Nonlinear springs for bandwidth-tolerant vibration energy harvesting".

Authors: Son Duy Nguyen and Einar Halvorsen.

Journal: *EEE/ASME Journal of Microelectromechanical Systems.*

Volume: 20**, Issue:** 6**, page(s):** 1225 – 1227

Date of Publication: Dec 2011

Times cited: 5 (from Web of Science, to Jan 2013).

Paper No. 6

Nguyen2012b JMEMS, Journal Article

Title: “Wideband MEMS Energy Harvester Driven by Colored Noise”.

Authors: Son Duy Nguyen, Einar Halvorsen and Geir Uri Jensen.

Submitted to: *EEE/ASME Journal of Microelectromechanical Systems,*

Date of submission: Nov 2012.

Wideband MEMS Energy Harvester Driven by Colored Noise

Son D. Nguyen, Einar Halvorsen, *Member, IEEE,* and Geir U. Jensen

***Abstract*—We experimentally investigate the usefulness of nonlinear springs in a MEMS electrostatic energy harvester under colored noise vibrations. The experimental characterisation of the energy harvester using nonlinear springs is compared to analytical and simulated results for an energy harvester with linear springs. For random vibrations with a bandwidth of 50 Hz and varying center frequencies, we found that the maximum output power of the nonlinear-spring harvester is 1.7 times lower than that of the linear-spring harvester but the 1-dB bandwidth is two times larger. For vibration center frequencies of 38 Hz and 58 Hz below the resonant frequency, the nonlinear-spring harvester always achieves more power than the linear-spring one regardless of the vibration bandwidth. By varying the bias voltage, we found that the nonlinear-spring harvester obtains an average power of about 1 μW at 180 V, corresponding to an efficiency of 92 % for a white noise excitation of 7.29×10^{-4} g^2/Hz and 1.2 μW at 36 V for a frequency down-sweep at 0.15 g. A design variety of the device reached an output power of 7 μW at 120-V bias and 0.36-g acceleration.**

***Index Terms*—Energy harvesting, Power generation, Microelectromechanical devices, Vibrations, Nonlinear systems.**

I. Introduction

THIS paper investigates the performance of a mechanically nonlinear microscale vibration energy harvester and is an expansion of a previously published JMEMS Letter [1].

Energy harvesting from environmental vibrations is a good candidate to power wireless sensors [2], [3]. Conventional vibration energy harvesters are designed as linear resonant structures. They have a very narrow bandwidth and operate efficiently only when the excitation frequency is very close to the resonant frequency of the harvesters. The narrow bandwidth limits their application in real-world environments which have a wide spectrum of frequencies or varying vibration spectra.

There have been several approaches to overcome this limitation by tuning the resonant frequency or widening the bandwidth of the harvesters [4]. Many methods have been developed to tune the resonant frequency so that it can match the excitation frequency such as using axially compressive pre-load [5] or centrifugal force [6]. To widen the harvester bandwidth, nonlinearities of suspensions have been reported recently as a promising solution. The nonlinear suspensions that have been considered can be classified into three types: hardening [7]–[10], bistable [11]–[15] and softening [16]–[18]. Besides, mechanical end stops, which gives a discontinuous restoring force, have been exploited to widen the harvester bandwidth [19]–[22].

The bistable suspensions have shown a great potential for increasing the harvester bandwidth [11]–[15]. To achieve the bistable characteristic, most such harvester designs reported so far make use of magnets. However, the presence of the magnets can introduce an undesired force on the proof mass of the harvester when placed close to magnetic materials. Conversely, the field from the magnets could affect other nearby electronic devices or magnetic sensors. Moreover, by adding magnets, the fabrication process requires an additional material and an additional device volume to allow space for two separated magnets.

The softening suspensions are a more promising solution than the hardening suspensions to widen the bandwidth and also potentially give as wide a bandwidth as bistable harvesters, especially when they are driven by white noise vibrations [23], [24]. Softening suspensions can be achieved by using magnets [16], but can also be obtained purely by their geometrical designs without any magnets [17], [18]. Different from piezoelectric energy harvesters where the piezoelectric material have to be deposited on the suspensions to exploit the their stress, electrostatic harvesters have separate transducers and suspensions. With in-plane motion, one then has the advantage of great freedom in designing the shape of the suspensions in the form of angled springs [17], curved springs [18], folded springs [25]–[27], segmented springs [28] or crab-leg springs [29]. Several of these methods allow tunability of the softening nonlinearity at the design stage and can span the whole range from linear or hardening springs, through softening springs to (asymmetric) bistable springs [17], [18], [28], [30].

Nonlinear harvesters are usually characterized with sinusoidal excitations [7], [9], [10], [19]–[21], white noise excitations [12] or both [8], [15], [17], [22]. Real world vibrations need not be close to these ideal cases. This is particularly important for a nonlinear harvester because it does not obey the superposition principle and has a spectrum that is dependent on the vibration strength. The degree to which a nonlinear harvester can respond effectively to a vibration depends in a nontrivial way on both the spectral shape and strength of the vibration. In addition one must expect some variability in vibration spectrum within the range of applications the harvester is intended for and over time. It is therefore of

Manuscript received ... This work was supported in part by The Research Council of Norway under grant no. 191282 .

S. D. Nguyen and E. Halvorsen are with the Department of Micro and Nano Systems Technology, Faculty of Technology and Maritime Sciences, Vestfold University College, Horten, Norway (e-mail: duy.s.nguyen@hive.no; einar.halvorsen@hive.no).

G. U. Jensen is with the Department of Microsystems and Nanotechnology, SINTEF Information and Communication Technology, 0314 Oslo, Norway (e-mail: Geir.U.Jensen@sintef.no).

Color versions of one or more of the figures in this paper are available online at http://ieeexplore.ieee.org.

interest to consider the influence of vibration center frequency and/or the bandwidth variations on the performance of nonlinear harvesters. Among the few previous works that considered finite-bandwidth random vibrations [14], [31]–[34], i.e. colored noise, only two are experimental [31], [34]. Hence very little is known about potential benefits of nonlinear energy harvesting outside the idealized cases of infinite or zero bandwidth.

In this paper, we present experiments on a nonlinear-spring harvester under colored-noise vibrations over a range of vibration bandwidths and center frequencies extending the work in our previously published letter [1]. Here, the experiments are presented in more details and compared to both analytical treatment of a linear harvester and SPICE simulations of a harvester with linear springs and nonlinear transducers. The use of sacrificial structures to protect the nonlinear springs during fabrication is presented. The effect of a bias voltage on the performance of the nonlinear-spring electrostatic energy harvester is experimentally investigated and compared to that of a linear-spring harvester.

II. Device description

Here we describe the key features of the device with an emphasis on those that are related to the nonlinear springs and different from previous devices. We also give the results of characterization with white noise and harmonic acceleration.

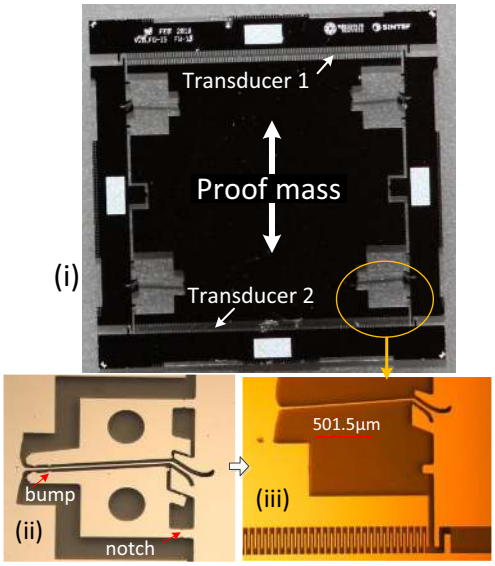

Fig. 1. (i) Photograph of a MEMS electrostatic energy harvester with nonlinear springs. (ii) Sacrificial structures to protect the nonlinear springs during DRIE. (iii) The nonlinear spring after removing the sacrificial structures.

A. Sacrificial structures and nonlinear springs

Fig. 1-i shows a MEMS electrostatic energy harvester after fabrication and dicing. The device is an in-plane overlap varying type made by deep reactive ion etch (DRIE). The fabrication process was presented in [17]. The main difference here is the use of sacrificial structures to protect the nonlinear springs during fabrication. The electrostatic energy harvester requires narrow openings between capacitor fingers to get large variable capacitance and narrow springs ($\approx 15\ \mu$m) to get low resonant frequency, but wide openings in regions close to the guided end of the springs (larger than 100 μm) in order to let the proof mass move freely. Therefore, it is important to consider the following DRIE issue: the profile of an etched wall in a narrow opening is nearly perpendicular to the wafer surface. However, as the opening increases, the wall profile becomes increasingly negative, i.e. the bottom of a spring becomes more and more narrow, while its top surface basically retains its width. Without countermeasures, the already narrow springs would be much narrower at their bottom. We solved this issue by adding sacrificial protective structures close to the springs as shown in Fig. 1-ii. This technique ensures narrow opening areas for all critical parts.

Different from the dummy protective structures in [17] which are still present after fabrication, the sacrificial structures here are manually broken off and removed from the device as the last step of the fabrication process to leave sufficient space for proof mass motion as shown in Fig. 1-iii. There are small bumps on the structures to avoid stiction of the springs. Each sacrificial structure has a hole in the middle allowing insertion of a needle to break it at a notch made in its suspension. The space around the sacrificial structures is designed at least big enough for them to rotate without touching the proof mass before breaking. The sacrificial structures not only make narrow and uniform opening areas along the nonlinear springs but also serve as mechanical end stops in the fabrication process. With the sacrificial structures, the proof mass displacement is limited to about 10 μm. Due to uniform opening areas, the nonlinear springs with the sacrificial structures have a better under-cut profile than the dummy protective structures in [17] have. However, removal of the sacrificial structures is a potentially risky process that could break the springs and requires some care. The amount of sacrificed chip area for these structures is a disadvantage compared to the previous technique.

Fig. 2 shows the restoring force versus displacement of the nonlinear springs calculated by the finite element method (FEM). The nonlinear springs have a softening characteristic in one direction of the displacement while the other side is hardening.

B. Optimal load and bandwidth

Fig. 3 shows the average output power vs. load resistance for both sinusoidal and white noise excitations. The optimal load resistance for the sinusoidal excitation is about 17.5 MΩ and 12.5 MΩ for transducer 1 and transducer 2 respectively. For white noise excitation, the optimal load is uncertain but close to these values. The excitation levels are small to make sure that the harvester works in the linear-spring regime. This choice ensures that the optimal loading does not artificially

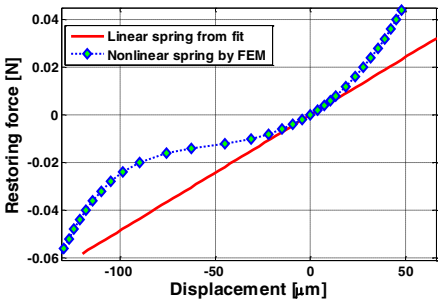

Fig. 2. Restoring force vs. displacement of the nonlinear springs showing a softening characteristic in the displacement of from -10 μm to -90 μm, calculated by FEM. The linear spring line is plotted to compare.

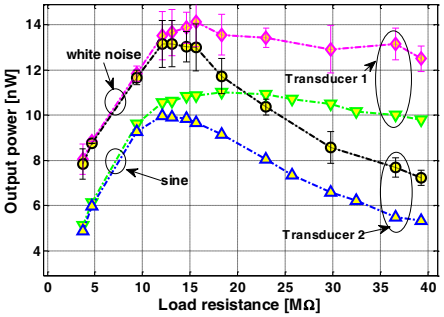

Fig. 3. Output power vs. load resistance for sinusoidal and white noise excitations. The bias voltage is 36 V. The sinusoidal excitation is at a resonance frequency of 668 Hz with root mean square (RMS) acceleration amplitude of 0.114 g. The white noise level is 8.21×10^{-5} g^2/Hz. The optimal load resistance is about 17.5 MΩ and 12.5 MΩ for transducer 1 and transducer 2 respectively.

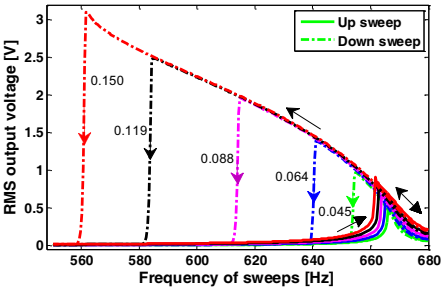

Fig. 4. Frequency-response curves for Transducer 1 under frequency up- and down-sweeps showing the softening characteristic of the nonlinear springs, RMS acceleration amplitudes of 0.045, 0.064, 0.088, 0.119 and 0.150 g. The bias voltage is 36 V.

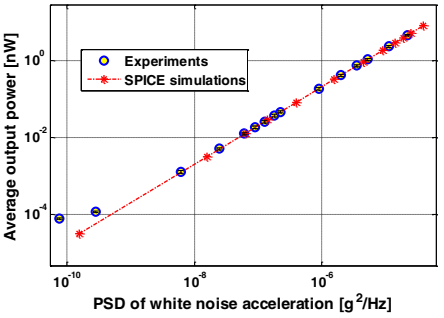

Fig. 5. Average output power (total) vs. acceleration PSD for low-level white noise acceleration. Circles: experiments. Dash-dotted lines with asterisks: SPICE model with nonlinear transducers and nonlinear springs. The bias voltage is 36 V.

favor the nonlinear operation. In the later experiments, the load resistors are fixed at 17.5 MΩ and 12.5 MΩ.

Fig. 4 shows the root mean square (RMS) output voltage on transducer 1 under linear frequency sweeps (up-sweep and down-sweep) with different constant acceleration amplitudes. The harvester responds with a narrow bandwidth for the up-sweeps, but with a wide bandwidth for the down-sweeps. The down-sweep bandwidth broadens with increasing acceleration amplitude. So, the overall effect of the nonlinear springs is softening. The down-sweep bandwidth ceases to increase when the acceleration amplitude reaches 0.150 g. In the experiments where the harvester is driven by colored noise reported in later sections, we focus on the frequency range from the resonant frequency f_0 of 668 Hz to the lowest jump-down frequency of 560 Hz.

The average output power as a function of power spectral density (PSD) of white noise acceleration is shown in Fig. 5. The PSD of white noise acceleration is calculated by averaging the relatively flat PSD obtained from the measured acceleration by Welch's method. It is averaged over a frequency range from 200 Hz to 1200 Hz [17]. By using a SPICE model with nonlinear springs and nonlinear transducers [17], the measured average output power is fitted with the SPICE simulation. The resultant mechanical quality factor is $Q_m = 450$.

III. Parameters and Lumped Model

To evaluate the usefulness of the nonlinear springs, the performance of the nonlinear-spring energy harvester is compared to that of a simulated linear-spring energy harvester. For a reasonable comparison, the parameters for the linear-spring harvester are extracted from the parameters of the nonlinear-spring one which are fitted to or directly taken from measurements. Different from the nonlinear-spring device with asymmetric transducers, the linear-spring harvester is symmetric. It has the same sum of initial overlaps for the two transducers as the nonlinear device has. Table I shows the parameters for the linear-spring harvester.

The linear-spring energy harvester with two symmetric transducers can be described by

$$m\ddot{x} + b\dot{x} + K_m x + F_e = ma, \qquad (1)$$

$$V_{Li} = \frac{q_i}{C_p + C_i(x)} + V_e, \quad i = 1, 2, \qquad (2)$$

where m is the proof mass, a is the negative of the package acceleration, b is the constant for linear mechanical damping

TABLE I
THE PARAMETERS FOR LINEAR-SPRING ENERGY HARVESTER

Parameter	Description	Value	Comment
m	Proof mass	30.4 mg	measured[a]
K_m	Linear spring stiffness	535 N/m	fitted
Q_m	Mechanical quality factor	450	fitted
V_e	Bias voltage	36 V	measured
x_0	Initial overlap	90 μm	layout
C_0	Initial capacitance	3.547 pF	fitted
C_p	Parasitic transducer capacitance	3.17 pF	FEM
C_L	Parasitic load capacitance	2 pF	datasheet
R_L	Load resistor	15 MΩ	measured
N	Number of fingers on stator	125	layout

[a]after the device was broken.

representing parasitic mechanical loss, K_m is the constant linear stiffness of the springs, V_e is the bias voltage, $C_i(x)$ and C_p are the variable capacitor on transducer number i (i = 1,2) and the parasitic transducer capacitor respectively, q_i is the charge on transducer number i, V_{Li} is the voltage across the load which consists of a load resistor R_L in parallel with a parasitic load capacitor C_L, F_e is the electrostatic force, and

$$C_{1/2}(x) = C_0(1 \mp \frac{x}{x_0}), \tag{3}$$

$$F_e = \frac{q_1^2}{2}\frac{d}{dx}(\frac{1}{C_p + C_1(x)}) + \frac{q_2^2}{2}\frac{d}{dx}(\frac{1}{C_p + C_2(x)}). \tag{4}$$

By linearization, see e.g. [35], of the electrostatic force F_e and the voltage for small displacement x and charge $q = (q_1 - q_2)/2$, the lumped model for the linear-transducer energy harvester with linear spring can be written as

$$m\ddot{x} + b\dot{x} + Kx + \frac{\Gamma}{C}q = ma, \tag{5}$$

$$-\dot{q}R = \frac{\Gamma}{C}x + \frac{q}{C}, \tag{6}$$

with

$$\Gamma = -\frac{C_0}{x_0}V_e = -2N\frac{\varepsilon_0 t}{g_0}V_e, \tag{7}$$

$$C = (C_0 + C_p + C_L)/2 \quad \text{and} \quad R = 2R_L, \tag{8}$$

$$K = K_m + \frac{\Gamma^2}{C}, \tag{9}$$

$$k^2 = \frac{\Gamma^2}{KC}, \tag{10}$$

where x_0 is the initial overlap, ε_0 is the vacuum permittivity, g_0 is the gap between capacitor fingers, t is the wafer thickness R and C are the equivalent load resistance and transducer capacitance respectively, K is the effective linear spring stiffness at open circuit and k is the electromechanical coupling factor. The nonlinear transducers expressed by equation (1) and (2) are used for SPICE simulation. For the fully linearized harvester governed by (5) and (6), analytical expressions for an output power with different types of excitations such as white and band-limited noise can be found in [36]. *The two theoretical models both have linear stiffness, but the SPICE simulation uses the nonlinear transducer model including the nonlinearity of the electrostatic force (4) and voltage (2).*

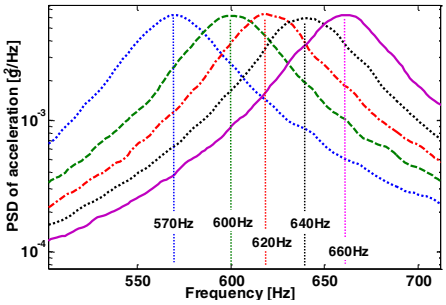

Fig. 6. PSD of acceleration for fixed RMS acceleration amplitude A and vibration bandwidth Δ of 50Hz, but different center frequencies f_c.

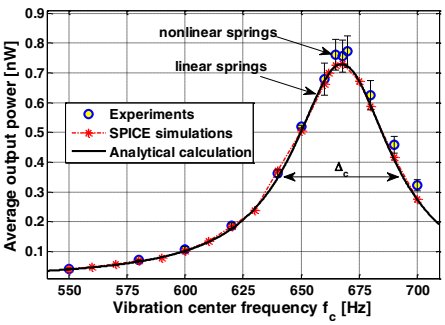

Fig. 7. Average output power vs. vibration center frequency for Δ = 50 Hz and small RMS acceleration amplitude of 0.024 g. Circles: experiments. Dash-dot curve with asterisks: SPICE simulations with nonlinear transducers. Solid curve: analytical calculation with linear transducers. At small acceleration amplitude, the power of the nonlinear harvester is approximate to that of linear device.

To model situations where the bandwidth and center frequency of the vibrations may vary, one can use white noise filtered by a band pass filter. For a second order filter, the two-sided power spectral density (PSD) of the acceleration is then given by

$$S_a(f) = \frac{1}{\pi}\frac{\Delta A^2 f^2}{(f_c^2 - f^2)^2 + \Delta^2 f^2} \tag{11}$$

where A is the RMS acceleration amplitude, f_c is the center frequency of the colored noise acceleration and Δ is the full bandwidth (at 3-dB). A is kept fixed when comparing the average output power under different bandwidths and center frequencies of the vibrations

IV. EFFECT OF THE VIBRATION CENTER FREQUENCY

Fig. 6 shows PSD of acceleration for different vibration center frequencies f_c but having the same RMS acceleration amplitude A and bandwidth Δ. The average output power of the harvester under these vibrations is shown in Fig. 7. In these experiments, the RMS acceleration amplitude is small so that the device works in the linear-spring regime. The analysis for linear-transducer harvester and SPICE simulation for nonlinear-transducer harvester using linear springs are also

plotted to compare. The 3-dB bandwidth Δ_c of the harvester's response under varying f_c is determined. It can be seen that Δ_c is approximately the vibration bandwidth Δ at this vibration level, i.e. $\Delta_c \approx \Delta = 50\ Hz$. In the linear-spring regime, a good agreement between the experiments, analytical calculation and SPICE simulations shows that it is reasonable to compare the experimental results of the nonlinear-spring harvester to the model of a linear-spring harvester.

The average output power vs. vibration center frequency f_c is shown for a higher acceleration amplitude in Fig. 8. Different from the response of the frequency sweeps (Fig. 4), there is no hysteresis phenomenon in the response of the nonlinear harvester under the colored noise excitations. Each value corresponds to the average over three different 60-s random time series of acceleration. The linear-spring energy harvester has maximum output power when f_c is centered at its resonant frequency. The maximum output power of the softening-spring harvester is found at lower frequency than its resonant frequency. While Δ_c of the linear-spring harvester does not change when increasing the RMS acceleration amplitude, Δ_c of the nonlinear-spring device increases with RMS acceleration amplitude. Particularly, Δ_c is about 75 Hz and 85 Hz for RMS acceleration amplitude of 0.360 g and 0.448 g, respectively. If the response bandwidth is taken instead at 1 dB below the peak power, 1-dB Δ_c is about 40 Hz and 50 Hz. The 1-dB bandwidth of the vibration is 25.4 Hz. The maximum output power of the nonlinear-spring harvester is about 1.7 times smaller than that of the linear-spring device (300 nW/172 nW), but the 1-dB Δ_c of the nonlinear-spring harvester is about two times larger (50 Hz/ 25.4 Hz). Hence peak power is traded for tolerance to frequency variations.

The measured output voltage PSD for some selected vibration center frequencies f_c (as shown in Fig. 6) at A = 0.488 g is shown in Fig. 9. For f_c = 660 Hz, the harvester's response bandwidth is about 48 Hz, which is approximately the vibration bandwidth. When tuning f_c toward the lower frequency, f_c = 640 Hz or 620 Hz, the harvester's response bandwidth is wider than the vibration bandwidth, but still keeps the high cut-off frequency around the resonant frequency. The response bandwidth is about 63 Hz for f_c = 640 Hz and 72 Hz for f_c = 620 Hz. At f_c = 600 Hz, the response bandwidth reduces to 22 Hz because of the lowered spectral weight of the vibration in the sensitive frequency range of the harvester. When f_c is further reduced to 570Hz, the harvester responds with a narrow bandwidth around the resonant frequency because the frequency mismatch is too large to excite the harvester into the strongly nonlinear regime of softening spring behavior. Though the peak value of the output PSD may appear high, the integrated PSD is not. It is proportional to the output power in Fig. 8, where we obtained 26.9 nW for f_c = 570Hz, which is 7.2 dB lower than 140.3 nW obtained for f_c = 660Hz.

V. Effect of the Vibration Bandwidth

Fig. 10 shows the acceleration PSD with fixed RMS acceleration and center frequency f_c of 668 Hz but with varying vibration bandwidth Δ from very narrow (2 Hz) to very wide (150 Hz).

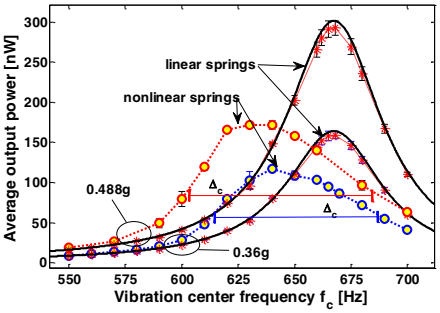

Fig. 8. Average output power vs. vibration center frequency f_c, the vibration bandwidth Δ = 50 Hz, the RMS acceleration amplitude of 0.360 g and 0.488 g. Dotted curves with circles: experiments. Dash-dot curves with asterisks: SPICE simulations. Solid curves: analytical calculation. Each output power value at each vibration center frequency is obtained by averaging the RMS values of three individual experiments. The peak power of the nonlinear harvester is traded for tolerance to frequency variations.

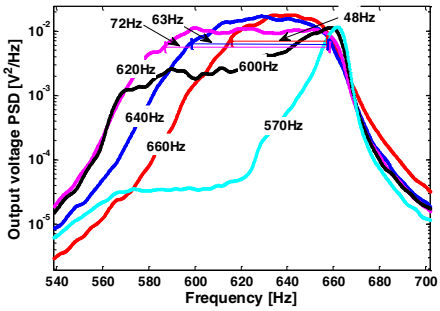

Fig. 9. PSD of the output voltage for different vibration center frequencies, f_c = 660 Hz, 640 Hz, 620 Hz, 600 Hz and 570 Hz, the vibration bandwidth Δ = 50 Hz, the RMS acceleration amplitude of 0.488 g. The response bandwidth of the nonlinear harvester is wider than the vibration bandwidth Δ for f_c = 620 Hz and 640 Hz.

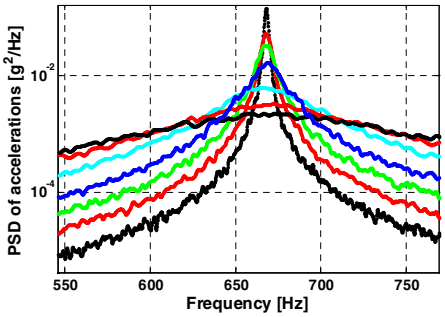

Fig. 10. PSD of accelerations for the same A of 1 g and center frequency of 668 Hz, but different bandwidth from 2 Hz, 5 Hz, 10 Hz, 30 Hz, 50 Hz, 100 Hz and 150 Hz.

The average output power of the harvester depends on the vibration bandwidth Δ for different vibration center frequencies f_c as shown in Fig. 11. The RMS acceleration amplitude

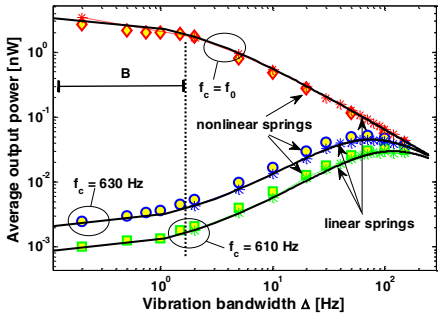

Fig. 11. Average output power vs. vibration bandwidth Δ for different center frequency f_c and RMS acceleration amplitude of 0.01 g. Circles/squares/diamonds: experiments. Solid curves: analytical calculation. Dash-dot curves with asterisks: SPICE simulations. The energy harvester with linear springs only works well when f_c is centered at its resonant frequency and Δ varies within its 3-dB bandwidth B.

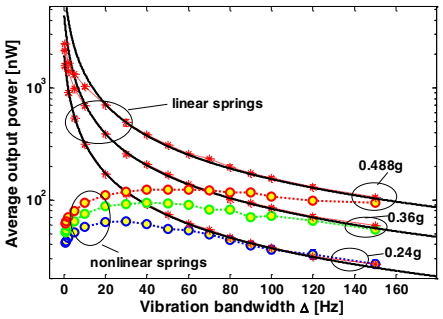

Fig. 12. Average output power vs. vibration bandwidth Δ, $f_c = f_0$ = 668 Hz, A = 0.240 g, 0.360 g and 0.488 g. Dotted curves with circles: experiments. Solid curves: analytical calculation. Dash-dot curves with asterisks: SPICE simulations. The linear-spring harvester obtains higher output power than the nonlinear one when f_c is centered at f_0 and Δ is smaller than 80 Hz for 0.24 g, 150 Hz for 0.36 g, and 160 Hz (estimated value) for 0.488 g.

A in this experiment is selected at very low level so that the spring nonlinearity is insignificant and the harvester works in the linear-spring regime. Again, the analytical results and the SPICE simulations for linear-spring harvester are plotted to compare.

When f_c is centered at the harvester resonant frequency f_0, i.e. $f_c = f_0$ = 668 Hz, the harvester operates best when Δ is less than the harvester 3-dB bandwidth B ($B \approx f_0/Q_m$). When Δ becomes larger than B, the average output power significantly reduces. The average output power is also very small when f_c is far, 38 Hz or 58 Hz, from the harvester resonant frequency, i.e. f_c = 630 Hz or 610 Hz, regardless of the vibration bandwidth Δ. In short, the energy harvester with linear springs only works well when f_c is centered at its resonant frequency and Δ varies within its 3-dB bandwidth B. It is noted that B tends to be rather small, about a few Hertz, due to the (desired) high mechanical factor Q_m. This small bandwidth is the main limitation of the energy harvester with linear springs.

The average output power as a function of the vibration bandwidth Δ when f_c is centered at f_0 and at large acceleration amplitude is shown in Fig. 12. The difference between the SPICE simulations and the analytical results for small Δ is due to the inclusion of mechanical end stops in the SPICE model. When Δ is small, which is the best operating condition for the harvester using linear springs, the nonlinear-spring harvester operates ineffectively. The output power of the nonlinear-spring harvester is smaller than that of the linear-spring harvester for a wide range of vibration bandwidth Δ. For increasing Δ, the output power of the nonlinear-springs device becomes comparable with the output power of the linear-spring one when Δ reaches a limit depending on the rms acceleration, e.g. Δ = 80 Hz for A = 0.24 g, Δ = 150 Hz for A = 0.36 g, and Δ = 160 Hz for A = 0.488 g (estimated based on the trend of experimental trace).

The average output power versus the vibration bandwidth Δ when f_c is lower 38 Hz than f_0, i.e. at 630 Hz, is shown in Fig. 13. In contrast with the linear-spring regime in Fig. 11, the power increases rapidly with increasing Δ and reaches the maximum at Δ = 30 Hz and then, decreases slowly. Compared to the linear-spring harvester, the nonlinear-spring harvester performance is much better in this situation, especially for higher A where the proof mass motion is deep into the softening-spring regime. In particular, for A = 0.488 g and Δ = 30 Hz, the average output power of the nonlinear-spring harvester is higher than that of the linear-spring harvester by a factor of 3.8.

The average output power as a function of the vibration bandwidth Δ for f_c = 610 Hz, which is 58 Hz from the resonant frequency is shown in Fig. 14. When Δ is smaller than about 10 Hz, the power is very small. For varying Δ larger than 10 Hz and A = 0.488 g, the output power of the nonlinear-spring harvester dramatically increases with increasing Δ and reaches its maximum value when Δ = 60 Hz. The power of the nonlinear-spring device is higher than that of the linear-spring harvester for a wide range of vibration bandwidths.

Fig. 15 shows the PSD of the output voltage at the maximum power value for different f_c and an RMS acceleration amplitude of 0.488 g. The acceleration PSD of each case is also plotted. For $f_c = f_0$ and Δ = 50 Hz, the harvester 3-dB bandwidth is about 34 Hz. For f_c = 630 Hz and Δ = 30 Hz, it is about 64 Hz which is two times larger than the vibration bandwidth Δ. For changing f_c down to 58 Hz from the harvester resonant frequency and Δ = 60 Hz, the harvester 3-dB bandwidth is about 68 Hz which is still larger than 3-dB bandwidth of the vibration.

VI. Effect of the Bias Voltage

Electrostatic energy harvesters need a bias to work. This bias must be provided internally, requiring additional fabrication steps, or be provided by the power conversion electronics. That is a disadvantage of electrostatic energy harvesters compared to piezoelectric or electromagnetic harvesters. However, different from the fixed electromechanical coupling of a piezoelectric harvester, the electromechanical coupling of the electrostatic harvester can be increased by increasing the bias

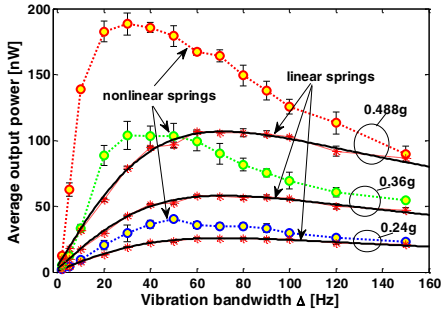

Fig. 13. Average output power vs. vibration bandwidth, f_c = 630 Hz, A = 0.240 g, 0.360 g and 0.488 g. Dotted curves with circles: experiments. Solid curves: analytical calculation. Dash-dot curves with asterisks: SPICE simulations. The nonlinear-spring harvester outperforms the linear-spring one when f_c is 38-Hz lower than the resonant frequency regardless the vibration bandwidth.

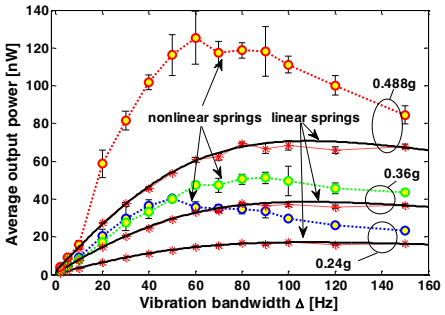

Fig. 14. Average output power vs. bandwidth, f_c = 610 Hz, A = 0.240 g, 0.360 g and 0.488 g. Dotted curves with circles: experiments. Solid curves: analytical calculation. Dash-dot curves with asterisks: SPICE simulations. The nonlinear-spring harvester outperforms the linear-spring one when f_c is 57-Hz lower than the resonant frequency regardless the vibration bandwidth.

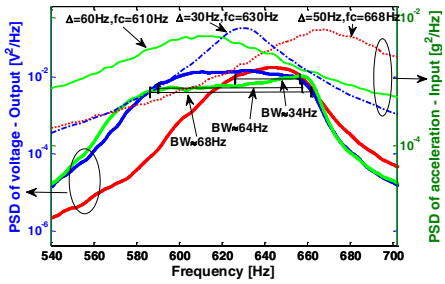

Fig. 15. PSD of output voltage for some selected vibration center frequencies f_c and vibration bandwidths Δ, A = 0.488 g. The response bandwidth (noted by BW) of the nonlinear-spring harvester exceeds the vibration bandwidth when f_c is tuned to the softening regime. In particular, BW = 64 Hz for Δ = 30 Hz and f_c = 630 Hz, BW = 68 Hz for Δ = 60 Hz and f_c = 610 Hz.

voltage. In this section, we experimentally study the effect of bias voltage on the nonlinear electrostatic energy harvester for both harmonic and white noise excitations.

The output power of general energy harvesters under white noise vibrations can be written $P = \eta P_{\text{in}}$ where $P_{\text{in}} = mS_a/2$ is the mechanical input power [37], S_a is the two-sided PSD of the acceleration and η is the efficiency of the energy harvester. As follows from the expression for output power in [36], the efficiency of an harvester with linear spring and linear transducer is given by

$$\eta = \frac{k^2 Q_m r}{1 + (1/Q_m + k^2 Q_m) r + r^2} \tag{12}$$

where $r = \omega_0 CR$. The coupling factor k^2 is given by (10) and is proportional to V_e^2 for small bias voltages V_e.

Fig. 16 shows the average output power as a function of the bias voltage under white noise excitations. The input power $P_{\text{in}} = mS_a/2$ is also plotted. Overall, increasing the bias voltage will increase the output power, but the detailed behavior differs depending on the bias voltage. The bias conditions can be roughly divided into three ranges: small bias voltage ($V_e \leq 30$ V), large bias voltage (30 V $< V_e <$ 120 V) and very large bias voltage ($V_e \geq$ 120 V). The output power quadratically increases at small bias voltage and linearly increases at large bias voltage. For very large bias voltage, the output power increases slowly showing a tendency to level out. It should be noted that the output power of the nonlinear-spring energy harvester is larger than that of the linear-spring harvester at very large bias voltages. This can be explained by the softening effect which reduces the effective spring stiffness and thereby increases the coupling to give a higher efficiency η for the nonlinear-spring device. Particularly, for $S_a = 7.29 \times 10^{-4}$ g^2/Hz and $V_e = 180$V, the output power of the nonlinear-spring harvester is 0.98 μW and the resulting efficiency is $\eta = 92\%$, while the efficiency of the linear-spring harvester is 80%. To reach the power value of the nonlinear-spring harvester, i.e. $P = 0.98\mu$W, the linear-spring harvester would need a bias of 320 V.

As shown in Fig. 4, for frequency down-sweep at acceleration amplitude of 0.15 g, a maximum voltage of 3.1 V was obtained on transducer 1. The corresponding value for transducer 2 (not shown) was 2.9 V. These voltages correspond to a maximum total output power of 1.2 μW at 36-V bias. Since the harvester reported upon above broke under a very large excitation test, another harvester with a larger proof mass and somewhat more compliant springs was used to study performance under frequency down-sweep at higher bias voltage. The experimental results are shown in Fig. 17. Similar to the above device, the frequency range from the resonant frequency to the lowest jump-down frequency is about 120 Hz. The harvester under higher bias voltage has larger total damping due to increased electrical damping. Therefore, for a given acceleration amplitude, increasing bias voltage reduces the response bandwidth of the harvester. So, to reach the same frequency-response bandwidth, the higher bias voltage requires larger acceleration amplitude. The harvester maintains a wide-band response with 3-dB bandwidth of 50 Hz at high bias voltage of 80 V and 120 V. A maximum output power of 7 μW is achieved at 120-V bias.

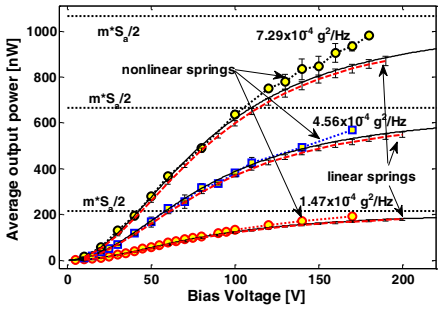

Fig. 16. Average output power vs. bias voltage for different white noise excitation levels. Dotted curves with circles/squares: experiments. Solid curves: analytical calculation. Dash-dot curves with asterisks: SPICE simulations, Dotted lines: the upper power bound. For $S_a = 7.29 \times 10^{-4}\ g^2/Hz$ and $V_e = 180$V, the output power of the nonlinear-spring harvester is 0.98 μW and the resulting efficiency is $\eta = 92\%$, while the efficiency of the linear-spring harvester is 80%.

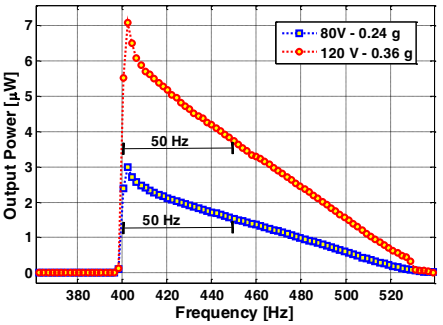

Fig. 17. Output power under frequency down-sweep for high bias voltages of 80 V and 120 V. R_{L1} = 18 $M\Omega$, R_{L2} = 17 $M\Omega$. The device maintains a wide bandwidth of 50 Hz at high bias voltages and obtains a maximum power of 7 μW at 120 V.

VII. Conclusion

We have experimentally investigated the usefulness of softening springs in a MEMS vibration energy harvester under colored noise excitations. Sacrificial structures to protect the nonlinear springs during the fabrication process were also presented. While a linear-spring energy harvester is a good choice when the vibrations have a known, constant, dominant frequency and tiny bandwidth, it is outperformed by the nonlinear-spring device when the vibrations have wide, but still finite, bandwidth and a center frequency that might vary over time or between different applications. The conclusion is adapted for any energy harvesters with softening springs, regardless of the transducer type.

In short, the nonlinear device is tolerant to variations both in vibration center frequency and bandwidth, and can perform close to its theoretical maximum with wideband vibrations.

References

[1] S. D. Nguyen and E. Halvorsen, "Nonlinear springs for bandwidth-tolerant vibration energy harvesting," *J. Microelectromech. Syst.*, vol. 20, no. 6, pp. 1225 –1227, dec. 2011.

[2] P. D. Mitcheson, E. M. Yeatman, G. K. Rao, A. S. Holmes, and T. C. Green, "Energy harvesting from human and machine motion for wireless electronic devices," *Proceedings of the IEEE*, vol. 96, no. 9, pp. 1457–1486, Sep. 2008.

[3] E. Mounier, "Mems markets & applications 2011-2017, an overview," in *dMEMS 2012*, Besancon, France, April 2nd - 3rd 2012.

[4] D. Zhu, M. J. Tudor, and S. P. Beeby, "Strategies for increasing the operating frequency range of vibration energy harvesters: a review," *Meas. Sci. Technol.*, vol. 21, no. 2, p. 022001, 2010.

[5] E. S. Leland and P. K. Wright, "Resonance tuning of piezoelectric vibration energy scavenging generators using compressive axial preload," *Smart Mater. Struct.*, vol. 15, no. 5, p. 1413, 2006.

[6] C. Gu, Lei; Livermore, "Passive self-tuning energy harvester for extracting energy from rotational motion," *Appl. Phys. Lett.*, vol. 97, p. 081904, 2010.

[7] M. Marzencki, M. Defosseux, and S. Basrour, "Mems vibration energy harvesting devices with passive resonance frequency adaptation capability," *J. Microelectromech. Syst.*, vol. 18, no. 6, pp. 1444 –1453, dec. 2009.

[8] L. G. W. Tvedt, D. S. Nguyen, and E. Halvorsen, "Nonlinear behavior of an electrostatic energy harvester under wide- and narrowband excitation," *J. Microelectromech. Syst.*, vol. 19, no. 2, pp. 305 –316, april 2010.

[9] X. Dai, X. Miao, L. Sui, H. Zhou, X. Zhao, and G. Ding, "Tuning of nonlinear vibration via topology variation and its application in energy harvesting," *Appl. Phys. Lett.*, vol. 100, p. 031902, 2012.

[10] B. Marinkovic and H. Koser, "Demonstration of wide bandwidth energy harvesting from vibrations," *Smart Mater. Struct.*, vol. 21, no. 6, p. 065006, 2012.

[11] S. G. Burrow and L. R. Clare, "A resonant generator with non-linear compliance for energy harvesting in high vibrational environmen," in *Proc. IEEE IEMDC*, 2007.

[12] F. Cottone, H. Vocca, and L. Gammaitoni, "Nonlinear energy harvesting," *Phys. Rev. Lett.*, vol. 102, no. 8, p. 080601, Feb 2009.

[13] M. Ferrari, V. Ferrari, M. Guizzetti, B. And, S. Baglio, and C. Trigona, "Improved energy harvesting from wideband vibrations by nonlinear piezoelectric converters," *Sensors Actuators A*, vol. 162, no. 2, pp. 425 – 431, 2010.

[14] S. C. Stanton, B. P. Mann, and B. A. M. Owens, "Melnikov theoretic methods for characterizing the dynamics of the bistable piezoelectric inertial generator in complex spectral environments," *Physica D: Nonlinear Phenomena*, vol. 241, no. 6, pp. 711–720, MAR 15 2012.

[15] A. Erturk and D. Inman, "Broadband piezoelectric power generation on high-energy orbits of the bistable duffing oscillator with electromechanical coupling," *J. Sound Vib.*, vol. 330, no. 10, pp. 2339 – 2353, 2011.

[16] S. C. Stanton, C. C. McGehee, and B. P. Mann, "Reversible hysteresis for broadband magnetopiezoelastic energy harvesting," *Appl. Phys. Lett.*, vol. 95, 2009.

[17] D. S. Nguyen, E. Halvorsen, G. U. Jensen, and A. Vogl, "Fabrication and characterization of a wideband MEMS energy harvester utilizing nonlinear springs," *J. Micromech. Microeng.*, vol. 20, no. 12, p. 125009, 2010.

[18] S. D. Nguyen, N.-H. T. Tran, E. Halvorsen, and I. Paprotny, "Design and fabrication of mems electrostatic energy harvester with nonlinear springs and vertical sidewall electrets," in *Power MEMS 2011 Technical Digest Poster Sessions*, vol. Oral Sessions, Seoul, Republic of Korea, Nov. 15–18 2011, pp. 126–129.

[19] M. Soliman, E. Abdel-Rahman, E. El-Saadany, and R. Mansour, "A design procedure for wideband micropower generators," *J. Microelectromech. Syst.*, vol. 18, no. 6, pp. 1288 –1299, dec. 2009.

[20] H. Liu, C. J. Tay, C. Quan, T. Kobayashi, and C. Lee, "Piezoelectric mems energy harvester for low-frequency vibrations with wideband operation range and steadily increased output power," *J. Microelectromech. Syst.*, vol. 20, no. 5, pp. 1131 –1142, oct. 2011.

[21] H. Liu, C. Lee, T. Kobayashi, C. J. Tay, and C. Quan, "Piezoelectric mems-based wideband energy harvesting systems using a frequency-up-conversion cantilever stopper," *Sensors Actuators A*, no. 0, pp. –, 2012.

[22] C. P. Le and E. Halvorsen, "Mems electrostatic energy harvesters with end-stop effects," *J. Micromech. Microeng.*, vol. 22, no. 7, p. 074013, 2012.

[23] D. S. Nguyen and E. Halvorsen, "Analysis of vibration energy harvesters utilizing a variety of nonlinear springs," in *Power MEMS 2010 Technical Digest Poster Sessions*, vol. Poster Sessions, Leuven, Belgium, Dec. 1–3 2010, pp. 331–334.

[24] E. Halvorsen, "Fundamental issues in nonlinear wide-band vibration energy harvesting," arXiv:1209.3184 [nlin.AO].

[25] Y. Suzuki, D. Miki, M. Edamoto, and M. Honzumi, "A mems electret generator with electrostatic levitation for vibration-driven energy-harvesting applications," *J. Micromech. Microeng.*, vol. 20, no. 10, p. 104002, 2010.
[26] D. Hoffmann, B. Folkmer, and Y. Manoli, "Analysis and characterization of triangular electrode structures for electrostatic energy harvesting," *J. Micromech. Microeng.*, vol. 21, no. 10, p. 104002, 2011.
[27] Z. J. Wong, J. Yan, K. Soga, and A. A. Seshia, "A multi-defree-of-freedom electrostatic mems power harvester," in *PowerMEMS 2009*, Washington DC, USA, 1-4 Dec 2009.
[28] B. Ando, S. Baglio, G. L'Episcopo, and C. Trigona, "Investigation on mechanically bistable mems devices for energy harvesting from vibrations," *J. Microelectromech. Syst.*, vol. 21, no. 99, pp. 779–790, 2012.
[29] M. Amri, P. Basset, F. Cottone, D. Galayko, F. Najar, and T. Bourouina1, "Novel nonlinear springs design for wideband vibration energy harvesters," in *PowerMEMS 2011*, Seoul, Republic of Korea, 15 - 18 Nov 2011, pp. 189–193.
[30] N.-H. T. Tran, S. D. Nguyen, and E. Halvorsen, "Design of nonlinear springs for MEMS vibration energy harvesting applications," in *Proceedings of the 22nd Micromechanics and Microsystem Technology Europe Workshop*, Tønsberg, Norway, Jun. 19–22 2011.
[31] D. A. W. Barton, S. G. Burrow, and L. R. Clare, "Energy harvesting from vibrations with a nonlinear oscillator," *J. Vib. Acoust.*, vol. 132, p. 021009 (7 pages), 2010.
[32] M. F. Daqaq, "Response of uni-modal duffing-type harvesters to random forced excitations," *J. Sound Vib.*, vol. 329, no. 18, pp. 3621 – 3631, 2010.
[33] A. M. Wickenheiser and E. Garcia, "Broadband vibration-based energy harvesting improvement through frequency up-conversion by magnetic excitation," *Smart Mater. Struct.*, vol. 19, no. 6, p. 065020, 2010.
[34] R. Masana and M. Daqqaq, "Performance of a randomly excited nonlinear energy harvester in mono- and bi-stable potentials: an experimental investigation," in *Proceedings of the IDETC*, Chicago, Illinois, USA, Aug 12-15 2012, pp. IDETC 2012–71 451.
[35] F. Peano and T. Tambosso, "Design and optimization of a MEMS electret-based capacitive energy scavenger," *J. Microelectromech. Syst.*, vol. 14, no. 3, pp. 429–435, Jun. 2005.
[36] E. Halvorsen, "Energy harvesters driven by broadband random vibrations," *J. Microelectromech. Syst.*, vol. 17, no. 5, pp. 1061–1071, Oct. 2008.
[37] J. Scruggs, "An optimal stochastic control theory for distributed energy harvesting networks," *J. Sound Vib.*, vol. 320, no. 4-5, pp. 707 – 725, 2009.

Son Duy Nguyen received the B.E. and M.E. degrees in electronics from Ho Chi Minh City University of Technology, Ho Chi Minh City, Vietnam, in 2004 and 2006, respectively. Since 2008, he has been working toward the Ph.D. degree at the Department of Micro and Nano Systems Technology, Vestfold University College, Horten, Norway, focusing on improving the bandwidth of electrostatic MEMS energy harvesters.

Einar Halvorsen (M′03) received the Siv.Ing. degree in physical electronics from the Norwegian Institute of Technology (NTH), Trondheim, Norway, in 1991, and the Dr.Ing. degree in physics from the Norwegian University of Science and Technology (NTNU, formerly NTH), Trondheim, Norway, in 1996. He has worked both in academia and the microelectronics industry. Since 2004, he has been with Vestfold University College, Horten, Norway, where he is a professor of micro- and nanotechnology. His current main research interest is in theory, design, and modeling of microeletromechanical devices.

Geir U. Jensen received the M.Sc. degree in physics and the Ph.D. degree in electrical engineering from the Norwegian Institute of Technology, Trondheim, in 1984 and 1989, respectively. His Ph.D. work was on Monte Carlo simulation of transport in III-V semiconductor devices. From 1989 to 1990, he was a Research Fellow at the University of Minnesota, Minneapolis, and from 1990 to 1991 he was a Research Scientist at the University of Virginia, Charlottesville. He was with SINTEF DELAB, Trondheim, from 1991 to 1993, and with Telenor R&D, Kjeller, Norway, from 1993 to 1995. His research in this period was in the area of design and fabrication of III-V semiconductor electronic and optoelectronic devices. Since 1995, Dr. Jensen has been with SINTEF ICT, Oslo, where he is involved in research and development of micromachined sensors and actuators as a Senior Scientist.

Paper No. 7

Nguyen2011b PowerMEMS, Conference paper

Title: "Design and fabrication of MEMS electrostatic energy harvester with nonlinear springs and vertical sidewall electrets".

Authors: Son D Nguyen, Ngoc Han T. Tran, Einar Halvorsen and Igor Paprotny.

Proceedings of: *PowerMEMS 2011*

Page: 126 - 129

Date: Nov 15 – 18, 2011

Place: Seoul, Republic of Korea.

DESIGN AND FABRICATION OF MEMS ELECTROSTATIC ENERGY HARVESTER WITH NONLINEAR SPRINGS AND VERTICAL SIDEWALL ELECTRETS

Son D. Nguyen[1*], Ngoc-Han T. Tran[1], Einar Halvorsen[1], Igor Paprotny[2]
[1]Department of Micro and Nano Systems Technology, IMST, Horten, Norway
[2]Departement of Electrical Engineering & Computer Sciences, BSAC, Berkeley, USA
*Presenting Author: duy.s.nguyen@hive.no

Abstract: This paper reports the design and fabrication of a MEMS electrostatic energy harvester with nonlinear springs and vertical sidewall electrets based on silicon MEMS fabrication technology. A SPICE model shows that the harvester can work in a wide bandwidth of 540 Hz under white noise acceleration at a level of 76.5 x 10^{-4} g^2/Hz. The harvester is fabricated using an SOI DRIE process. The sidewall angle of our 150 µm silicon device thickness is typically 89.1^0 for the nonlinear spring and 89.7^0 for the capacitor fingers. The SiO_2/Si_3N_4 electrets layer on the sidewall capacitor finger has a thickness of about 700 – 800 nm.

Keywords: MEMS energy harvester, nonlinear springs, vertical electrets

INTRODUCTION

Traditional vibration energy harvesters are designed as linear resonating structures [1]. They have a very narrow bandwidth and operate efficiently only when the excitation frequency is very close to the resonant frequency of the harvesters. These resonant harvesters are limited in their application in real-world environments with stochastic or varying vibration spectra. There have been several attempts to overcome this limitation by tuning the resonant frequency or widening the bandwidth of the harvesters [2]. Several authors have exploited nonlinear suspensions, often created with magnets, to extend the bandwidth of the harvesters by hardening [3-5] and/or softening nonlinearities [6-8]. Electrostatic energy harvesters have been developed as a preferred choice for silicon MEMS fabrication technology [8-9]. An issue with electrostatic energy harvesters is the need for a bias or priming voltage. Electrets provide a viable means for self-bias of electrostatic energy harvesters [10], even for the vertical structures of in-plane gap closing or overlap varying transducers [11-12].

In this paper, we will present the design and fabrication of a MEMS electrostatic energy harvester with nonlinear springs and vertical sidewall electrets. The nonlinearity of springs is obtained purely by mechanical design.

DESIGN AND SIMULATION

Nonlinear spring design

Figure 1 shows the shape of a nonlinear spring at its equilibrium position. The un-deformed spring shape is constructed equal to the deformed shape of a straight clamped-guided spring with a tip displacement of y_0 [13]. The spring force vs. displacement for different y_0 is shown in Figure 2. Clearly, the behavior of the nonlinear spring is different depending on y_0. When the guided end moves in the positive direction, the spring appears increasingly stiffer. If it moves in the opposite direction, it becomes more compliant until it ultimately stiffens again at large displacements. For large enough initial displacement y_0, e.g. $y_0 = 40$ µm and $y_0 = 50$ µm in Figure 2, the force is zero at three points representing two stable local minima and one local maximum of the corresponding potential energy. By varying y_0, the nonlinear spring design can thus be varied continuously from linear to asymmetrically bi-stable. This design degree of freedom can be used to shape an energy harvester's spectrum. In particular it can be used to design for large bandwidths [8, 13].

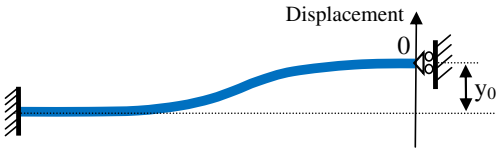

Figure 1: The shape of the nonlinear spring at its equilibrium position.

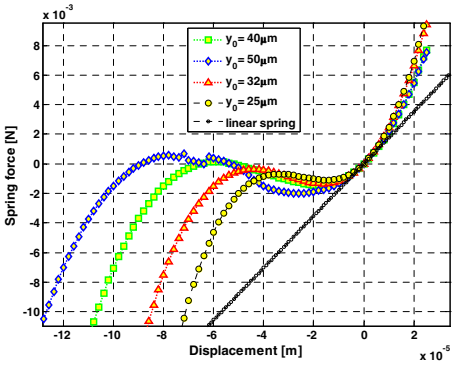

Figure 2: Spring force vs. displacement for different initial displacements y_0, calculated by the finite element method.

Energy harvester design

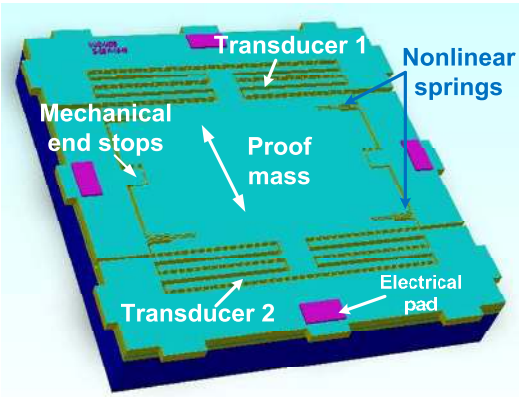

Figure 3: Schematic drawing of electrostatic energy harvester using nonlinear springs.

Table 1: Design parameters for the harvester

Symbol	Description	Value
S	Die size	10 mm x 10 mm
t	Thickness of device structure	200 µm
m	Proof mass	16.58 mg
K_1	Linear spring stiffness	770 N/m
K_2	Coefficients of the nonlinear spring stiffness	2.43×10^{7} Nm^{-2}
K_3		1.34×10^{11} Nm^{-3}
K_4		8.62×10^{14} Nm^{-4}
K_5		5.03×10^{19} Nm^{-5}
K_6		5.24×10^{23} Nm^{-6}
K_7		1.68×10^{27} Nm^{-7}
f_0	Resonant frequency at very small acceleration	1080 Hz
b	Damping coefficient (estimate)	7.5×10^{-4} Nms^{-1}
g_0	Capacitor gaps	15 µm
x_{01}	Overlap, transducer 1	22 µm
x_{02}	Overlap, transducer 2	100 µm
N	Number of capacitor pairs per transducer	315
C_{01}	Transducer 1 capacitance	1.64 pF
C_{02}	Transducer 2 capacitance	7.43 pF

The electrostatic energy harvester using nonlinear springs is designed to work in a wide vibration frequency range of 400 Hz – 1000 Hz at sufficiently high levels of acceleration. Figure 4 shows the schematic drawing of the device. It is an in-plane overlap varying type with two asymmetric transducers. To increase the coupling of the energy harvester, there is a large number of electrodes on each transducer. The device layout is fit within a 1-cm^2 area. Because the aspect ratio of deep reactive ion etch (DRIE) and the vertical sidewall electrets could potentially be affected by the device thickness, the prototypes are made with a variety of device thicknesses (125 µm, 150 µm and 200 µm). The prototypes are also designed with variety of initial displacements y_0 (25 µm, 32 µm, 40 µm and 50 µm). Typical parameters of the energy harvester with y_0 = 40 µm is shown in Table 1.

We built a lumped model for SPICE simulation as in our previous works [7-8] to simulate the harvester's responses under sinusoidal accelerations and white noise accelerations. Figure 5 shows the response of the harvester (y_0 = 40 µm) under the increasing and decreasing frequency sweeps at constant acceleration amplitudes of 1 *g* and 1.2 *g*. The softening spring effect is clearly exhibited with the widening frequency response for decreasing frequency sweeps. The output power spectral density (PSD) under white noise acceleration is shown on Figure 6. At the white noise level of 76.5×10^{-4} g^2/Hz, a wide bandwidth of about 540 Hz is obtained.

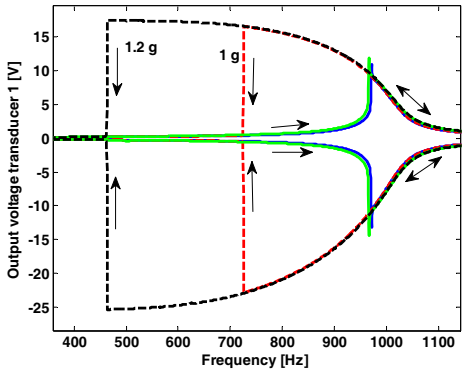

Figure 4: The increasing and decreasing frequency sweeps for many acceleration amplitudes. The bias is 150V, the load resistor of transducer 1 and transducer 2 is 20 MΩ and 21.2 MΩ respectively.

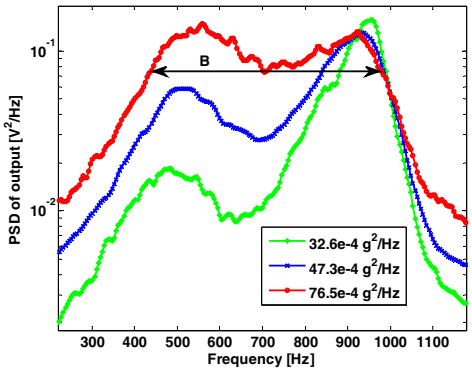

Figure 5: PSD of output voltage for few values of the white noise acceleration PSD.

FABRICATION

Fabrication process

The fabrication process aims to achieve high aspect ratio Si device structures by DRIE on silicon on isolator (SOI) wafers and SiO_2/Si_3N_4 electret layer on

the vertical sidewalls of the capacitor fingers. The harvester is fabricated on 6 inch SOI wafers with 125 µm, 150 µm or 200 µm device layer thickness, 2 µm buried oxide and 500 µm substrate thickness. The process starts with deposition of titanium (Ti) for the electrical bonding pads. Ti is selected due to its high melting temperature (1668^0C) so that it can be allowed in the furnace for oxidation and low pressure vapor chemical deposition (LPVCP) in later steps. The Ti layer is then wet etched using Hydrogen peroxide plus a few percents of Ammonium hydroxide (step 1). In step 2, 200 - 300 nm silicon nitride (Si_3N_4) is deposited by LPCVD method as a passivation layer for local oxidation of silicon in later step. In the next step, the wafers are coated by spinning a thick SPR 220-7 photoresist (about 10 – 11 µm at 1800 revolutions per minute) as a mask for DRIE. In the lithography step, a multiple exposure process is used to avoid cracking of the thick photoresist in the development step. The wafers are then DRIE etched in a Surface Technology Systems Advanced Silicon Etch equipment. The (SF_6 + O_2) gas in the DRIE process will etch the thin Si_3N_4 layer and then the Si device layer. The etching process stops on the buried oxide layer (step 3).

The wafers are then thermally oxidized at 1000^0C to grow about 500-nm silicon dioxide on the sidewalls for the electret layer. Only the silicon on the sidewall is oxidized, since the silicon on the topside is passivated by Si_3N_4 on the topside (step 4). The Si_3N_4 is then subsequently removed using 160^0C hot phosphoric which has a good selectivity of etching Si_3N_4 over SiO_2 and Si (step 5). To make a thin Si_3N_4 layer on the SiO_2 forming a suitable structure for the sidewall electrets, a 300 – 400 nm Si_3N_4 layer is deposited by LPCVD (step 6) and subsequently removed from the top structure by an anisotropic plasma etch (step 7). The wafers are then DRIE etched from the backside. To etch the 500-µm silicon of the substrate layer, the wafers need to be bonded on a handle wafer using cool grease which is a high thermal conductivity material. As a mask for DRIE of the substrate, the thick photoresist is again used. The post-bake step lasts much longer (from 8 to 10 hours) to increase the selectivity of photoresist mask (step 8). Since the SiO_2 on the vertical sidewall is protected by the Si_3N_4 layer, Buffered Hydrofluoric is used to etch the buried oxide layer to release the proof mass.

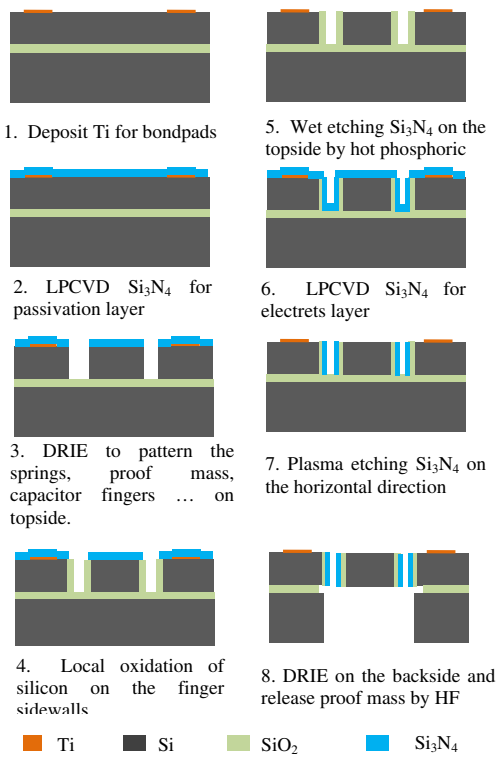

Figure 6: Fabrication process for MEMS electrostatic energy harvester with nonlinear springs and vertical sidewall electrets.

Fabrication results

Figure 8 shows the picture of the harvester die after fabrication. The backside view of the harvester with the nonlinear spring and the capacitor fingers is shown in Figure 9. Due to the non-uniform etching in the DRIE process – the fastest etching is near the rim of the wafer and gradually reduces towards the center. The sidewall profile of the nonlinear springs is somewhat different from die to die, depending on its position on the wafer. A typical sidewall angle of a nonlinear spring is about 89.1^0 for 150-µm Si device thickness. Figure 10 shows the cross-section view of the capacitor fingers. A profile angle of 89.7^0 is observed in this situation. The SiO_2/Si_3N_4 electret layer on the sidewall finger has a thickness of about 700 – 800 nm (Figure 11).

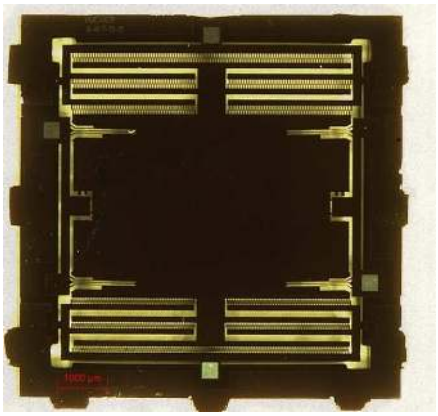

Figure 7: The picture of the harvester after fabrication

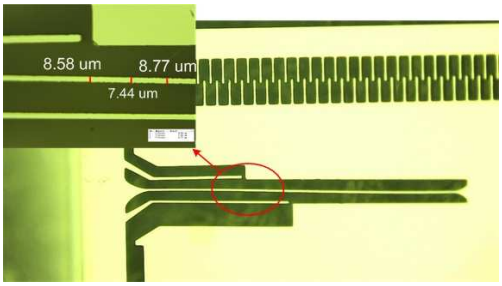

Figure 8: The back side view of the nonlinear spring and the capacitor fingers.

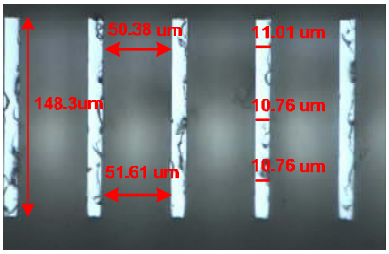

Figure 9: The cross-section view of the capacitor fingers.

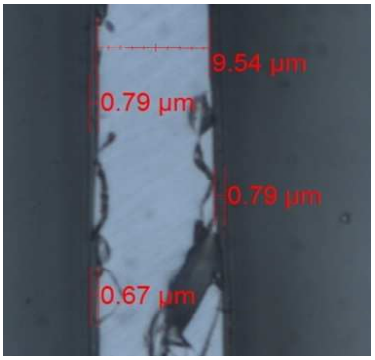

Figure 10: The cross-section view of a capacitor finger with SiO_2/Si_3N_4 electret layer.

CONCLUSION

We have presented the design and fabrication of a MEMS electrostatic energy harvester with nonlinear springs and vertical sidewall electrets based on SOI DRIE fabrication technology. Simulations indicate that a wide bandwidth of 540 Hz can be achieved by this design under white noise acceleration at a level of 76.5 $\times 10^{-4}$ g^2/Hz. The harvester is fabricated using an SOI DRIE process. The sidewall angle of our 150 µm silicon device thickness is typically 89.1^0 for the nonlinear spring and 89.7^0 for the capacitor fingers. The SiO_2/Si_3N_4 electret layer on the sidewall capacitor fingers has a thickness of about 700 – 800 nm. Charging of the vertical sidewall SiO_2/Si_3N_4 electrets and characterization of the nonlinear-spring energy harvester will be pursued in the future.

ACKNOWLEDGEMENT

The authors grateful thank to Sia Parsa (Marvell Nanolab) and Antwi Nimo (IMTEK) for the useful and stimulating discussion on the fabrication. This work is supported by The Norwegian Centre for International Cooperation in Higher Education (SIU) contract no. MNA-2008/10004 and the Research Council of Norway (RCN) Grant no. 191282. The devices were fabricated at the U.C. Berkeley nanofabrication facility.

REFERENCES

[1] Mitcheson P D, Yeatman E M, Rao G K, Holmes A S and Green T C 2008 Energy Harvesting From Human and Machine Motion for Wireless Electronic Devices *Proceedings of the IEEE* **96** 1457--86

[2] Zhu D, Tudor J and Beeby S 2009 Strategies for increasing the operating frequency range of vibration energy harvesters: a review *Meas. Sci. Technol.* **21** 022001

[3] Burrow S G and Clare L R 2007 A resonant generator with non-linear compliance for energy harvesting in high vibrational environments *IEEE Int. Electric Machines & Drives Conference, IEMDC '07* **1** 715

[4] Marinkovic B and Koser H 2009 Smart Sand---a wide bandwidth vibration energy harvesting platform *Appl. Phys. Lett.* **94** 103505

[5] Marzencki M, Defosseux M and Basrour S 2009 MEMS Vibration Energy Harvesting Devices With Passive Resonance Frequency Adaptation Capability *J. Microelectromech. Syst.* **18** 1444-53

[6] Stanton S C, McGehee C C and Mann B P 2009 Reversible hysteresis for broadband magnetopiezoelastic energy harvesting *Appl. Phys. Lett.* **95** 174103

[7] Tvedt L G W, Nguyen D S and Halvorsen E 2010 Nonlinear Behavior of an Electrostatic Energy Harvester Under Wide- and Narrowband Excitation *J. Microelectromech. Syst.* **19** 305-16

[8] Nguyen D S, Halvorsen E, Jensen G U and Vogl A 2010 Fabrication and characterization of a wideband MEMS energy harvester utilizing nonlinear springs *J. Micromech. Microeng.* **20** 125009

[9] Hoffmann D, Folkmer B and Manoli Y 2009 Fabrication, characterization and modelling of electrostatic micro-generators *Journal of Micromechanics and Microengineering* **19** 094001 (11pp)

[10] Suzuki Y 2011 Recent Progress in MEMS Electret Generator for Energy Harvesting *IEEJ Trans. Elec. Electron. Eng.* **6** 101-11

[11] Nimo A, Mescheder U, Müller B and Elkeir A S A 2011 3D Capacitive Vibrationional Micro Harvester using Isotropic Charging of Electrets Deposited on Vertical Sidewalls *Proc. of SPIE* **8066** 80661Q1 - Q14

[12] Yamashita K, Honzumi M, Hagiwara K, Iguchi Y and Suzuki Y 2010 Vibration-driven MEMS energy harester with vertical electrets *PowerMEMS 2010 (Dec 1-4, Leuven, Belgium)* 165-8

[13] Tran N-H T, Nguyen S D and Halvorsen E 2011 Design of nonlinear springs for MEMS vibration energy harvesting applications *Micromechanics and Micro systems Europe Workshop (June 19-22, 2011, Toensberg, Norway).*

Paper No. 8

Nguyen2013 APL, Journal Article

Title: "Bistable springs for wideband MEMS energy harvesters".

Authors: Son Duy Nguyen, Einar Halvorsen and Igor Paprotny.

Journal: *Applied Physics Letters.*

Volume: 102**, Issue:** 02**, page(s):** 3904 1-4

Date of Publication: Jan 2013.

Bistable springs for wideband microelectromechanical energy harvesters

Son D. Nguyen,[1,a)] Einar Halvorsen,[1,b)] and Igor Paprotny[2,c)]
[1]*Department of Micro and Nano Systems Technology, Faculty of Technology and Maritime Sciences, Vestfold University College, Horten, Norway*
[2]*Berkeley Sensor & Actuator Center (BSAC), University of California, Berkeley, California 94720-1774, USA*

(Received 24 October 2012; accepted 26 December 2012; published online 15 January 2013)

This paper presents experimental results on a microelectromechanical energy harvester with curved springs that demonstrates an extremely wide bandwidth. The springs display an asymmetrical bistable behavior obtained purely through their geometrical design. The frequency down-sweep shows that the harvester 3-dB bandwidth is about 587 Hz at 0.208-g acceleration amplitude. For white noise excitation at $4 \times 10^{-3}\ g^2/\text{Hz}$, we found that the bandwidth reaches 715 Hz, which is more than 250 times wider than in the linear-spring regime. By varying the bias voltage, an output power of 3.4 μW is obtained for frequency down-sweep at 1-g amplitude and 150-V bias. © *2013 American Institute of Physics*. [http://dx.doi.org/10.1063/1.4775687]

In recent years, energy harvesting from ambient environmental vibrations has been proposed for powering wireless sensors.[1,2] However, linear resonating energy harvesters with a narrow bandwidth are not suited for real world applications since ambient vibration sources usually have a wide spectrum of frequencies or varying vibration spectra. For example, the vibration of car tires have very wide frequency spectrum, spread from 300 Hz to about 800 Hz.[3,4] Developing techniques to widen the bandwidth of vibration energy harvesters has become the next important problem in this field.

Three common nonlinearities of suspensions—hardening, softening, and bistability have been recently exploited to increase the harvester bandwidth.[5–24] Symmetric bistable suspensions have shown a great potential for increasing energy harvester bandwidth.[5,9,11,13] To achieve bistable behavior, these harvesters use permanent magnets. It has been proposed[24,25] that asymmetric bistable behavior without the use of magnets can be obtained for energy harvesters with three-segmented springs[26] or curved springs.[27] However, such asymmetric bistability has not yet been experimentally verified.

In this paper, we present experimental results for a wideband electrostatic energy harvester with curved springs based on microelectromechanical systems (MEMS) technology. It can operate from 373 Hz to 1088 Hz for sufficiently large white noise vibration. The curved springs demonstrate asymmetrical bistable behavior obtained purely through their geometrical design.

Fig. 1 shows the MEMS electrostatic energy harvester with curved springs. It has two asymmetrical in-plane overlap-varying transducers, referred to as transducer 1 and transducer 2. The device is fabricated on a silicon-on-insulator wafer using bulk microfabrication technology.[28] The chip area is 1×1 cm and the device layer is 150-μm thick. The sidewalls of the capacitor fingers are oxidized to allow for vertical-electret biasing.[29] In this work, we focus on studying broadband performance of the harvester using an external voltage to bias the device.

Fig. 2 shows the restoring force versus displacement for the curved springs calculated using the finite element method (FEM). The FEM model includes the undercut of the deep

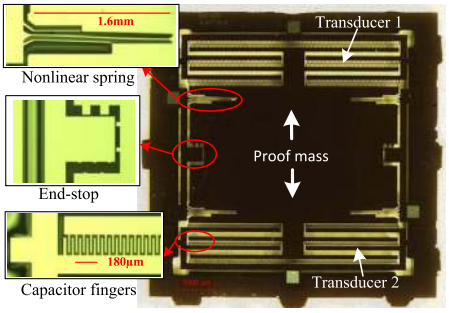

FIG. 1. Optical micrograph of MEMS electrostatic energy harvester with curved springs.

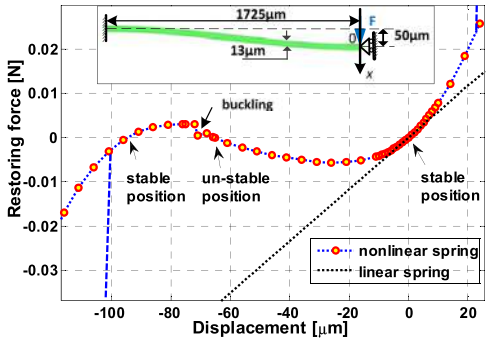

FIG. 2. Restoring force vs. displacement for the curved springs calculated by the FEM. The proof mass displacement is limited to -100 μm and 22 μm by mechanical end stops. Inset: schematic drawing of the curved spring. Spring dimensions: length 1725 μm, width 13 μm (top) and 8.5 μm (bottom), thickness 150 μm.

[a)]duy.s.nguyen@hive.no.
[b)]einar.halvorsen@hive.no.
[c)]igorpapa@eecs.berkeley.edu.

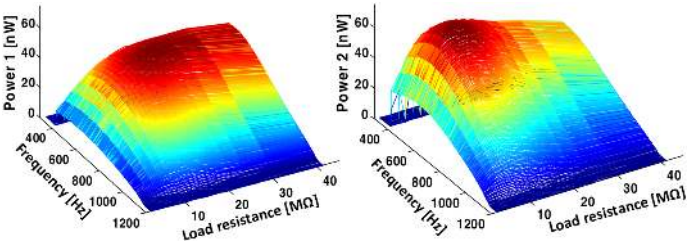

FIG. 3. Output power on transducer 1 (left) and transducer 2 (right) vs. frequency and load resistance.

reactive ion etch process resulting in a non-rectangular cross section. For small displacements, the springs behave linearly. For further displacement in the positive direction, the curved springs have increasing stiffness. In the negative direction they first exhibit softening behavior, reach an unstable equilibrium point at $-65\ \mu$m displacement, then a stable equilibrium position at $-95\ \mu$m. Beyond this point, the stiffness increases (hardening behavior). Consequently, these curved springs are asymmetrically bistable. The springs buckle at a displacement of about $-71\ \mu$m.

Fig. 3 shows the output power versus load resistance on transducer 1 and 2, respectively. Since the optimal load depends on the excitation frequency, the output power for each resistance value is measured by frequency down-sweep. When the frequency varies from 1149 Hz (the resonant frequency) to 400 Hz, the optimal load of transducer 1 changes from 9 MΩ to about 22 MΩ while the optimal load of transducer 2 changes from about 7 MΩ to about 14 MΩ. In the later experiments, the load is fixed at the optimal load in the softening spring regime, e.g., $R_{L1} = 14.5\,\text{M}\Omega$ and $R_{L2} = 10\,\text{M}\Omega$.

Fig. 4 shows the frequency-response curves of the harvester under frequency up-sweep at very small acceleration amplitudes such that the device works in the linear-spring regime. As a resonant energy harvester, the device works with very narrow bandwidth of about 2.8 Hz (3-dB bandwidth), corresponding to a total quality factor of about 410.

The response curves for frequency sweeps at larger acceleration amplitudes are shown in Fig. 5. For frequency up-sweeps, the harvester responds with a narrow bandwidth. For frequency down-sweeps, the bandwidth is broadened in a somewhat complex manner with increasing acceleration amplitude. The sensitivity of bandwidth increase to acceleration-amplitude increase becomes very small when approaching 0.200 g and a jump-down frequency of 800 Hz. This is illustrated by the 0.125 g, 0.176 g, and 0.200 g traces. A small increase beyond this threshold, e.g., to 0.208 g, results in an abrupt transition to a jump-down frequency of 380 Hz. This can be explained by the proof mass reaching the unstable point (see Fig. 2) at the threshold. The harvester 3-dB bandwidth in this case reaches 587 Hz, which is about 209 times wider than the 3-dB bandwidth in the linear-spring regime.

During the experiments at larger than 0.200 g amplitude, we sometimes observed down-sweeps indicating a resonant frequency of about 820 Hz instead of 1149 Hz, e.g., the lower frequency-response curve for 0.208-g amplitude in Fig. 5. We interpret this as the initial position of the proof mass being at the locally stable point ($-95\ \mu$m in Fig. 2) and therefore a direct observation of the bistable behavior.

The output power versus down-sweep frequency for several bias voltages is shown in Fig. 6. The jump-down frequency depends on the bias since increasing the bias voltage will increase the electrical damping and the total damping. So, to get the same jump-down frequency point, higher bias requires higher acceleration amplitude. The harvester still maintains wide bandwidth response at high bias voltages. At the bias voltage of 150 V, a maximum output power of 3.4 μW is achieved, corresponding to $226\mu\text{W}/\text{cm}^3$.

Fig. 7 shows the average output power versus power spectral density (PSD) of acceleration for white noise vibrations. The output power increases with increasing acceleration PSD, but at different rates for small

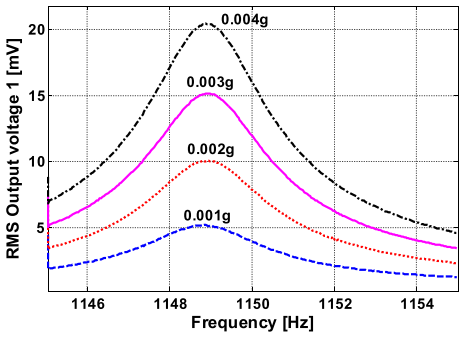

FIG. 4. RMS output voltage vs. frequency for very small acceleration amplitudes, $R_{L1} = 14.5\,\text{M}\Omega$, $R_{L2} = 10\,\text{M}\Omega$, bias voltage $V_e = 36$ V.

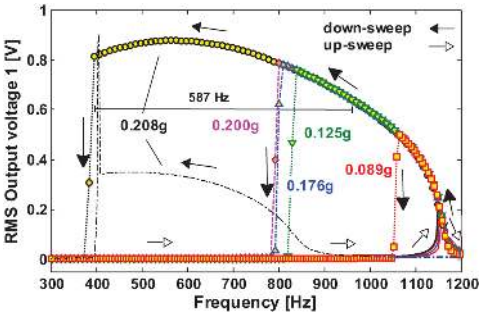

FIG. 5. RMS output voltage vs. frequency for both up- and down-sweeps at different acceleration amplitudes of 0.089, 0.125, 0.176, 0.200 and 0.208 g. $R_{L1} = 14.5\,\text{M}\Omega$, $R_{L2} = 10\,\text{M}\Omega$, $V_e = 36$ V.

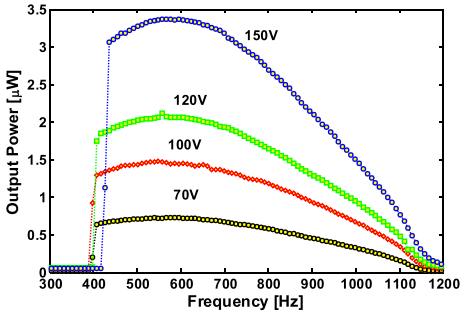

FIG. 6. Output power vs. down-sweep frequency for several bias voltages and acceleration amplitudes: 70 V-0.358 g, 100 V-0.541 g, 120 V-0.702 g, and 150 V-0.998 g.

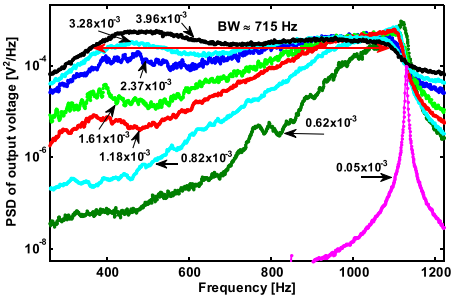

FIG. 8. Output voltage PSD for increasing acceleration PSD of the white noise vibrations, acceleration PSD of 0.05×10^{-3}, 0.62×10^{-3}, 0.82×10^{-3}, 1.18×10^{-3}, 1.61×10^{-3}, 2.37×10^{-3}, 3.28×10^{-3}, and $3.96\times10^{-3}\,g^2/\text{Hz}$.

($\leq 0.8\times10^{-3}\,g^2/\text{Hz}$) and large acceleration PSD ($\geq 0.8\times10^{-3}\,g^2/\text{Hz}$). The reason for this difference in slope may be that the proof mass impacts the mechanical end stops more frequently for larger acceleration PSDs.

The PSDs of output voltage for some selected acceleration PSD values are shown in Fig. 8. At small acceleration level of $5\times10^{-5}\,g^2/\text{Hz}$, where the harvester works in the linear-spring regime, the harvester responds with narrow bandwidth. Increasing the acceleration levels, the response bandwidth dramatically increases. At the acceleration level of $3.96\times10^{-3}\,g^2/\text{Hz}$, a harvester 3-dB bandwidth of 715 Hz (cut-off frequency from 373 Hz to 1088 Hz) is achieved. Compared to the 3-dB bandwidth in the linear-spring regime, this bandwidth is more than 250 times larger.

The coupling of an electrostatic energy harvester increases with increasing a bias voltage and results in a corresponding overall increase of the average output power when driven by white noise. The power versus bias voltage for the white noise vibration of $3.96\times10^{-3}\,g^2/\text{Hz}$ is shown in Fig. 9. Because the output voltage is measured through a buffer amplifier OPA2137 which has an input-voltage limit of 18 V, the highest bias voltage in this experiment is limited to 200 V. An average output power of about 1.5 μW is achieved at this maximum voltage.

Table I shows the comparison of the measured 3-dB bandwidths of some wideband energy harvesters reported in the literature. The MEMS energy harvester with curved springs obtains the largest 3-dB bandwidth and the second largest normalized frequency 3-dB bandwidth of nearly 1.

The bistable characteristic of the springs is attained purely by geometrical design. This approach is better suited for micro-fabrication than the use of permanent magnets. The bandwidth enhancement of the nonlinear harvester hinges on sufficiently large proof mass displacements. The device is therefore only suited to wide-band operation for ambient vibrations beyond a certain acceleration level.

The maximum output powers of 3.4 μW for frequency sweep and 1.5 μW for white noise were obtained at bias voltages of 150 V and 200 V, respectively. These high bias voltages are potentially challenging to obtain for vertical electrets. However, the achievement of 95 V from the demonstration of a vertical electret in Reference 29, shows that it is not unrealistic to expect electret-voltages in our bias-voltage range.

In conclusion, we presented experimental results for a MEMS energy harvester using curved springs that demonstrated an extremely wide bandwidth. The fabricated curved springs displayed an asymmetrical bistable behavior, which was obtained purely by their geometrical design. Under the frequency down-sweep, a harvester 3-dB bandwidth of 587 Hz was achieved at an acceleration amplitude of 0.208 g. The device responded with wide bandwidth and obtained a

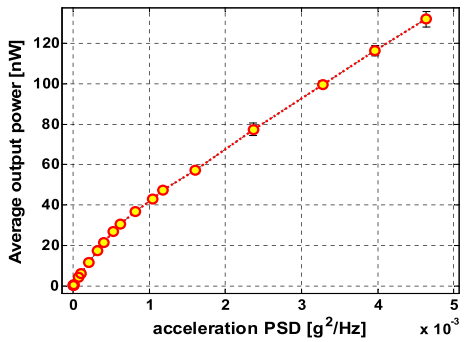

FIG. 7. Average output power vs. acceleration PSD of white noise excitations, the bias voltage Ve = 36 V.

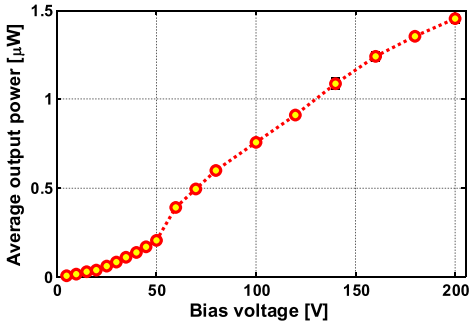

FIG. 9. Average output power vs. bias voltage for the white noise vibration with the acceleration PSD of $3.96\times10^{-3}\,g^2/\text{Hz}$.

TABLE I. Comparison of the measured normalized bandwidth of some wideband energy harvesters (A: the rms acceleration, BW: 3-dB bandwidth, f_c: the central frequency of 3-dB bandwidth, NFB $= BW/f_c$: normalized frequency 3-dB bandwidth).

Ref.	Approach	Non-linearity	Device scale	A (g)	BW (Hz)	f_c (Hz)	NFB
6	End-stops	Hardening	Macro	0.1	5	96.5	0.05
7	Magnetic forces (MF)	Softening	Macro	0.3	3	12.1	0.25
11	MF	Bistable	Macro	0.35	1.5	7.25	0.21
14	MF	Bistable	Macro	2	4.5	11.5	0.39
13	MF	Bistable	Macro	0.3	7	14.5	0.48
18	MF	…	Macro	1	16	30	0.53
30	End-stops	Hardening	MEMS	1.4	14	33	0.42
21	End-stops	Hardening	MEMS	3.2	70	55	1.27
19	End-stops	Hardening	MEMS	1	17	36	0.47
22	Stretching	Hardening	MEMS	0.8	12	186	0.07
16	Beam shape	Softening	MEMS	$7 \times 10^{-4}\ g^2/\text{Hz}$	60	543	0.11
This work	Beam shape	Bistable	MEMS	$4 \times 10^{-3}\ g^2/\text{Hz}$	715	730	0.98

maximum output of 3.4 μW at high bias voltage of 150 V. For a white noise excitation at the level of $4 \times 10^{-3}\ g^2/\text{Hz}$, the harvester 3-dB bandwidth reached 715 Hz, which is more than 250 times wider than in linear-spring regime.

Such wideband MEMS energy harvesters are well-suited to extract power from wide spectrum vibrations such as in car tires or from sources with a wide range of variability in the spectrum. Charging the dielectric layers on the sidewall of capacitor fingers to create electrets to bias the harvester is the topic of our future work.

This work was supported by The Norwegian Centre for International Cooperation in Higher Education (SIU) contract no. MNA-2008/10004 and the Research Council of Norway (RCN) Grant no. 191282. The devices were fabricated at the Marvell Nanofabrication Laboratory-U.C. Berkeley and HiVe MST-Lab-Vestfold University College.

[1]P. D. Mitcheson, E. M. Yeatman, G. K. Rao, A. S. Holmes, and T. C. Green, Proc. IEEE **96**, 1457 (2008).
[2]E. Mounier, in *dMEMS 2012*, Besancon, France, 2-3 April 2012.
[3]M. Lohndorf, T. Kvisterøy, E. Westby, and E. Halvorsen, in *PowerMEMS 2007 Technical Digest, Freiburg*, 2007, pp. 331–334.
[4]S. Roundy, in *Proceedings of PowerMEMS 2008+ microEMS 2008, Sendai, Japan, 9–12 November, 2008* (2008), pp. 1–6.
[5]S. G. Burrow and L. R. Clare, in *Proceedings of IEEE IEMDC, May 3–5, Antalya, Turkey* (IEEE, 2007), pp. 715–720, DOI: 10.1109/IEMDC.2007.382755.
[6]M. S. M. Soliman, E. M. Abdel-Rahman, E. F. El-Saadany, and R. R. Mansour, J. Micromech. Microeng. **18**, 115021 (2008).
[7]S. C. Stanton, C. C. McGehee, and B. P. Mann, Appl. Phys. Lett. **95**, 174103 (2009).
[8]B. P. Mann and N. D. Sims, J. Sound Vib. **319**, 515 (2009).
[9]F. Cottone, H. Vocca, and L. Gammaitoni, Phys. Rev. Lett. **102**, 080601 (2009).
[10]L. Gammaitoni, I. Neri, and H. Vocca, Appl. Phys. Lett. **94**, 164102 (2009).
[11]A. Erturk, J. Hoffmann, and D. J. Inman, Appl. Phys. Lett. **94**, 254102 (2009).
[12]M. Marzencki, M. Defosseux, and S. Basrour, J. Microelectromech. Syst. **18**, 1444 (2009).
[13]M. Ferrari, V. Ferrari, M. Guizzetti, B. Andò, S. Baglio, and C. Trigona, Sens. Actuators A **162**, 425 (2010).
[14]A. F. Arrieta, P. Hagedorn, A. Erturk, and D. J. Inman, Appl. Phys. Lett. **97**, 104102 (2010).
[15]L. G. W. Tvedt, D. S. Nguyen, and E. Halvorsen, J. Microelectromech. Syst. **19**, 305 (2010).
[16]D. S. Nguyen, E. Halvorsen, G. U. Jensen, and A. Vogl, J. Micromech. Microeng. **20**, 125009 (2010).
[17]A. Hajati and S.-G. Kim, Appl. Phys. Lett. **99**, 083105 (2011).
[18]T. Galchev, H. Kim, and K. Najafi, J. Microelectromech. Syst. **20**, 852 (2011).
[19]H. Liu, C. J. Tay, C. Quan, T. Kobayashi, and C. Lee, J. Microelectromech. Syst. **20**, 1131 (2011).
[20]S. D. Nguyen and E. Halvorsen, J. Microelectromech. Syst. **20**, 1225 (2011).
[21]B. Marinkovic and H. Koser, Smart Mater. Struct. **21**, 065006 (2012).
[22]X. Dai, X. Miao, L. Sui, H. Zhou, X. Zhao, and G. Ding, Appl. Phys. Lett. **100**, 031902 (2012).
[23]B. P. Mann, D. A. W. Barton, and B. A. M. Owens, J. Intell. Mater. Syst. Struct. **23**, 1451 (2012).
[24]B. Andò, S. Baglio, G. L'Episcopo, and C. Trigona, J. Microelectromech. Syst. **21**, 779 (2012).
[25]N.-H. T. Tran, S. D. Nguyen, and E. Halvorsen, in Proceedings of the 22nd Micromechanics and Microsystem Technology Europe Workshop, Tønsberg, Norway, June 19–22, 2011.
[26]J. Wittwer, M. Baker, and L. Howell, J. Microelectromech. Syst. **15**, 33 (2006).
[27]S. Krylov and Y. Bernstein, Sens. Actuators A **130–131**, 497 (2006).
[28]S. D. Nguyen, N.-H. T. Tran, E. Halvorsen, and I. Paprotny, in *PowerMEMS 2011, Seoul, Republic of Korea, 15–18 November 2011* (Cell Bench Research Center, KAIST, 2011), pp. 126–129.
[29]K. Yamashita, M. Honzumi, K. Hagiwara, Y. Iguchi, and Y. Suzuki, in *PowerMEMS 2010, Leuven, Belgium, November 30-December 3, 2010* (2010), pp. 165–168.
[30]K. Matsumoto, K. Saruwatari, and Y. Suzuki, in *PowerMEMS 2011, Seoul, Republic of Korea, 15–18 November 2011* (Micropower Generation group, imec/Holst Centre, Department of Mechanical Engineering, Katholieke Universiteit Leuven, 2011), pp. 134–137.

Appendix A

Modeling of MEMS electrostatic energy harvester

In this appendix, we present a nonlinear dynamic model of MEMS electrostatic energy harvester with nonlinear springs and its lumped model for SPICE simulation. All energy harvesting devices in this work can be modeled as the schematic drawing shown in Fig. A.1-ii. They are an in-plane overlap varying type with two symmetrical transducers [131] or two asymmetrical transducers [132; 134]. The suspensions of the proof mass display a nonlinear characteristic and therefore are expressed by a nonlinear spring in the model.

A.1 Mathematical model

In modeling the variable capacitances, the parallel plate capacitor formula for the inter-electrode capacitances $C_{\mathrm{T},1}$ and $C_{\mathrm{T},2}$ can be used together with stray capacitances $C_{\mathrm{p},1}$ and $C_{\mathrm{p},2}$ as indicated in the Fig. A.1-ii. The two anti-phase capacitors of the first prototype [131] are made equal, but due to asymmetries in the nonlinear springs of the later prototypes [132; 134], asymmetrical transducers is considered with different nominal overlaps x_1 and x_2 of the electrode fingers. The capacitances are then given by

$$C_{1/2}(x) = C_{p,1/2} + C^0_{1/2}(1 \mp \frac{x}{x_{1/2}}) \tag{A.1}$$

A. MODELING OF MEMS ELECTROSTATIC ENERGY HARVESTER

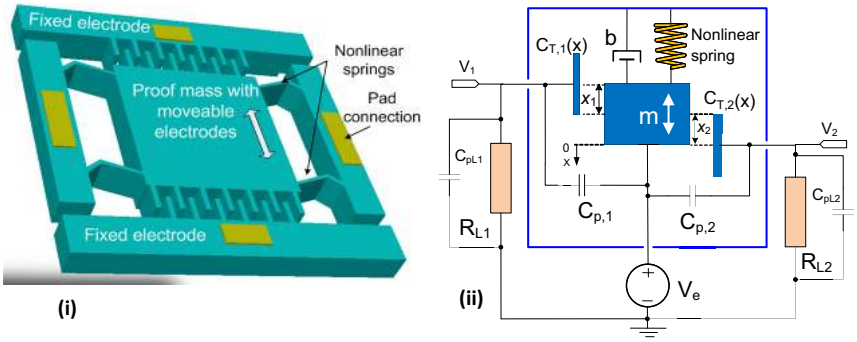

Figure A.1: In-plane overlap varying electrostatic energy harvester, (i) geometry [132] , (ii) schematic drawing model.

where $C^0_{1/2} = 2N\epsilon_0 t x_{1/2}/g_0$, N is the number of fingers of the comb structure, ϵ_0 is the permittivity of vacuum, t is the thickness the fingers and g_0 is the gap between the fingers.

From the Newton's second law for the proof mass and the Ohm's law for the circuitry, the equations for the harvester are

$$m\ddot{x} = -F_{\mathrm{r}} - F_{\mathrm{e}} - b\dot{x} - F_{\mathrm{s}} + ma \tag{A.2}$$

$$V_{1/2} = \frac{Q_{1/2}}{C_{1/2}(x)} + V_e \tag{A.3}$$

where m is the mass, a is the negative of the package acceleration, b is the constant for linear mechanical damping representing parasitic mechanical loss, Q_1 and Q_2 are the charge on capacitors C_1 and C_2 respectively, and V_e is the bias voltage. F_{r}, F_{s} and F_{e} are a restoring force (or spring force), an end-stop force and a electrical force respectively.

The electrical force is given by

$$F_{\mathrm{e}} = \frac{1}{2}Q_1^2\frac{d}{dx}\frac{1}{C_1(x)} + \frac{1}{2}Q_2^2\frac{d}{dx}\frac{1}{C_2(x)}. \tag{A.4}$$

The end-stop force can be modeled as a spring-damper system that is engaged at sufficiently large displacements. For such rigid end-stops, the simple spring-

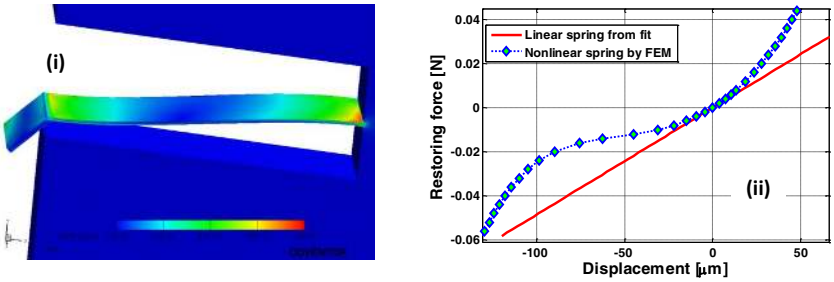

Figure A.2: (i) FEM CoventorWare model to calculate the restoring force-displacement curve of the angled spring. (ii) Restoring force-displacement curve of the angled spring.

dashpot model is adequate [107; 126]. A simple model of ideal rigid end-stops can be given as [144]

$$\mathrm{F_s} = \begin{cases} 0, & \text{if } x_{s,2} \leq x \leq x_{s,1} \\ k_\mathrm{s}(x - x_{\mathrm{s},2}), & \text{if } x < x_{s,2} \\ k_s(x - x_{\mathrm{s},1}), & \text{if } x > x_{s,1}. \end{cases} \tag{A.5}$$

where k_s is the end-stop stiffness, $x_{\mathrm{s},1}$ and $x_{\mathrm{s},2}$ are the maximum displacement of the proof mass.

The restoring force is modeled as a polynomial in displacement x found by fitting to numerical calculations (Fig. A.2, [133; 136]) or to experimental data [131]. For accuracy with large displacement of asymmetric transducers, the restoring force is expressed by a septic equation, a seventh degree polynomial, in displacement x, i.e.,

$$F_r = K_1 x + K_2 x^2 + K_3 x^3 + K_4 x^4 + K_5 x^6 + K_6 x^6 + K_7 x^7 \tag{A.6}$$

where K_1 is the linear spring stiffness and K_i $(i = 2 \div 7)$ is the coefficient of the nonlinear spring stiffness.

A.2 Linear regime

We now consider symmetric transducers - e.g. a harvester with clamped-guided springs [131],

$$x_1 = x_2 = x_0, \tag{A.7}$$

$$C_{p,1} = C_{p,2} = C_p, C_1^0 = C_2^0 = C_0, \tag{A.8}$$

$$R_{L1} = R_{L2} = R_L, C_{pL1} = C_{pL2} = C_L \tag{A.9}$$

and a small displacement of the proof mass around the equilibrium position. There are no end-stop effects in this regime. By linearization, see e.g. [145] of the electrostatic force F_e and the voltage for small displacement x and charge $q = (Q_1 - Q_2)/2$, the dynamic model for the *linear-transducer* energy harvester with *linear spring* can be written as

$$m\ddot{x} + b\dot{x} + Kx + \frac{\Gamma}{C}q = ma, \tag{A.10}$$

$$-\dot{q}R = \frac{\Gamma}{C}x + \frac{q}{C}, \tag{A.11}$$

with

$$\Gamma = -\frac{C_0}{x_0}V_e = -2N\frac{\epsilon_0 t}{g_0}V_e, \tag{A.12}$$

$$C = (C_0 + C_p + C_L)/2 \quad \text{and} \quad R = 2R_L, \tag{A.13}$$

$$K = K_1 + \frac{\Gamma^2}{C}, \tag{A.14}$$

$$k^2 = \frac{\Gamma^2}{KC}, \tag{A.15}$$

where R and C are the equivalent load resistance and transducer capacitance respectively, K is the effective linear spring stiffness at open circuit and k is the electromechanical coupling factor.

For the fully linearized harvester governed by (A.10) and (A.11), analytical expressions for output power with different types of excitations such as white and band-limited noise can be found in[146].

A.3 Nonlinear regime, lumped model for SPICE simulations

Finding a precise solution for a nonlinear harvester governed by (A.2) and (A.3) including the asymmetrical transducers, the nonlinear electrical force F_e (Eq. (A.4) and the nonlinear springs F_r (Eq. (A.6)) by analytical analysis is a challenge, especially when the input acceleration is white noise or band-limited noise (colored noise). Instead, numerical solutions have been used in the nonlinear regimes such as the harmonic balance method for harmonic accelerations [147].

Here, we use SPICE simulator, in particular LTspice IV (Linear Technology Corporation [148]), for numerical solutions. *Arbitrary behavioral sources - bv* in SPICE can be used to implement the variable capacitors Eq. (A.1) (as shown Fig. A.3), the electrical force Eq. (A.4), the nonlinear spring Eq. (A.6). A complex equation, such as the mechanical end-stops and the variable capacitances including end-stop effects, can be modeled with behavioral sources and *user defined functions - func.* in SPICE. Voltage sources in SPICE can use a wave (.wav) file as an input. This allows to simulate the harvester driven by white noise or colored noise signals which can be generated externally [149]. An example of a lumped model for SPICE simulation of MEMS electrostatic energy harvester with nonlinear springs driven by white noise is shown in Fig. A.4.

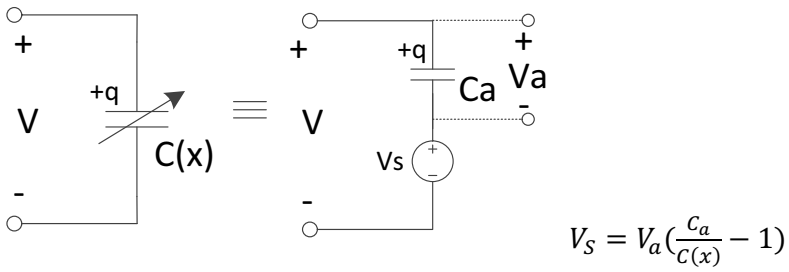

Figure A.3: Variable capacitor $C(x)$ is implemented by an arbitrary capacitor C_a and a behavioral source V_S in SPICE.

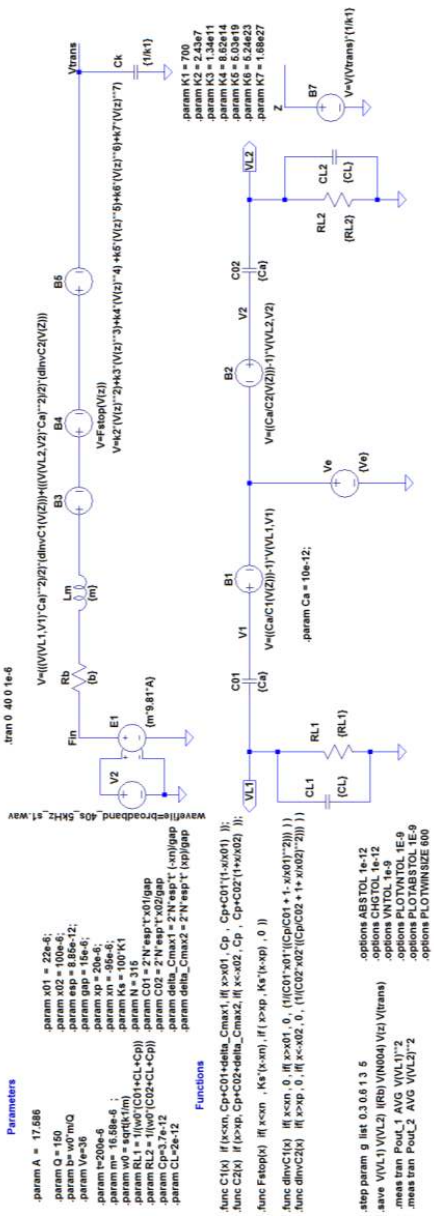

Figure A.4: Lumped model for SPICE simulation of MEMS electrostatic energy harvester with nonlinear springs.

A. MODELING OF MEMS ELECTROSTATIC ENERGY HARVESTER

Appendix B

The fabrication process

B.1 Fabrication issue of the angled-spring harvesters

As stated in *Paper 4* [132] and *Paper 6* [134], the fabrication of angled springs posed an issue regarding their protection during the process. As shown in Fig. B.1, the maximum tensile stress is about 2.2 GPa at maximum displacement 125 μm. We resolved this by using dummy structures [132] to reduce the under-cut of the springs during DRIE process. Another method is the use of sacrificial structures [134] which are designed to protect the springs from under-cuts and shocks during handling in fabrication. Before finally solving the problem, though, there was one un-successful attempt. The cause of the failure was poor dummy protective structures for the angled springs. As seen in Fig. B.2, the dummy structures are short and the spring has large opening areas at middle. Consequently, the springs were deeply undercut and very narrow at their bottom (Fig. B.4) after DRIE process. One or more of the springs were broken in almost all harvesters during fabrication (Fig. B.3).

With improved protective structures, the second fabrication batch had a higher yield (Fig. B.6). As shown in Fig. B.2-ii, the protective structures and the proof mass were designed so that the opening areas along the spring were as small as necessary to protect it during DRIE process. The spring width on the backside (Fig. B.7) is wider than that of the previous design.

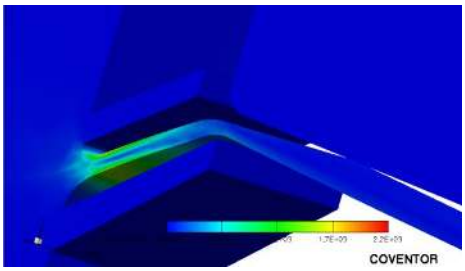

Figure B.1: Maximum stress on the angled spring at the maximum displacement of 125 μm.

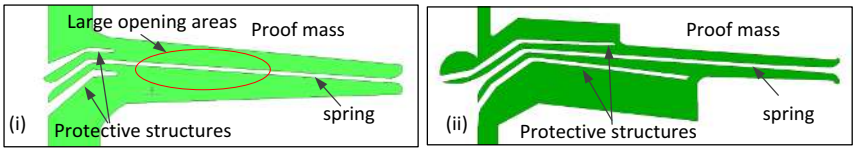

Figure B.2: Layout of angled spring with its dummy protective structures (i) old design (ii) new design.

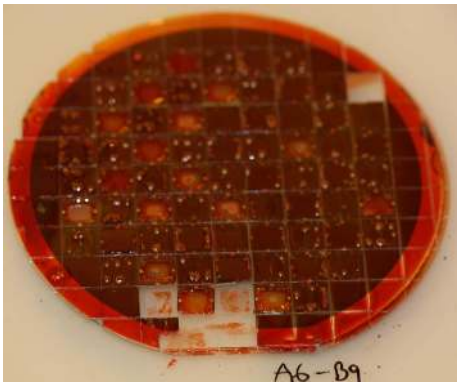

Figure B.3: Wafer after fabrication. The dies have already been sawed and covered by photoresist to fix the moving parts for transfer. The nonlinear harvesters are with other prototypes, dual mass harvesters [14] in a single wafer. 60% of the angled-spring harvester dies had broken suspensions and severed proof masses (the empty places in the wafer). Harvesters on the left side of the wafer have one or more springs broken off.

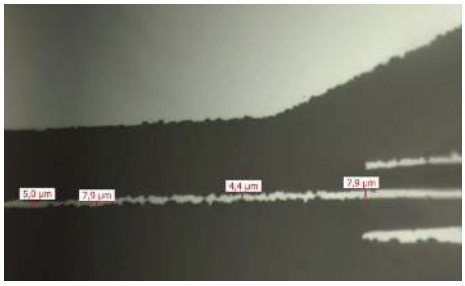

Figure B.4: Bottom view of the angled spring showing signs of being deeply undercut. The layout width of the spring is 15 μm.

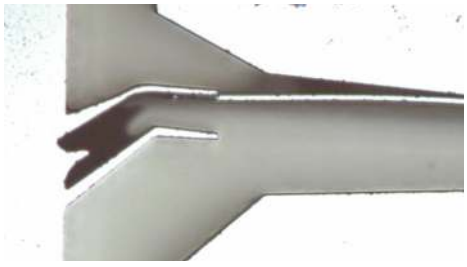

Figure B.5: Top view of a broken angled spring.

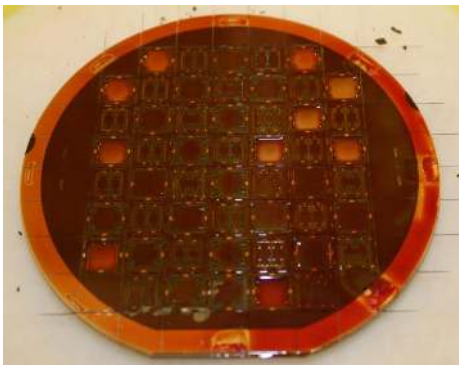

Figure B.6: New fabrication batch with improved dummy protective structures for the angled springs. About ten angled-spring-harvester dies (among total twenty eight dies) had broken suspensions. A six dies among left ones have one or more broken springs.

Figure B.7: Top view of the angled spring with improved dummy protective structures.

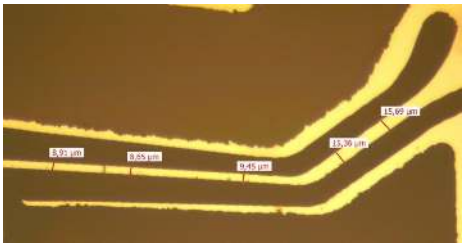

Figure B.8: Bottom view of the angled spring with improved dummy protective structures. The spring width is wider than that in the old design (Fig. B.4).

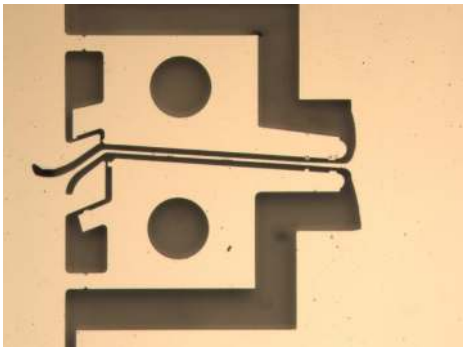

Figure B.9: Sacrificial structures to protect the angled spring.

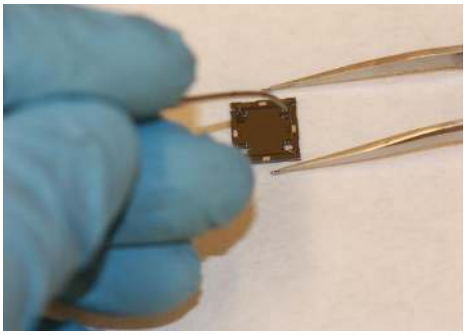

Figure B.10: Sacrificial structures being manually broken off. Each device has eight sacrificial structures. Some of these break off during fabrication.

The higher yield from the later batch compared with the previous one was also due to the use of the sacrificial structures (see Fig. B.9, Figs. B.10 and B.11). Among about twelve successful dies (without any broken springs), there were seven dies with sacrificial structures (during the removal of the sacrificial structures, the spring(s) of three of these were broken). Details of the sacrificial structures are described in *Paper 6* [134].

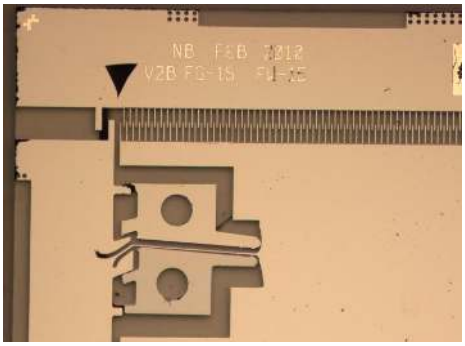

Figure B.11: Separated sacrificial structures. In the next step, the chip is dipped upside down in water for safe removal of the sacrificial structures.

B.2 Fabrication process of the curved-spring harvesters

An angled spring with dummy protective structures was broken in a strong vibration testing of about 7.0×10^{-4} g^2/Hz, before impacting mechanical end-stops. The curved springs, shown Fig. B.12, were designed at smaller maximum tensile stress, around 600 MPa.

The fabrication process for the curved-spring harvesters is presented in *Paper 7*. Here, we illustrate the process with more photos of the process as well as present the challenges in fabrication. The process requires only three masks for the 6-inch wafers: the metal layer, the structure layer (springs, capacitor fingers, stoppers,...) and the backside cavity. Prototypes were attempted with different structure thicknesses: 125 μm, 150 μm and 200 μm of SOI wafers with 2-μm buried oxide and 500-μm substrate thickness.

The pictures of the wafer through the fabrication process are shown in Fig. B.13, B.14, B.17, B.18, and B.19.

The fabrication yield of the curved-spring harvesters is much higher than for angled-spring harvesters. There were about twelve successful dies, i.e. angled-spring harvesters without any broken springs, among a total 28 on the 4-inch wafer after fabrication. In fabricating the curved springs, about 90% of the devices (100 among 110 dies on a 6-inch wafer) had no broken springs. The

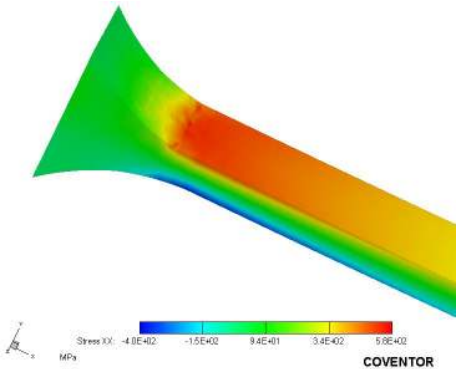

Figure B.12: Maximum stress of the curved spring, calculated using FEM.

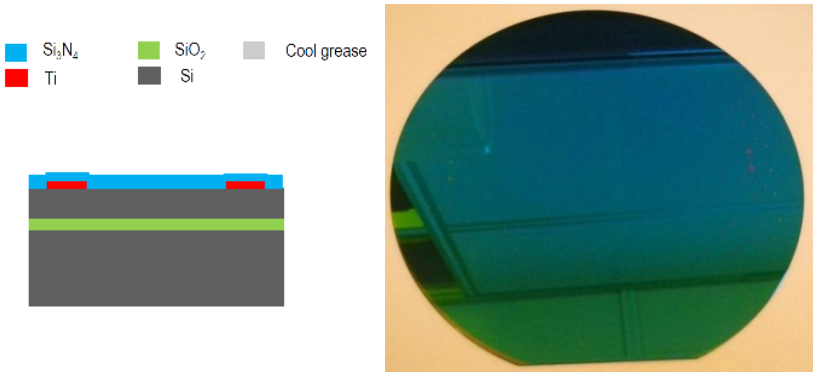

Figure B.13: Wafer after the deposition 120-nm Titanium (Ti) for electrical contact pads and 200-300 nm Si_3N_4 as a passivation layer for local oxidation of Si.

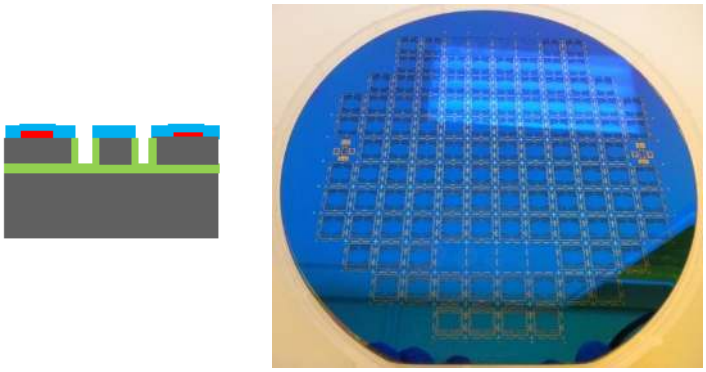

Figure B.14: DRIE of both Si_3N_4 and Si on top to create top structures. The wafers are then thermally oxidized at 1000^0C to grow about 500-nm SiO_2 on the sidewalls.

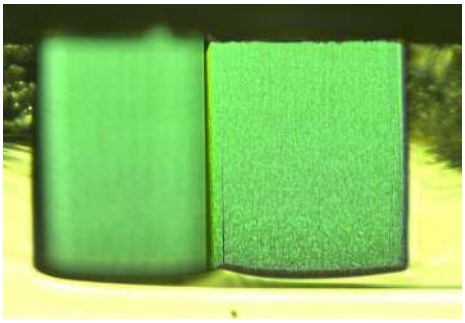

Figure B.15: SiO_2 on the sidewall of capacitor finger. Some wafers skipped the deposition Si_3N_4 in next step to retain only SiO_2 on the sidewall for potential electret charging.

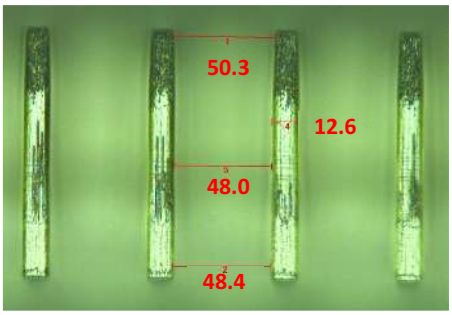

Figure B.16: Profile of the capacitor fingers. The layout distance between two fingers is 50 μm and the layout finger thickness is 15 μm. The fingers are under-cut about 1 μm on each side.

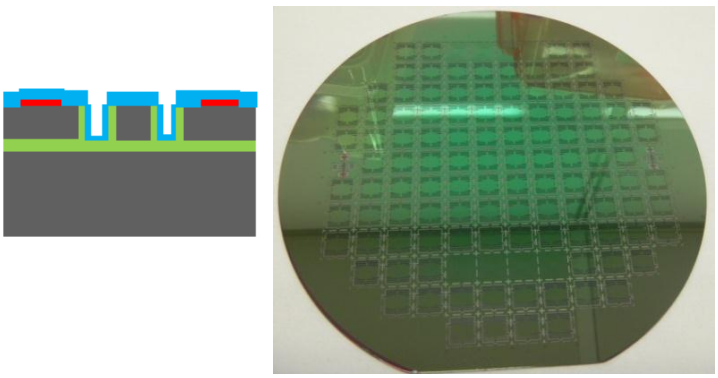

Figure B.17: Depositing the next layer of Si_3N_4 to create a SiO_2/Si_3N_4 dielectric layer on the capacitor sidewall.

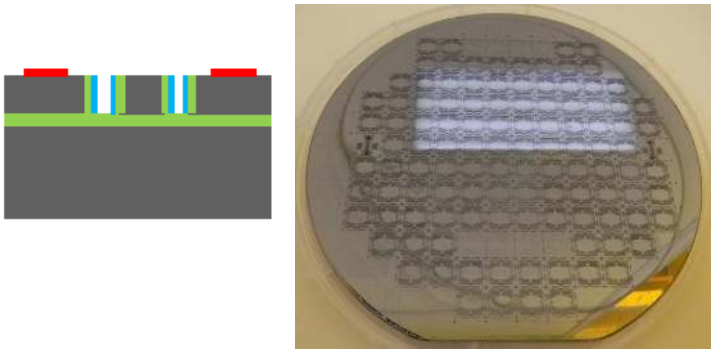

Figure B.18: Wafer after DRIE to etch the Si_3N_4 layer horizontally and maintain Si_3N_4 on the sidewall sidewall.

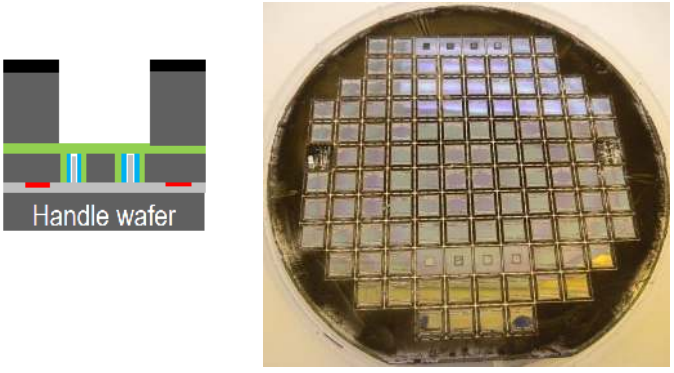

Figure B.19: DRIE of 500-μm Si on the backside to create a cavity.

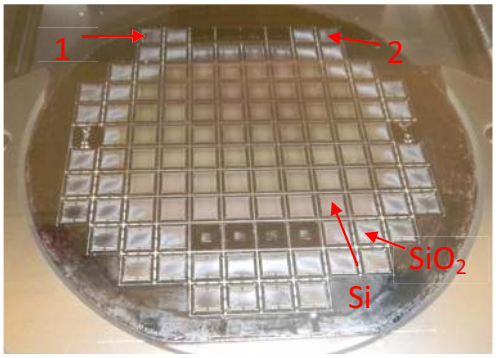

Figure B.20: Non-uniform etching rate on the backside. The opening areas near the wafer rim are etched faster than those near the wafer center.

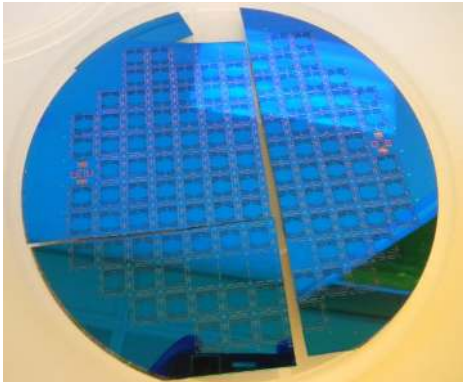

Figure B.21: Wafer broken during handling.

Table B.1: Recipe in etching 500-μm Si on the backside of SOI wafers (used for the Surface Technology Systems Advanced Silicon Etch machine - Marvell Nanofabrication Laboratory, U.C. Berkeley).

Parameter	Passivation	Etch
Cycle times	7 sec	14 sec
Pressure	18 mT	18 mT
C_4F_8 flow	80 sccm	0 sccm
SF_6 flow	0 sccm	130 sccm
Coil Power	600 W	600 W
Bias Power	0 W	30 W
Platen Chiller	25^0C	25^0C

curved springs presented no issue in fabrication but there were some other issues. First, the surface of the Ti electrical contact pads adhered for wire bonding. The Ti pads can suffer from oxidization at 1000^0C despite being covered by a 200-300 nm Si_3N_4 layer. Second, because of the high temperatures during oxidization as well as deposition of Si_3N_4 (850^0C), there is a large residual stress on the curved springs, especially for the chips near the wafer rim where the etching rate is highest (see Fig. B.20).

To etch the 500-μm silicon of the substrate layer, the wafers need to be bonded on a handle wafer using cool grease which is a high thermally conductive material. The cool grease though is hard to clean off (with acetone) in the next step of the process as it is trapped in trenches of the small capacitor fingers.

The layout design also makes fabrication problematic. Two chips (marked as 1 and 2 in Fig. B.20) were the cause for wafer fracturing in handling. Two wafers were broken during handling and become hard to handle in the following process steps (Fig. B.21). The opened area on the backside corresponds to more than 53% of a 6-inch wafer area; thus, the amount of Si to be etched is too large for the DRIE machine. The effect of Si grass formation is an issue for etching Si on the backside. We avoided the effect by increasing the etching time cycle, and reducing the pressure as well as increasing the bias power. A typical recipe is shown in Table B.1. The etching rate is quite low, about 1.4 μm/min.

Appendix C

Bistable-spring harvester driven by real car-tire vibrations

In this Appendix, the response of the bistable-spring harvester driven by actual car-tire vibrations is presented. The car-tire vibration signal was measured at a car speed of 50 km/h on the E18 Highway, Norway. The vibration signal was recorded and stored in a file. We used the actual recorded signal to drive the shaker to re-produce the real car-tire vibration for characterization the bistable-spring harvester.

The PSD of the tangential acceleration is shown in Fig. C.1. There is a very high spectral weight at about 6 Hz, dominated by the tire revolutiona at 50 km/h, but quite narrow, and many high peaks of comparable magnitude up to 100 Hz.

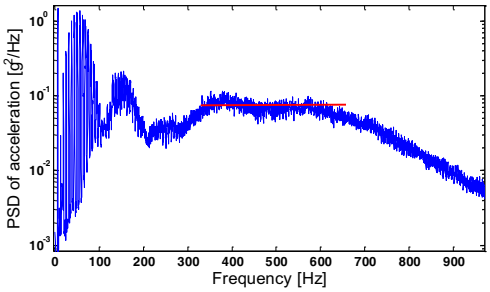

Figure C.1: PSD of the tangential acceleration at a car speed of 50 km/h on the E18 Highway, Norway [6; 7].

C. BISTABLE-SPRING HARVESTER DRIVEN BY REAL CAR-TIRE VIBRATIONS

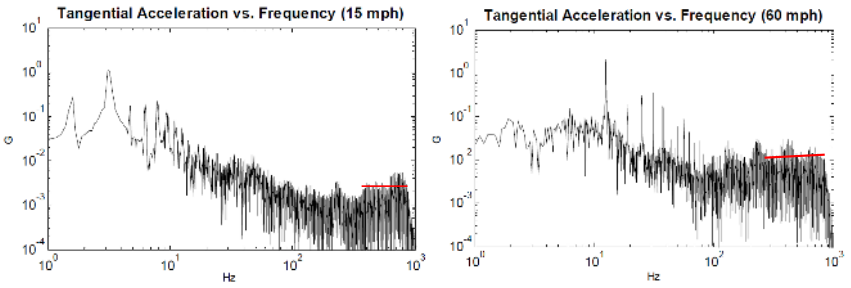

Figure C.2: Spectrum of the tangential acceleration at the different car speeds of 15 mph (24 km/h) and 60 mph (96 km/h) from Roundy [15]. The vibration spectrum is almost flat over a wide range frequencies from 300 Hz to 800 Hz and the spectrum does not change when changing car speeds.

The most interesting portion from harvesting perspective is the flat portion in a frequency range from 300 Hz to 700 Hz since it is wide and does not change spectrum when changing the car speed, only the strength changes.

The characteristic of the vibration spectrum was replicated with the other recorded car-tire vibrations of Roundy [15] as shown in Fig. C.2.

In this experiment, we scaled the vibration strength of the measured vibration at 50 km/h (Fig. C.1) to mimic different car speeds. The output power as a function of acceleration PSD is shown in Fig. C.3. The acceleration PSD is calculated by the average PSD in the range frequency of 300 Hz to 700 Hz. The high spectral weight, i.e. from 300 Hz to 700 Hz, is outside the harvester's resonant frequency. Consequently, the output power increases slowly when the acceleration PSD is smaller than $8{\times}10^{-3}$ g^2/Hz. When acceleration is larger than this value, the output power increases at a rate of 63.3 μW/(g^2/Hz) (for 100-V bias). This is because the acceleration is sufficiently strong to drive the harvester operating into the low frequency regime (see Fig. C.4). This is because output voltage is measured through a buffer amplifier OPA2137 which has an input voltage limit of 18 V, the highest acceleration in this experiment is limited to $2{\times}10^{-2}$ g^2/Hz. The actual acceleration at 50-km/h car speed is $7.3{\times}10^{-2}$ g^2/Hz. An average output power of 1.1 μW is obtained at the PSD acceleration of $2{\times}10^{-2}$ g^2/Hz and the bias voltage of 100 V. The output reading of 4.4 μW

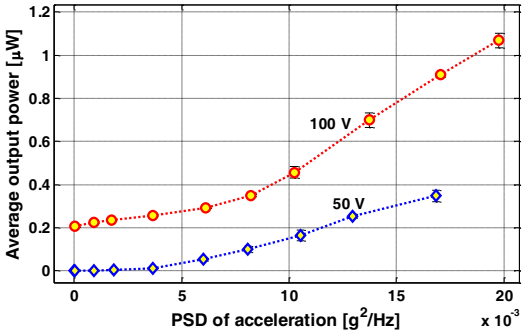

Figure C.3: Output power vs. acceleration PSD for 50-V and 100-V bias voltages.

can be reached under actual acceleration (estimated when the proof mass does not impact mechanical end-stops).

Based on this experiment, a new design of MEMS electrostatic energy harvester with lower resonant frequency and lager variable capacitance can potentially give higher output power. The resonance of the current harvester is further outside the high spectral weight of the car-tire vibration. A resonant frequency of 700 Hz is supposed to give a higher efficiency. The variable capacitance can be increased by increasing the number of capacitors as well as the distance travel of the proof mass.

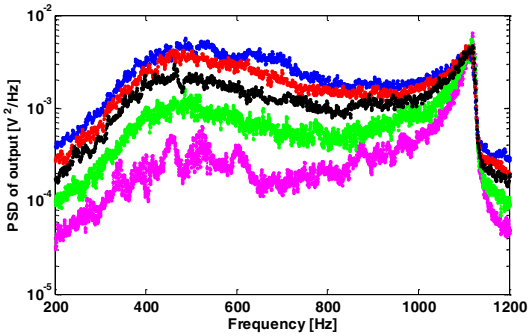

Figure C.4: PSD of the output voltage for acceleration PSD of $8{\times}10^{-3}$, $10{\times}10^{-3}$, $14{\times}10^{-3}$, $17{\times}10^{-3}$, $20{\times}10^{-3}$ g^2/Hz (from lower to upper curve). The harvester responds to a wide bandwidth in the frequency range 300 Hz - 700 Hz.

Bibliography

[1] R. Rajan, "Ultra-low power short range radio transceivers," Microsemi CMPG, Tech. Rep., May 2012. xi, 2

[2] R. Elfrink, T. M. Kamel, M. Goedbloed, S. Matova, D. Hohlfeld, Y. van Andel, and R. van Schaijk, "Vibration energy harvesting with aluminum nitride-based piezoelectric devices," *J. Micromech. Microeng.*, vol. 19, no. 9, pp. 094005, 2009. xi, 3

[3] R. Torah, P. Glynne-Jones, M. Tudor, T. O'Donnell, S. Roy, and S. Beeby, "Self-powered autonomous wireless sensor node using vibration energy harvesting," *Meas. Sci. Technol.*, vol. 19, no. 12, p. 125202 (8pp), 2008. xi, 3

[4] S. Meninger, J. Mur-Miranda, R. Amirtharajah, A. Chandrakasan, and J. Lang, "Vibration-to-electric energy conversion," *IEEE Trans. VLSI Syst.*, vol. 9, pp. 64–76, 2001. xi, 3, 4

[5] InfinitePowerSolutions, "THINERGY micro-energy cell (MEC) product overview," Tech. Rep., Jul 2012. xi, 6, 14

[6] M. Lohndorf, T. Kvisterøy, E. Westby, and E. Halvorsen, "Evaluation of energy harvesting concepts for tire pressure monitoring systems," in *Tech. Dig. PowerMEMS 2007*, Freiburg, Nov 2007, pp. 331–334. xi, xv, 5, 6, 7, 127

[7] E. R. Westby and E. Halvorsen, "Design and modeling of a patterned-electret-based energy harvester for tire pressure monitoring systems," *IEEE Trans. Mechatronics*, vol. 17, no. 5, pp. 995–1005, 2011. xi, xv, 5, 7, 127

[8] M. Wischke, G. Biancuzzi, G. Fehrenbach, Y. Abbas, and P. Woias, "Vibration harvesting in railway tunnels," in *Proc. PowerMEMS 2010*, Leuven, Belgium, Nov 30 - Dec 3 2010. xi, 6, 7

[9] S. C. Stanton, C. C. McGehee, and B. P. Mann, "Reversible hysteresis for broadband magnetopiezoelastic energy harvesting," *Appl. Phys. Lett.*, vol. 95, p. 174103, 2009. xi, 10, 12, 29

[10] S. G. Burrow and L. R. Clare, "A resonant generator with non-linear compliance for energy harvesting in high vibrational environmen," in *Proc. IEEE IEMDC*, Antalya, Turkey, 3-5 May 2007 2007, pp. 715–720. xi, 10, 12

[11] S. G. Burrow, L. R. Clare, A. Carrella, and D. Barton, "Vibration energy harvesters with non-linear compliance," *Proc. SPIE 6928*, vol. 692807, no. 10, 2008. xi, 10, 12

[12] C. V. Jutte and S. Kota, "Design of nonlinear springs for prescribed load-displacement functions," *J. Mech. Design*, vol. 130, no. 8, AUG 2008. xii, 11, 21

[13] J. Wittwer, M. Baker, and L. Howell, "Robust design and model validation of nonlinear compliant micromechanisms," *J. Microelectromech. Syst.*, vol. 15, no. 1, pp. 33 – 41, feb. 2006. xii, 11

[14] L.-C. Blystad, "Modelling and design MEMS energy harvesters," Ph.D. dissertation, University of Oslo, 2010. xiv, 116

[15] S. Roundy, "Energy harvesting for tire pressure monitoring systems desing considerations," in *Tech. Dig. PowerMEMS + μEMS 2008*, Sendai, Japan, Nov 9-12 2008, pp. 1–6. xv, 5, 128

[16] "Charging at high and low temperatures". [Online]. Available: http://batteryuniversity.com/learn/article/charging_at_high_and_low_temperatures 1

[17] S. Roundy, D. Steingart, L. Frechette, P. Wright, and J. Rabaey, "Power Sources for Wireless Sensor Networks", *Lect. Notes Comput. Sci.* 2920,pp.1-17, 2004. 1

[18] P. Smith, "Comparing low-power wireless technologies - wireless solutions," CSR plc, Tech. Rep., 2011. 1

[19] A. Ricci, M. Grisanti, I. De Munari, and P. Ciampolini, "Improved pervasive sensing with RFID: An ultra-low power baseband processor for UHF tags," *IEEE Trans. VLSI Syst.*, vol. 17, no. 12, pp. 1719 –1729, dec. 2009. 1

[20] V. Pillai, H. Heinrich, D. Dieska, P. Nikitin, R. Martinez, and K. Rao, "An ultra-low-power long range battery/passive RFID tag for UHF and microwave bands with a current consumption of 700 nA at 1.5 V," *IEEE Trans. Circuits Syst.*, vol. 54, no. 7, pp. 1500 –1512, july 2007. 2

[21] A. Shameli, A. Safarian, A. Rofougaran, M. Rofougaran, and F. De Flaviis, "Power harvester design for passive UHF RFID tag using a voltage boosting technique," *IEEE Trans. Microwave Theory Tech.*, vol. 55, no. 6, pp. 1089 –1097, june 2007. 2

[22] U. Karthaus and M. Fischer, "Fully integrated passive UHF RFID transponder ic with 16.7- μw minimum RF input power," *IEEE J. Solid-State Circuits*, vol. 38, no. 10, pp. 1602 – 1608, oct. 2003. 2

[23] A. El-Hoiydi and J.-D. Decotignie, "WiseMAC: an ultra low power MAC protocol for the downlink of infrastructure wireless sensor networks," *Comput. and Commun., 2004. Proc.. ISCC 2004. Ninth Int. Symp. on*, vol. 1, pp. 244 – 251 Vol.1, 28 june-1 july 2004. 2

[24] C. Enz, A. El-Hoiydi, J.-D. Decotignie, and V. Peiris, "WiseNET: an ultralow-power wireless sensor network solution," *Computer*, vol. 37, no. 8, pp. 62 – 70, aug. 2004. 2

[25] C. B. Williams and R. B. Yates, "Analysis of a micro-electric generator for microsystems," *Sens. Actuators A, Phys.*, vol. 52, no. 1-3, pp. 8–11, 1996. 3, 6

[26] P. D. Mitcheson, E. M. Yeatman, G. K. Rao, A. S. Holmes, and T. C. Green, "Energy harvesting from human and machine motion for wireless electronic devices," *Proc. IEEE*, vol. 96, no. 9, pp. 1457–1486, Sep. 2008. 3

[27] E. Mounier, "MEMS markets & applications 2011-2017, an overview," in *dMEMS 2012*, Besancon, France, April 2nd - 3rd 2012. 3

[28] M. Hayakawa, "Electronic wristwatch with generator," U.S. Patent 5 001 685, Mar. 1991. 4

[29] W. H. Ko, "Piezoelectric energy converter for electronic implants," US Patent 3 456 134, Jul 15, 1969. 4, 6

[30] E. A. Schroeppel, "Pacing lead with piezoelectric power generating means," US Patent 4 690 143, 1987. 4, 6

[31] P. Glynne-Jones, S. Beeby, and N. White, "Towards a piezoelectric vibration-powered microgenerator," *IEE Proc. Sci. Meas. Technol.*, vol. 148, no. 2, pp. 68–72, 2001. 4

[32] N. M. White, P. Glynne-Jones, and S. P. Beeby, "A novel thick-film piezoelectric micro-generator," *Smart Mater. Struct.*, vol. 10, no. 4, pp. 850–852, Aug. 2001. 4

[33] N. E. duToit, "Modeling and design of a MEMS piezoelectric vibration energy harvester," M.S. thesis, Massachusetts Institute of Technology, May 2005. 4

[34] A. Erturk, "Electromechanical modeling of piezoelectric energy harvesters," Ph.D. dissertation, Virginia Polytechnic Institute and State University, 2009. 4

[35] R. Elfrink, S. Matova, C. de Nooijer, M. Jambunathan, M. Goedbloed, J. van de Molengraft, V. Pop, R. Vullers, M. Renaud, and R. van Schaijk, "Shock induced energy harvesting with a MEMS harvester for automotive applications," in *2011 IEEE IEDM*, no. 677-680, Hilton Washington and Towers Washington, DC, USA, 05 Dec - 07 Dec 2011 2011. 4

[36] R. Xu, A. Lei, C. Dahl-Petersen, K. Hansen, M. Guizzetti, K. Birkelund, E. V. Thomsen, and O. Hansen, "Fabrication and characterization of MEMS-based PZT/PZT bimorph thick film vibration energy harvesters," *J. Micromech. Microeng.*, vol. 22, no. 9, p. 094007, 2012. 4

[37] L. M. Miller, E. Halvorsen, T. Dong, and P. K. Wright, "Modeling and experimental verification of low-frequency MEMS energy harvesting from ambient vibrations," *J. Micromech. Microeng.*, vol. 21, no. 4, p. 045029, 2011. 4, 6

[38] L.-C. Blystad, E. Halvorsen, and S. Husa, "Piezoelectric MEMS energy harvesting systems driven by harmonic and random vibrations," *Trans. Ultrason., Ferroelectr., Freq. Control*, vol. 57, no. 4, pp. 908 –919, april 2010. 4

[39] Perpetuum Ltd. [Online]. Available: http://www.perpetuum.com/ 4

[40] MicroGen Systems, Inc. [Online]. Available: http://www.microgensystems.co/default.asp 4

[41] R. Amirtharajah, S. Meninger, J. O. Mur-Miranda, A. P. Chandrakasan, and J. H. Lang, "BA micropower programmable DSP powered using a MEMS-based vibration-to-electric energy converter," in *Proc. IEEE Int. Conf. Solid State Circuits*, 2000, pp. 362–363. 4

[42] S. Roundy, K. S. J. Pister, and P. K. Wright, "Micro-electrostatic vibration-to-electricity converters," in *Proc. IMECE2002*, ASME International Mechanical Engineering Congress & Exposition. ASME, November 2002. 4

[43] T. Sterken, K. Baert, R. Puers, G. Borghs, and R. Mertens, "A new power MEMS component with variable capacitance," in *Proc. Pan Pacific Microelectron. Symp. 2003*, 2003, pp. 27–34. 4

[44] A. Nimo and U. Mescheder, "3-d capacitive vibrational harvester for autonomous low power sensors," in *Proc. PowerMEMS 2010*, Leuven, Belgium, Nov 30-Dec 3 2010, pp. 165–168. 4, 5, 32

[45] K. Yamashita, M. Honzumi, K. Hagiwara, Y.Iguchi, and Y. Suzuki, "Vibration-driven MEMS energy harvester with vertical electrets," in *Proc. PowerMEMS 2010*, Leuven, Belgium, Nov 30-Dec 3 2010, pp. 165–168. 4, 5, 32

[46] Y. Suzuki, "Recent progress in MEMS electret generator for energy harvesting," *IEEJ Trans. Electr. Electron. Eng.*, vol. 6, no. 2, pp. 101–111, 2011. 4

[47] M. Honzumi, K. Hagiwara, Y. Iguch, and Y. Suzuki, "High-speed electret charging method using vacuum UV irradiation," in *Proc. PowerMEMS 2010*, Leuven, Belgium, Nov 30-Dec 3 2010, pp. 173–176. 4, 5

[48] K. Hagiwara, M. Goto, Y. Iguchi, T. Tajima, Y. Yasuno, K. Kodama, H.and Kidokoro, and Y. Suzuki, "Effect of high-absorbance gas introductuon on soft-X-ray charning properties for electret generator," in *Proc. PowerMEMS 2010*, Leuven, Belgium, Nov 30-Dec 3 2010, pp. 165–168. 4, 5

[49] E. Blokhina, D. Galayko, P. Basset, and O. Feely, "Steady-state oscillations in resonant electrostatic vibration energy harvesters," *IEEE Trans. Circuits Syst.*, vol. PP, no. 99, p. 1, 2012. 4, 14

[50] W. Ma, R. Zhu, L. Rufer, Y. Zohar, and M. Wong, "An integrated floating-electrode electric microgenerator," *J. Microelectromech. Syst.*, vol. 16, no. 1, pp. 29–37, 2007. 4

[51] D. Hoffmann, B. Folkmer, and Y. Manoli, "Fabrication, characterization and modelling of electrostatic micro-generators," *J. Micromech. Microeng.*, vol. 19, no. 9, p. 094001 (11pp), 2009. 4

[52] D. Hoffmann, B. Folkmer, and Y. Manoli, "Analysis and characterization of triangular electrode structures for electrostatic energy harvesting," *J. Micromech. Microeng.*, vol. 21, no. 10, p. 104002, 2011. 4

[53] S. Boisseau, A.-B. Duret, J.-J. Chaillout, and G. Despesse, "New DRIE-patterned electrets for vibration energy harvesting," in *Proc. European Energy Conf.*, 2012. 5

[54] Y. Sakane, Y. Suzuki, and N. Kasagi, "The development of a high-performance perfluorinated polymer electret and its application to micro power generation," *J. Micromech. Microeng.*, vol. 18, no. 10, p. 104011 (6pp), 2008. 5

[55] U. Mescheder, B. Mller, S. Baborie, and P. Urbanovic, "Properties of SiO_2 electret films charged by ion implantation for MEMS-based energy harvesting systems," *J. Micromech. Microeng.*, vol. 19, no. 9, p. 094003, 2009. 5

[56] D. Chong, W. Lee, J. Pang, T. Low, and B. Lim, "Mechanical failure strength characterization of silicon dice," in *EPTC 2003*, dec. 2003, pp. 600 – 605. 5

[57] D. Gang Zong, C. Wo Ong, M. Aravind, M. Po Tsang, C. Loong Choy, D. Lu, and D. Ma, "Tensile strength of aluminium nitride films," *Philosophical Magazine*, vol. 84, no. 31, pp. 3353–3373, 2004. 5

[58] Y. Suzuki and Y.-C. Tai, "Micromachined high-aspect-ratio parylene spring and its application to low-frequency accelerometers," *J. Microelectromech. Syst.*, vol. 15, no. 5, pp. 1364 – 1370, oct 2006. 5, 32

[59] European Parliamenth. [Online]. Available: http://www.europarl.europa.eu/sides/getDoc.do?pubRef=-//EP//TEXT+TA+P6-TA-2009-0092+0+DOC+XML+V0//EN&language=EN#BKMD-13 5

[60] L. Wu, Y. Wang, C. Jia, and C. Zhang, "Battery-less piezoceramics mode energy harvesting for automobile TPMS," in *ASIC, 2009. ASICON '09. IEEE 8th Int. Conf.*, oct. 2009, pp. 1205 –1208. 5

[61] A. Frey, J. Seidel, and I.Kuehne, "System design of a piezoelectric MEMS energy harvesting module based on pulsed mechanical excitation," in *Proc. of PowerMEMS 2010*, Lueven, Belgium, Nov 30-Dec 3 2010, pp. 29–32. 5

[62] N. Makki and R. Pop-Iliev, "Piezoelectric power generation for sensor applications: design of a battery-less wireless tire pressure sensor," *Proc. SPIE, Smart Sens., Actuators, and MEMS V*, vol. 8066, p. 806618, 2011. 5

[63] R. Elfrink, S. Matova, C. de Nooijer, M. Jambunathan, M. Goedbloed, J. van de Molengraft, V. Pop, R. Vullers, M. Renaud, and R. van Schaijk, "Shock induced energy harvesting with a MEMS harvester for automotive applications," in *IEEE Int. IEDM 2011* , 5-7 Dec 2011, pp. 29.5.1– 29.5.4. 5, 8

[64] A. L. Chait, "Solving the last milli-mile problem in vehicle safety and the eoplex approach to powering wireless tire pressure sensors," EoPlex Technologies, Tech. Rep., 2012. 5

[65] VisiTyre, "Batery-less tyre pressure monitoring system," Available: http://www.etv.com.au/default.htm. 5

[66] Piezotag Limited. Piezo power source for tyre pressure monitoring systems. [Online]. Available: http://www.piezotag.com/index.htm 5

[67] E. Sazonov, H. Li, D. Curry, and P. Pillay, "Self-powered sensors for monitoring of highway bridges," *IEEE Sensors J.*, vol. 9, no. 11, pp. 1422–1429, Nov 2009. 6

[68] A. M. Hedayetullah, "Analysis of piezoelectric energy harvesting for bridge health monitoring systems," M.S. thesis, University of Wales Swansea, 2010. 6

[69] G. Park, T. Rosing, M. Todd, C. Farrar, and W. Hodgkiss, "Energy harvesting for structural health monitoring sensor networks," *J. Infrastruct. Syst., SPECIAL ISSUE: New Sens., Instrum., Sign. Interpretation*, vol. 14, pp. 64–79, 2008. 6

[70] E. Romero, R. O. Warrington, and M. R. Neuman, "Energy scavenging sources for biomedical sensors," *Physiol. Meas.*, vol. 30, no. 9, p. R35, 2009. 6

[71] P. Mitcheson, "Energy harvesting for human wearable and implantable biosensors," in *IEEE EMBC*, 2010, pp. 3432–3436. 6

[72] S. P. Beeby, M. J. Tudor, and W. N. M., "Energy harvesting vibration sources for microsystems applications," *Meas. Sci. Technol.*, vol. 17, no. 12, pp. R175–R195, Dec. 2006. 6

[73] E. S. Leland, P. K. Wright, and R. M. White, "A MEMS ac current sensor for residential and commercial electricity end-use monitoring," *J. Micromech. Microeng.*, vol. 19, no. 9, p. 094018, 2009. 6

[74] I. Paprotny, E. S. Leland, R. M. White, and P. K. Wright, "Optimization of a die-sized (10x10x4 mm^3) MEMS ac energy scavenger for residential and commercial electricity end-use monitoring." in *Tech. Dig. PowerMEMS 2009*, Washington DC, USA, Dec 1-4 2009. 6

[75] Q. Xu, R. M. White, I. Paprotny, and P. K. Wright, "Improved performance of nonlinear piezoelectric AC energy scavengers," in *Proc. PowerMEMS 2010*, Leuven, Belgium, Nov 30-Dec 3 2010. 6

[76] I. Neri, F. Travasso, R. Mincigrucci, H. Vocca, F. Orfei, and L. Gammaitoni, "A real vibration database for kinetic energy harvesting application," *J. Intell. Mater. Syst. Struct.*, 2012. 6

[77] D. Zhu, M. J. Tudor, and S. P. Beeby, "Strategies for increasing the operating frequency range of vibration energy harvesters: a review," *Meas. Sci. Technol.*, vol. 21, no. 2, p. 022001, 2010. 8

[78] G. Piazza, R. Abdolvand, G. K. Ho, and F. Ayazi, "Voltage-tunable piezoelectrically-transduced single-crystal silicon micromechanical resonators," *Sens. Actuators A, Phys.*, vol. 111, no. 1, pp. 71 – 78, 2004. 8

[79] K. B. Lee, L. Lin, and Y.-H. Cho, "A closed-form approach for frequency tunable comb resonators with curved finger contour," *Sens. Actuators A, Phys.*, vol. 141, no. 2, pp. 523 – 529, 2008. 8

[80] V. R. Challa, M. G. Prasad, Y. Shi, and F. T. Fisher, "A vibration energy harvesting device with bidirectional resonance frequency tunability," *Smart Mater. Struct.*, vol. 17, no. 1, p. 015035, 2008. 8

[81] S. Roundy, "On the effectiveness of vibration-based energy harvesting," *J. Intell. Mater. Syst. Struct.*, vol. 16, no. 10, pp. 809–823, 2005. 8

[82] W.-J. Wu, Y.-Y. Chen, B.-S. Lee, J.-J. He, and Y.-T. Peng, "Tunable resonant frequency power harvesting devices," *Proc. SPIE*, vol. 6169, pp. 61 690A–61 690A–8, 2006. 8

[83] J. F. Gieras, J.-H. Oh, M. Huzmezan, and H. S. Sane, "Electromechanical energy harvesting system," US Patent US 2009/0 079 200 A1, 2011. 8

[84] E. S. Leland and P. K. Wright, "Resonance tuning of piezoelectric vibration energy scavenging generators using compressive axial preload," *Smart Mater. Struct.*, vol. 15, no. 5, p. 1413, 2006. 8, 21

[85] G. A. Lesieutre, G. K. Ottman, and H. F. Hofmann, "Damping as a result of piezoelectric energy harvesting," *J. Sound Vib.*, vol. 269, no. 3-5, pp. 991–1001, Jan. 2004. 8

[86] I. Sari, T. Balkan, and H. Kulah, "A wideband electromagnetic micro power generator for wireless microsystems," in *Solid-State Sens. Actuators Microsyst. Conf., 2007. TRANSDUCERS 2007. Int.*, june 2007, pp. 275 –278. 9

[87] S. Shahruz, "Design of mechanical band-pass filters for energy scavenging," *J. Sound Vib.*, vol. 292, no. 35, pp. 987 – 998, 2006. 9

[88] J.-Q. Liu, H.-B. Fang, Z.-Y. Xu, X.-H. Mao, X.-C. Shen, D. Chen, H. Liao, and B.-C. Cai, "A MEMS-based piezoelectric power generator array for vibration energy harvesting," *Microelectron. J.*, vol. 39, no. 5, pp. 802 – 806, 2008. 9

[89] R. G. Andosca and J. Wu, "Piezoelectric vibrational energy harvesting MEMS-based solutions," in *APEC 2011 Special Presentation - Energy Harvesting & Power Electronics*, Fort Worth, Texas, USA, March 2011. 9

[90] C. Gu, Lei; Livermore, "Passive self-tuning energy harvester for extracting energy from rotational motion," *Appl. Phys. Lett.*, vol. 97, p. 081904, 2010. 9, 12

[91] R. Miles, "An approximate solution for the spectral response of Duffing's oscillator with random input," *J. Sound Vib.*, vol. 132, p.43 – 49, 1989. 9

[92] I Kovacic; M J Brennan (eds), "The duffing equation," *Wiley*, Chichester, West Sussex, 2011. 9

[93] Y. Kao, C. Wang, and T. Yang, "Influences of harmonic coupling on bifurcations in duffing oscillator with bounded potential well," *J. Sound Vib.*, vol. 159, no. 1, pp. 13 – 21, 1992. 10

[94] M. Soliman, "Non-linear vibrations of hardening systems: Chaotic dynamics and unpredictable jumps to and from resonance," *J. Sound Vib.*, vol. 207, no. 3, pp. 383 – 392, 1997. 10

[95] R. Ramlan, M. Brennan, B. Mace, and I. Kovacic, "Potential benefits of a non-linear stiffness in an energy harvesting device," *Nonlinear Dynamics*, vol. 59, pp. 545–558, 2009. 10

[96] B. Mann and N. Sims, "Energy harvesting from the nonlinear oscillations of magnetic levitation," *J. Sound Vib.*, vol. 319, no. 12, pp. 515 – 530, 2009. 10, 12

[97] M. Marzencki, M. Defosseux, and S. Basrour, "MEMS vibration energy harvesting devices with passive resonance frequency adaptation capability," *J. Microelectromech. Syst.*, vol. 18, no. 6, pp. 1444 –1453, dec. 2009. 10, 12

[98] D. Spreemann, B. Folkmer, and Y. Manoli, "Realization of nonlinear hardening springs with predefined characteristic for vibration transducers based on beam structures," in *Proc. PowerMEMS 2010*, Leuven, Belgium, Nov 30-Dec 3 2010, pp. 371–374. 10, 12

[99] A. Hajati and S.-G. Kim, "Ultra-wide bandwidth piezoelectric energy harvesting," *Appl. Phys. Lett.*, vol. 99, p. 083105, 2011. 10, 12

[100] X. Dai, X. Miao, L. Sui, H. Zhou, X. Zhao, and G. Ding, "Tuning of nonlinear vibration via topology variation and its application in energy harvesting," *Appl. Phys. Lett.*, vol. 100, p. 031902, 2012. 10, 12, 29

[101] B. Marinkovic and H. Koser, "Demonstration of wide bandwidth energy harvesting from vibrations," *Smart Mater. Struct.*, vol. 21, no. 6, p. 065006, 2012. 10, 12, 28, 29

[102] P. Constantinou, P. Mellor, and P. Wilcox, "A magnetically sprung generator for energy harvesting applications," *IEEE Trans. Mechatron.*, vol. 17, no. 3, pp. 415 –424, june 2012. 10, 12

[103] M. Soliman, E. Abdel-Rahman, E. El-Saadany, and R. Mansour, "A design procedure for wideband micropower generators," *J. Microelectromech. Syst.*, vol. 18, no. 6, pp. 1288 –1299, dec. 2009. 10

[104] L.-C. J. Blystad and E. Halvorsen, "An energy harvester driven by colored noise," *Smart Mater. Struct.*, vol. 20, no. 2, p. 025011, 2011. 10

[105] H. Liu, C. J. Tay, C. Quan, T. Kobayashi, and C. Lee, "Piezoelectric MEMS energy harvester for low-frequency vibrations with wideband operation range and steadily increased output power," *J. Microelectromech. Syst.*, vol. 20, no. 5, pp. 1131 –1142, oct. 2011. 10, 12, 29

[106] H. Liu, C. Lee, T. Kobayashi, C. J. Tay, and C. Quan, "Piezoelectric MEMS-based wideband energy harvesting systems using a frequency-up-conversion cantilever stopper," *Sens. Actuators A, Phys.*, vol. 186, pp. 242–248, 2012. 10

[107] C. P. Le and E. Halvorsen, "MEMS electrostatic energy harvesters with end-stop effects," *J. Micromech. Microeng.*, vol. 22, no. 7, p. 074013, 2012. 10, 109

[108] R. Ramlan, "Effects of non-linear stiffness on performance of an energy harvesting device," Ph.D. dissertation, University of Southampton, 2009. 10

[109] F. Cottone, H. Vocca, and L. Gammaitoni, "Nonlinear energy harvesting," *Phys. Rev. Lett.*, vol. 102, no. 8, p. 080601, Feb 2009. 10, 12

[110] D. A. W. Barton, S. G. Burrow, and L. R. Clare, "Energy harvesting from vibrations with a nonlinear oscillator," *J. Vib. Acoust.*, vol. 132, p. 021009 (7 pages), 2010. 10, 12

[111] M. Ferrari, V. Ferrari, M. Guizzetti, B. And, S. Baglio, and C. Trigona, "Improved energy harvesting from wideband vibrations by nonlinear piezoelectric converters," *Sens. Actuators A, Phys.*, vol. 162, no. 2, pp. 425 – 431, 2010. 10, 12, 29

[112] S. C. Stanton, C. C. McGehee, and B. P. Mann, "Nonlinear dynamics for broadband energy harvesting: Investigation of a bistable piezoelectric inertial generator," *Phys. D: Nonlinear Phenomena*, vol. 239, no. 10, pp. 640 – 653, 2010. 10

[113] A. M. Wickenheiser and E. Garcia, "Broadband vibration-based energy harvesting improvement through frequency up-conversion by magnetic excitation," *Smart Mater. Struct.*, vol. 19, no. 6, p. 065020, 2010. 10

[114] S. C. Stanton, B. P. Mann, and B. A. M. Owens, "Melnikov theoretic methods for characterizing the dynamics of the bistable piezoelectric inertial generator in complex spectral environments," *Phys. D: Nonlinear Phenomena*, vol. 241, no. 6, pp. 711–720, MAR 15 2012. 10

[115] A. Erturk and D. Inman, "Broadband piezoelectric power generation on high-energy orbits of the bistable duffing oscillator with electromechanical coupling," *J. Sound Vib.*, vol. 330, no. 10, pp. 2339 – 2353, 2011. 10

[116] R. Ramlan, M. J. Brennan, B. R. Mace, and S. G. Burrow, "On the performance of a dual-mode non-linear vibration energy harvesting device," *J. Intell. Mater. Syst. Struct.*, vol. 23, p. 14231432, 2012. 10, 12, 29

[117] L. Tang, Y. Yang, and C.-K. Soh, "Improving functionality of vibration energy harvesters using magnets," *J. Intell. Mater. Syst. Struct.*, vol. 23, p. 14331449, 2012. 10, 12

[118] I.-H. Hwang, Y.-S. Shim, and J.-H. Lee, "Modeling and experimental characterization of the chevron-type bi-stable microactuator," *J. Micromech. Microeng.*, vol. 13, no. 6, p. 948, 2003. 11

[119] J. Tsay, H.-A. Chang, and C.-K. Sung, "Design and experiments of fully compliant bistable micromechanisms," *Mechanism. and Machine. Theory*, vol. 40, pp. 17–31, 2005. 11

[120] B. B. Cherry, L. L. Howell, and B. D. Jensen, "Evaluating three-dimensional effects on the behavior of compliant bistable micromechanisms," *J. Micromech. Microeng.*, vol. 18, no. 9, p. 095001, 2008. 11

[121] B. Ando, S. Baglio, G. L'Episcopo, and C. Trigona, "Investigation on mechanically bistable MEMS devices for energy harvesting from vibrations," *J. Microelectromech. Syst.*, vol. 21, no. 99, pp. 779–790, 2012. 11, 12

[122] J. Grade, H. Jerman, and T. Kenny, "Design of large deflection electrostatic actuators," *J. Microelectromech. Syst.*, vol. 12, no. 3, pp. 335 – 343, june 2003. 11, 27

[123] S. Krylov and Y. Bernstein, "Large displacement parallel plate electrostatic actuator with saturation type characteristic," *Sens. Actuators A, Phys.*, vol. 130131, no. 0, pp. 497 – 512, 2006. 11, 27

[124] N.-H. T. Tran, S. D. Nguyen, and E. Halvorsen, "Design of nonlinear springs for MEMS vibration energy harvesting applications," in *Proc. 22nd Micromech. Microsyst. Technol. Europe Workshop*, Tønsberg, Norway, Jun. 19–22 2011. 11, 12

[125] M. S. M. Soliman, E. M. Abdel-Rahman, E. F. El-Saadany, and R. R. Mansour, "A wideband vibration-based energy harvester," *J. Micromech. Microeng.*, vol. 18, no. 11, p. 115021 (11pp), 2008. 12, 29

[126] L.-C. Blystad and E. Halvorsen, "A piezoelectric energy harvester with a mechanical end stop on one side," *Microsyst. Technol.*, vol. 17, pp. 505–511, 2011. 12, 109

[127] K. Matsumoto, K. Saruwatari, and Y. Suzuki, "Vibration-powered batteryless sensor node using MEMS electret generator," in *Proc. PowerMEMS 2011*, Seoul, The Republic of Korea, Nov. 15–18 2011, pp. 134–137. 12, 29

[128] B. Marinkovic and H. Koser, "Smart sand—a wide bandwidth vibration energy harvesting platform," *Appl. Phys. Lett.*, vol. 94, no. 10, p. 103505, 2009. 12

[129] A. Erturk, J. Hoffmann, and D. J. Inman, "A piezomagnetoelastic structure for broadband vibration energy harvesting," *Appl. Phys. Lett.*, vol. 94, p. 254102, 2009. 12, 29

[130] L. G. W. Tvedt, "Design, modeling and characterization of a MEMS electrostatic energy harvester," M.S. thesis, Vestfold University College, 2008. 13, 17

[131] L. G. W. Tvedt, D. S. Nguyen, and E. Halvorsen, "Nonlinear behavior of an electrostatic energy harvester under wide- and narrowband excitation," *J. Microelectromech. Syst.*, vol. 19, no. 2, pp. 305 –316, april 2010. 15, 17, 107, 109, 110

[132] S. D. Nguyen, E. Halvorsen, G. U. Jensen, and A. Vogl, "Fabrication and characterization of a wideband MEMS energy harvester utilizing nonlinear springs," *J. Micromech. Microeng.*, vol. 20, no. 12, p. 125009, 2010. xiii, 15, 17, 25, 107, 108, 115

[133] S. D. Nguyen and E. Halvorsen, "Nonlinear springs for bandwidth-tolerant vibration energy harvesting," *J. Microelectromech. Syst.*, vol. 20, no. 6, pp. 1225 –1227, dec. 2011. 15, 17, 109

[134] S. D. Nguyen, E. Halvorsen, and I. Paprotny, "Bistable springs for wideband MEMS energy harvesters." *Appl. Phys. Lett*, vol. 102, no. 02, p.023904, 2013. 15, 17, 25, 107, 115, 119

[135] S. D. Nguyen, E. Halvorsen, and G. U. Jensen., "Wideband MEMS energy harvester driven by colored noise," Nov 2012, submitted to *J. Microelectromech. Syst.* 15, 17

[136] S. D. Nguyen and E. Halvorsen, "Wideband vibration energy harvesting utilizing nonlinear springs," in *Tech. Dig. PowerMEMS 2009*, Washington DC, USA, Dec. 1–4 2009, pp. 411–414. 15, 17, 109

[137] S. D. Nguyen and E. Halvorsen, "Analysis of vibration energy harvesters utilizing a variety of nonlinear springs," in *Proc. PowerMEMS 2010*, vol. Poster Sessions, Leuven, Belgium, Dec. 1–3 2010, pp. 331–334. 15, 17

[138] S. D. Nguyen, N.-H. T. Tran, E. Halvorsen, and I. Paprotny, "Design and fabrication of MEMS electrostatic energy harvester with nonlinear springs and vertical sidewall electrets," in *Proc. PowerMEMS 2011*, vol. Oral Sessions, Seoul, Republic of Korea, Nov. 15–18 2011, pp. 126–129. 15, 17

[139] G. A. Lesieutre and C. L. Davis, "Can a coupling coefficient of a piezoelectric device be higher than those of its active material?" *J. Intell. Mater. Syst. Struct.*, vol. 8, pp. 859–867, Oct. 1997. 21

[140] A. F. Arrieta, P. Hagedorn, A. Erturk, and D. J. Inman, "A piezoelectric bistable plate for nonlinear broadband energy harvesting," *Appl. Phys. Lett.*, vol. 97, p. 104102, 2010. 29

[141] T. Galchev, H. Kim, and K. Najafi, "Micro power generator for harvesting low-frequency and nonperiodic vibrations," *J. Microelectromech. Syst.*, vol. 20, no. 4, pp. 852 –866, aug. 2011. 29

[142] M. Wischke, M. Masur, F. Goldschmidtboeing, and P. Woias, "Electromagnetic vibration harvester with piezoelectrically tunable resonance frequency," *J. Micromech. Microeng.*, vol. 20, no. 3, p. 035025, 2010. 29

[143] G. Sebald, H. Kuwano, D. Guyomar, and B. Ducharne, "Experimental Duffing oscillator for broadband piezoelectric energy harvesting," *Smart Mater. Struct.*, vol. 20, no. 10, p. 102001, 2011. 32

[144] L. G. W. Tvedt, L. J. Blystad, and E. Halvorsen, "Simulation of an Electrostatic Energy Harvester at Large Amplitude Narrow and Wide Band Vibrations," *Proceedings DTIP 2008*, French Riviera, France, Apr. 2008, pp. 296-301. 109

[145] F. Peano, and T. Tambosso, "Design and optimization of a MEMS electret-based capacitive energy scavenger," *J. Microelectromech. Syst.*, vol. 14, pp. 429-435, 2005. 110

[146] E. Halvorsen, "Energy Harvesters Driven by Broadband Random Vibrations", *J. Microelectromech. Syst.*, vol. 17, no. 5, pp. 1061-1071, 2008. 111

[147] D. Galayko, and P. Basset, "A General Analytical Tool for the Design of Vibration Energy Harvesters (VEHs) Based on the Mechanical Impedance Concept," *IEEE Trans Circ Syst I*, vol. 58, no. 2, pp.299-311, 2011. 111

[148] Linear Technology Corporation. [Online]. Available: http://www.linear.com/. 111

[149] E. Halvorsen, L. J. Blystad, S. Husa, and E. Westby, "Simulation of Electromechanical Systems Driven by Large Random Vibrations," *MEMSTECH'2007*, May 23-26, 2007, Lviv-Polyana, UKRAINE. 111